17552

NATIONAL LIBRARY
OTTAWA

CANADA

BIBLIOTHÈQUE NATIONALE
OTTAWA

NAME OF AUTHOR........William.....D.......Hogg..

TITLE OF THESIS.........Boundary....Layer....Fluxes
........Above.....A....Hot....Water
........Plume..........................

UNIVERSITY....of.....Alberta..........................

DEGREE FOR WHICH THESIS WAS PRESENTED..Master...of...Science

YEAR THIS DEGREE GRANTED.........1973....................

Permission is hereby granted to THE NATIONAL LIBRARY OF CANADA to microfilm this thesis and to lend or sell copies of the film.

The author reserves other publication rights, and neither the thesis nor extensive extracts from it may be printed or otherwise reproduced without the author's written permission.

(Signed).William....D...Hogg.

PERMANENT ADDRESS:

..753.....Sunnypoint. Dr.
..Newmarket........
...Ontario.............

DATED....June....28....1973

NL-91 (10-68)

THE UNIVERSITY OF ALBERTA

BOUNDARY-LAYER FLUXES ABOVE A HOT WATER PLUME

by

© WILLIAM D.HOGG

A THESIS

SUBMITTED TO THE FACULTY OF GRADUATE STUDIES AND RESEARCH

IN PARTIAL FULFILMENT OF THE REQUIREMENTS FOR THE DEGREE

OF MASTER OF SCIENCE

IN

METEOROLOGY

DEPARTMENT OF GEOGRAPHY

EDMONTON, ALBERTA

FALL, 1973

THE UNIVERSITY OF ALBERTA

RELEASE FORM

NAME OF AUTHOR WILLIAM D. HOGG

TITLE OF THESIS BOUNDARY-LAYER FLUXES ABOVE A HOT WATER PLUME

DEGREE FOR WHICH THESIS WAS PRESENTED MASTER OF SCIENCE IN METEOROLOGY

YEAR THIS DEGREE GRANTED FALL, 1973

Permission is hereby granted to THE UNIVERSITY OF ALBERTA LIBRARY to reproduce single copies of this thesis and to lend or sell such copies for private, scholarly or scientific research purposes only.

The author reserves other publication rights, and neither the thesis nor extensive extracts from it may be printed or otherwise reproduced without the author's written permission.

(Signed) William D. Hogg

PERMANENT ADDRESS:

753 SUNNYPOINT DR.
NEWMARKET, ONTARIO

DATED June 28 1973

THE UNIVERSITY OF ALBERTA

FACULTY OF GRADUATE STUDIES AND RESEARCH

The undersigned certify that they have read, and recommend to the Faculty of Graduate Studies and Research for acceptance, a thesis entitled "Boundary-Layer Fluxes Above a Hot Water Plume," submitted by William D. Hogg in partial fulfilment of the requirements for the degree of Master of Science in Meteorology.

Keith D. Hage
Supervisor

Edward Lozowski

John B. Nuttall

Date . . . JUNE 25, 1973

ABSTRACT

Fluxes of momentum, heat and water vapour above Lake Wabamum, Alberta are dealt with in this investigation. Two power-generating plants discharge heated water from condenser-cooling systems into the lake and the fluxes above this heated water are the main concern. Measurements of the fluxes by fast-response instruments are presented for two warm days in August and one cold day in October. Temperature, dew-point and wind profiles are included for the October date only.

The August fluxes are calculated from one day's data collected above the heated water and from a similar day's data collected above the undisturbed lake. It is shown that the fluxes of heat and water vapour above the heated water were approximately 5 times greater than those above the natural lake.

It is noted that free convection conditions exist above the heated water for the October situation because of a 15°C difference between air and water temperature. The October profile and fast-response instrument estimates of fluxes are compared and found to agree well for sensible heat flux, less so for vapour flux and not at all for momentum flux. An upward momentum flux as measured by the fast-response shear-stress meter is discussed and is shown to be linked with a large-scale turbulence upon which the normal small-scale turbulence is superimposed. The possibility of the large-scale turbulence being associated with organized convective eddies is pointed out.

A liquid water flux associated with a dense fog during the October data collection is considered and found to be an order of magnitude less than the water vapour flux.

Sensible and latent heat fluxes due to an observed positive mean vertical velocity in October are calculated and discussed. Each is shown to be significant but less than the corresponding turbulent flux.

ACKNOWLEDGEMENTS

The assistance I received in the preparation of this thesis was invaluable and I wish to express my gratitude to all those who helped.

In particular I am very appreciative of the advice and guidance of my departmental supervisor, Dr. K. D. Hage. I would also like to thank Dr. E. P. Lozowski and Professor J. B. Nuttall for their willingness to serve on my examining committee.

The mobile micrometeorological unit and associated equipment for the field tests were supplied by the Institute of Earth and Planetary Physics under a Negotiated Development Grant from the National Research Council of Canada. Operating expenses were provided by the Atmospheric Environment Service, Environment Canada, under its Grants-In-Aid of Research Program. Calgary Power Ltd. expended considerable effort to supply the site with electrical power.

I am grateful to Dr. J. Honsaker for his advice and assistance in data analysis and to all those who braved the mud and flies of Lake Wabamun to help at the site.

The experienced assistance of Mrs. Marilyn Wahl who typed the final draft is greatly appreciated.

I would also like to thank my friends and fellow students for the discussions and suggestions which were

most helpful. Finally, I am very grateful to my wife for her patience, understanding and encouragement during the two years of graduate study.

This study was undertaken while I was on leave from the Atmospheric Environment Service of the Department of the Environment.

TABLE OF CONTENTS

CHAPTER PAGE

I. INTRODUCTION 1

II. COLLECTION OF THE DATA 8

2.1 The Observing Site 8

2.2 Instrumentation

2.2.1 Slow-Response Instruments 11

2.2.2 Fast-Response Instruments 14

2.2.3 Instrumental-Array 16

2.3 Calibrations 18

2.4 Water Temperature Surveys 20

2.5 Local Weather Conditions 21

III. THEORETICAL ANALYSIS 24

3.1 Introduction 24

3.2 Profile Theories 25

3.2.1 Introduction 25

3.2.2 Profiles in Neutral and Near-Neutral Conditions 29

3.2.3 Profiles in Free Convection . . . 36

3.2.4 General Profiles in Unstable Air . 41

3.2.5 Actual Method of Profile Analysis 45

3.3 Vertical Fluxes by Eddy Correlation . . 48

CHAPTER PAGE

3.3.1 Introduction 48

3.3.2 Turbulent Fluxes 49

3.3.3 Fluxes Associated with a Mean Vertical Wind 54

IV. RESULTS

4.1 Introduction 56

4.2 August Tests 59

4.2.1 Local Weather Conditions 59

4.2.2 Stability 59

4.2.3 Fluxes 63

4.3 October Tests 67

4.3.1 Stability 67

4.3.2 October Profiles 68

4.3.3 Directly Measured Fluxes 77

4.3.4 The Anomalous Momentum Fluxes . . . 82

4.3.5 Turbulent Flux of Liquid Water . . 107

4.3.6 Fluxes Associated With the Mean Vertical Wind 108

V. CONCLUSIONS 113

BIBLIOGRAPHY 118

LIST OF TABLES

TABLE	DESCRIPTION	PAGE
1	Morphometry of Lake Wabamun	9
2	Slow-Response Instrumentation	12
3	Fast-Response Instrumentation	15
4	Slow-Response Instrument Error	57
5	Fast-Response Instrument Error	58
6	August z/L Values	64
7	August Fluxes	65
8	October Ri and z/L' Values	69
9	Actual and Theoretical Temperature Profiles, October 21.	70
10	Actual and Theoretical Wind Profiles, October 21	72
11	Profile Estimates of Turbulent Fluxes, October 21	78
12	Sensible Heat Flux Assocated with Mean Vertical Wind	111
13	Latent Heat Flux Associated with Mean Vertical Wind	112

LIST OF FIGURES

FIGURE PAGE

1 Lake Wabamun, Alberta -- showing experimental site at Point Alison. 10

2 Point Alison and Vicinity, Lake Wabamun, Alberta. 10

3 Point Alison Instrumentation Site, Lake Wabamun, 1972. 17

4 Lake Wabamun Surface Temperature, August 24. . 60

5 Lake Wabamun Surface Temperature, August 25. 61

6 Surface Temperature Upwind from Tower Site Lake Wabamun, October 21. 62

7 August Wind Profiles. 66

8 October Temperature Profiles. 74

9 October Wind Profiles. 75

10 Heat Flux Comparison, October. 80

11 Latent Heat Flux Comparisons, October. 81

12 Five Minute Heat Fluxes (Sonic) 1830-2130 MDT. 83

13 Five Minute Momentum Fluxes (Shear-Stress Meter) 1830-2130 MDT. 83

14 October 30-second Means 1833-1845 MDT. 85

15 October 30-second Means 1900-1913 MDT. 85

16 October 30-second Means 1916-1924 MDT. 86

17 October 30-second Means 1925-1938 MDT. 86

18 October 30-second Means 1938-1950 MDT. 87

FIGURE PAGE

19 October 30-second Means 2105-2116 MDT. . . . 87

20 October 30-second Means 2118-2130 MDT. . . . 88

21 October Half-Second Values 1835-1836 MDT Fluxatron T. 88

22 October Half-Second Values 1835-1836 MDT Sonci T. 90

23 October Half-Second Values 1835-1836 MDT Sonic W. 90

24 October Half-Second Values 1835-1836 MDT Total Horizontal wind. 91

25 October Half-Second Values 1835-1836 MDT Shear-Stress Meter W. 91

26 October Half-Second Values 1842-1843 MDT Sonic T. 92

27 October Half-Second Values 1842-1843 MDT Sonic W. 92

28 October Half-Second Values 1842-1843 MDT Total Horizontal Wind. 93

29 October Half-Second Values 1842-1843 MDT Shear-Stress w. 93

30 October Half-Second Values 1842-1843 MDT V component. 94

31 October Half-Second Values 1842-1843 MDT Mean Direction Component. 94

32 October Half-Second Values 1843-1844 MDT Sonic T. 95

33 October Half-Second Values 1843-1844 MDT Sonic W. 95

34 October Half-Second Values 1843-1844 MDT Total Horizontal Wind. 96

FIGURE PAGE

35 October Half-Second Values 1843-1844 MDT Shear-Stress W. 96

36 October Half-Second Values 1843-1844 MDT V Component. 97

37 October Half-Second Values 1843-1844 MDT Mean Direction Component. 97

38 October Half-Second Values 1919-1920 MDT Total Horizontal Wind. 98

39 October Half-Second Values 1919-1920 MDT Shear-Stress W. 98

40 October Half-Second Values 1919-1920 MDT V Component. 99

41 October Half-Second Values 1919-1920 MDT Mean Direction Component. 99

42 October Half-Second Values 1919-1920 MDT Sonic T. 100

43 October Half-Second Values 1920-1921 MDT Fluxatron T. 100

44 October Half-Second Values 1920-1921 MDT Sonic T. 101

45 October Half-Second Values 1920-1921 MDT Sonic W. 101

46 October Half-Second Values 1920-1921 MDT Total Horizontal Wind. 102

47 October Half-Second Values 1920-1921 MDT Shear-Stress w. 102

48 October Half-Second Values 1920-1921 MDT V Component. 103

49 October Half-Second Values 1920-1921 MDT Mean Direction Component. 103

CHAPTER I

INTRODUCTION

Over the past few years in Central Alberta, considerable scientific and community interest has been focussed on a body of water about forty miles west of Edmonton. This lake, Lake Wabamun, is both large enough, (three by twelve miles) and close enough (42 miles) to a large urban population centre to serve as a well-used recreation area. Thus, summer cottages, beaches, and other similar facilities including a provincial park border much of the lake. In addition, accessible coal has been found on the shores of the lake making the area an ideal location for thermal power plants. Coal for fuel and water for steam and condensing purposes are convenient and abundant. As a result, Calgary Power has established two generators (599 and 300 MW) on opposite shores of the lake and these generators discharge water from their cooling systems back into the lake. It has been claimed that the resultant plumes of heated water have caused increased weed growth and other biological and zoological changes detrimental to the recreational aspects of the lake. Consequently biologists, zoologists and civil engineers from the University of Alberta became involved in determining the validity of such claims through the Wabamun Lake Thermal Project (e.g. see Nursall and Gallup, 1971). During 1972 the Meteorology Division of the University entered the investigation in an attempt to examine the fluxes of momentum, heat and water substance from both the heated plumes and the ambient lake surface. I was fortunate enough to take part in this micro-meteorological project and the following chapters deal with the techniques of this project, and some of the results.

Although the bulk of boundary-layer flux measurements have been made over land, the problem of estimating heat and water exchanges between air and a water surface has received worldwide attention for many decades. At first most estimates of evaporation were obtained from empirical flux-gradient relationships involving wind speed, surface water temperature and air temperature and moisture content. These formulae were frequently used in water-level studies of lakes and reservoirs and similar hydrologic investigations.

A logical extension of this flux-gradient relationship assumption leads to estimates of all the boundary-layer fluxes. The technique is simply to apply a mixing-length type approach, where the flux of a quantity is given by a constant times the gradient of the concentration of the quantity. As is pointed out by Robinson (1966), this approach could be extremely useful as it relates phenomena physically compounded of micro-scale interactions with standard meteorological observations. Thus, using synoptic-scale data only, estimates of the boundary-layer fluxes are available, e.g. for input into dynamic models. Such a method is very approximate, however, and the resultant flux estimates approach the real fluxes only when averages over vast areas of ocean are considered. The same method can be applied to lakes that exhibit horizontal homogeneity in atmospheric moisture and temperature and in surface water temperature. Edge-effects complicate the procedure, but for sufficiently long time intervals, fairly accurate estimates of the fluxes can be obtained if the above restrictions are met.

One of the most comprehensive studies of evaporation from a lake was the well-known Lake Hefner project (e.g. U.S. Dept. Interior, 1954). The purpose of the investigation was to obtain formulae to predict evaporation from Lake Mead before Lake Mead existed. Because inflow and outflow for Lake Hefner were well known, a water-budget method was used as a control estimate of evaporation. Observations from a meso-scale network around the lake were used to compute evaporation estimates using an energy-budget technique as well as various empirical flux-gradient procedures similar to those mentioned previously. Generally successful comparisons were then made between these estimates, and the water-budget estimates, of average monthly evaporation.

As the Monin-Obukhov Similarity Theory (e.g. Lumley and Panofsky; 1964) gained rapid, widespread acceptance, and with improved instrumentation and computing facilities profile methods became more sophisticated, while direct measurement of the turbulent fluxes became possible. Similarity theory provided a sound theoretical basis for the form of the profile-flux relations and also introduced the inclusion of stability effects. Thus, estimates of flux averaged over minutes, instead of days, were feasible. Additionally, the last fifteen years has seen increased use of instruments with responses fast enough to measure all significant turbulence fluctuations. If the responses of the instruments are properly matched, then the covariance of two measurements is directly proportional to the appropriate flux. Fast-response temperature and wind sensors have been used for some time to measure heat and momentum flux. More recently, the use of the Lyman-alpha humidiometer has permitted direct measurement of turbulent water-vapour flux. The disadvantages of these methods are the cost of the instruments, and the large amount of data and data anlaysis required for even short-period calculations. The data collection and analysis problems become practicable only with the use of modern computers. These are hardly the methods for calculating evaporation on a long-term or large-scale basis, but they are the only methods which give information about the structure of the boundary layer itself.

Two of the largest expeditions to use the improved profile methods, and direct-measurement approach to the problem of evaluating fluxes over water, were the Indian Ocean Expedition (Badgley, Paulson, and Miyake, 1968) and the Barbados Oceanogrophic and Meteorological Expedition (BOMEX) (e.g. Holland 1972). Both projects were concerned with determining fluxes in the atmosphere above large expanses of fairly warm ocean. BOMEX, in particular, attempted to evaluate the fluxes using every possible technique for comparison purposes. Thus, in addition to the two previously-mentioned methods, budget methods, and a procedure based on Kolmogoroff's Law were also used (Pond et al. 1971). Budget methods employ conservation equations for heat, water vapour, or horizontal velocity to express boundary-layer fluxes as a function of observable quantities. The fourth procedure involves calculation of the turbulent-transfer coefficients and vertical fluxes through the use of Kolmogoroff's Law, which relates the energy spectrum and wave number in the inertial subrange. The observations used for the direct covariance calculation of fluxes can also be used in this method.

Both profile and fast-response type measurements were made recently at Lough Neagh, a lake in Northern Ireland, by Sheppard, et al. (1972). In fact, the Lake Wabamun experiment was similar in design to the Lough Neagh operation, though far less extensive in scope than the latter. The combination of profile and fast-response measurements, allowed both groups to make use of three of the four independent methods of determining fluxes in the atmospheric boundary layer.

As was mentioned previously, the empirical flux-gradient relationships described earlier are intended for use over large bodies of water that exhibit horizontal homogeneity. This is hardly the situation at Lake Wabamun, where it is the departures from horizontal homogeneity which we wish to examine. The water-budget method, used on Lake Mead, provides only an estimate of evaporation averaged over the entire lake for fairly long time periods. For this reason, and because of the probable existence of a large underground source for Lake Wabamun, it was deemed to be unsuitable. Thus, the only techniques appropriate to the Wabamun project were those supplying information about the vertical fluxes at some point in the atmosphere. Of the four independent methods left, three can be utilized if profile and fast-response measurements are available. With this in mind, these were the two types of measurements made at Lake Wabamun during 1972.

Useful data were obtained on three days, two of which were warm days in August, while the third, in October, had air temperatures near freezing. Different wind directions permitted measurement of fluxes above both the heated plume and the undisturbed lake surface for the August situation, but only the fluxes above the plume were obtained in October. It is the intent of this thesis to compare various methods of estimating fluxes at some point in the atmosphere, as well as to compare fluxes from the heated and unheated water of the lake.

CHAPTER II

COLLECTION OF THE DATA

2.1 The Observing Site

Lake Wabamun is situated in gently rolling, forested terrain, 67 km west of Edmonton, Alberta. The lake lies in an east-west direction, being approximately 19 km long and on the average 4.3 km wide. A more complete list of the physical characteristics can be found in Table 1. The Wabamun power plant, the larger of the two generating stations, is on the north shore of the lake near the eastern end. The eastern tip of Point Alison was selected as the observing site for the 1972 experiments in order to take advantage of air flow over the heated water discharged from this station (see Figure 1). The point protrudes into the lake between the power plant's intake canal to the west, and the discharge canal to the east. The only acceptable wind directions at this site were east to southeast with an over-water fetch of not less than 2.2 km, and west to southwest with an overwater fetch of not less than 5.6 km. East to southeast winds carry warm water from the outlet westward around Point Alison and the air reaching the observing site has a fetch of at least 0.5 km over the heated water plume.

TABLE 1

Morphometry of Lake Wabamun

Elevation	722.7 m
Area	82.5 km^2
Volume	ca. 0.455 km^3
Length	19.2 km
Maximum breadth	6.6 km
Mean breadth	4.3 km
Maximum depth	11.6 m
Mean depth	5.4 m
Shoreline lehgth	57.3 km
Area of Surface drainage	372.4 km^2

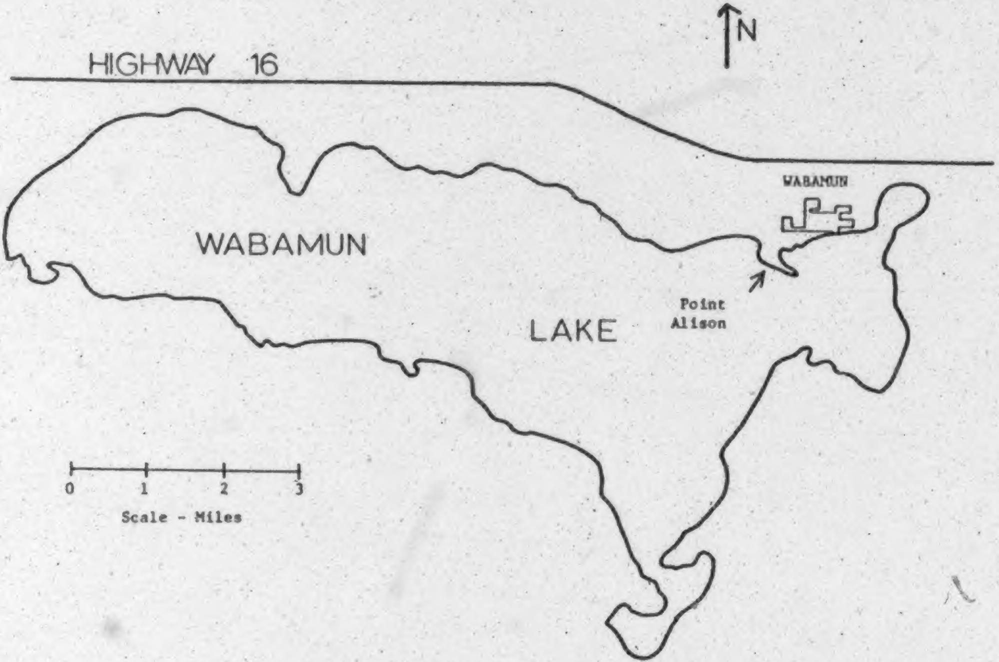
HIGHWAY 16
N
WABAMUN
Point Alison
WABAMUN
LAKE
0
1
2
3
Scale - Miles

Figure 1. Lake Wabamun, Alberta - showing experimental site at Point Alison.

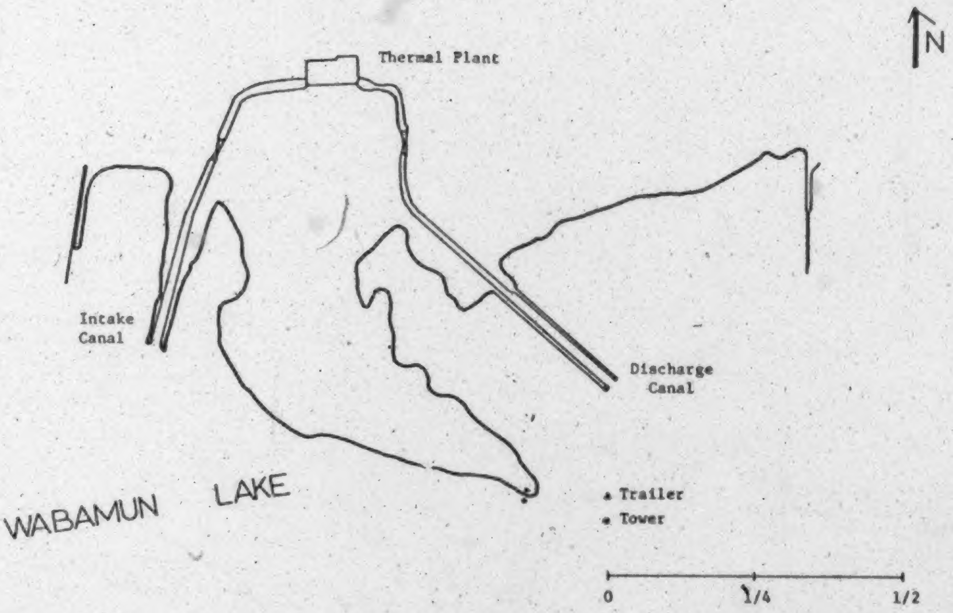
Thermal Plant
N
Intake Canal
Discharge Canal
WABAMUN LAKE
▲ Trailer
● Tower
0
1/4
1/2
Scale - Miles

Figure 2. Point Alison and vicinity, Lake Wabamun, Alberta.

In a southwest wind the warm water plume is carried east of the point and air reaching the site has a trajectory over the normal lake surface only.

An enlarged view of Point Alison showing the experimental site is shown in Figure 2. A trailer, housing recording and data processing equipment, was located near the water line, and an 8 m tower was erected in water of depth 0.5 m about 25 m out from the lakeshore. Point Alison itself is heavily forested and rises to a maximum elevation of 18 m approximately 0.6 km westnorthwest of the tower site. As is shown by Figure 2, the tip of the point may cause flow interference in a wind from due east.

2.2 Instrumentation

2.2.1 Slow-Response Instruments

The slow-response instruments listed in Table 2 were used to obtain average values of wind, temperature, humidity, and net radiation for time periods of fifteen minutes or more. The wind speed, air temperature and air dew-point instruments were mounted at the four listed heights on an 8 m tower to provide the profile data. The non-logarithmic heights were necessitated by the use of a tower with fixed booms, designed for use on land, but sitting in 0.5 m of water at Lake Wabamun. Net radiation and wind direction instruments were located on separate

Table 2 Slow Response Instrumentation

Element	Height Above Water (m)	Sampling Period (min)	Sensor
Wind Speed	0.5, 1.5, 3.5, 7.5	15	Cup Anemometers[1]
Wind Direction	2.0	1	Vane
Air Temperature	0.5, 1.5, 3.5, 7.5	15	Thermistors[2]
Dew Point	0.5, 1.5, 3.5, 7.5	8	Hygrometers[3]
Water Temperature	Surface	8	Thermistor[4]
Net Radiation	1.0	1	Funk Radiometer[5]

[1] Rauchfuss Instruments and Staff Pty. Ltd. Model R/ASC

[2] Yellow Springs Instrument Co. Ltd., Model 44203

[3] Cambridge Systems, Model 880

[4] Yellow Springs Instrument Co. Ltd., Model 42SL

[5] Solar Radiation Instruments, Model SRI 4

masts away from the tower and their signals were recorded in analog form on strip charts. Dew-point temperatures and water temperatures were read and recorded periodically from meters, while Assman psychrometer readings were taken at irregular intervals at low heights on the tower as additional independent checks of air temperature and moisture.

The temperature profile utilized linear thermistors and a set of operational amplifiers. The thermistors were mounted in reentrant shielded tubes which were ventilated. The output was arranged to give the ambient temperature at one level, and differences from that temperature at the other levels. Maximum sensitivity to the temperature gradient can be obtained in this way. Data readouts were accomplished by driving integrating motors with number wheels, which were photographed every fifteen minutes to give a mean temperature.

The dew-point profile instrument had four sensing heads. They were connected to the thermistor elements of the temperature profile, and ventilated together by a small suction pump. The dew-point detection was accomplished by sensing light scattered from condensate on a mirror which was cooled to dew-point by a thermoelectric cooler (Peltier effect). To obtain profiles, the four elements had to be switched on manually in turn, and read in sequence.

The sensitive cup anemometers mounted on the end of each of the tower booms measured total horizontal wind at each level. The cup generators operated counters located in the trailer which were photographed every fifteen minutes, permitting the calculation of mean wind speeds for periods of a quarter hour or more.

2.2.2 Fast-Response Instruments

Fast-response instruments at the tower site are listed in Table 3. All channels were sampled at 100 readings per second and filtered at a cut-off frequency of 20 Hz before conversion from analog to digital form. Analog-to-digital conversion, gross error checks, and recording of up to 8 channels of data on digital magnetic tape were carried out in the field following procedures described by Honsaker, McDougall, and Oracheski (1972).

A shear-stress meter, consisting of three Gill propeller anemometers mounted on orthogonal axes, was used for the measurement of eddy flux of momentum. It was mounted on a separate mast so that it could be moved independently of the main tower, thus avoiding wind interference effects.

The sonic anomemeter-thermometer was a continuous-wave model similar to that described by Kaimal and Businger (1963). The instrument was capable of measuring fluctuations

Table 3 Fast Response Instrumentation

Element	Height Above Water (m)	Response Time (sec)*	Sensor
Vertical Wind Speed	3.0	0.4	Propeller Anemometer[1]
Vertical Wind Speed	3.0	0.1	Sonic Anemometer[2]
Horizontal Wind Speed	2.5	0.4	Propeller Anemometers[1]
Air Temperature	3.0	0.02	Resistance Thermometer
Air Temperature	3.0	0.1	Sonic Thermometer[2]
Vapour Pressure	3.0	0.007	Lyman α Humidiometer[3]

[1] R. M. Young Company, Model 27101

[2] Kaimal, J. C., and J. A. Businger, 1963: A continuous wave sonic anemometer-thermometer. J. Appl. Meteor., 2, pp. 156-164.

[3] Electromagnetic Research Corp., Model BR

*Evaluated for a mean wind speed of 2.0 m sec^{-1}

in the vertical wind component and temperature simultaneously. It was mounted on the main tower 3 m above the surface of the water.

A Lyman-alpha Humidiometer was attached to the same mounting as the sonic anemometer-thermometer. The Humidiometer produces a signal from the absorption of ultraviolet light around the Lyman-alpha wavelength (121.5 nm). In air, Lyman-alpha absorption is almost entirely due to water vapour, and thus provides a measure of absolute humidity. The strength of the absorption permits the measurement to be made over a short sampling path (15 mm) which in turn means that the instrument is capable of very fast response. It was used in conjunction with the sonic anemometer to measure the eddy flux of latent heat.

The fine-wire resistance thermometer was mounted on its own mast with a Gill propeller anemometer measuring vertical wind either on the same mast or on the adjacent shear-stress meter mast. The resulting simultaneous measurements of temperature and vertical wind provided an estimate of the sensible heat flux which was independent of the sonic anemometer-thermometer estimate.

2.2.3 Instrumental Array

The arrangement of instrumentation at the site is shown in Figure 3, a photograph of the tower looking southward

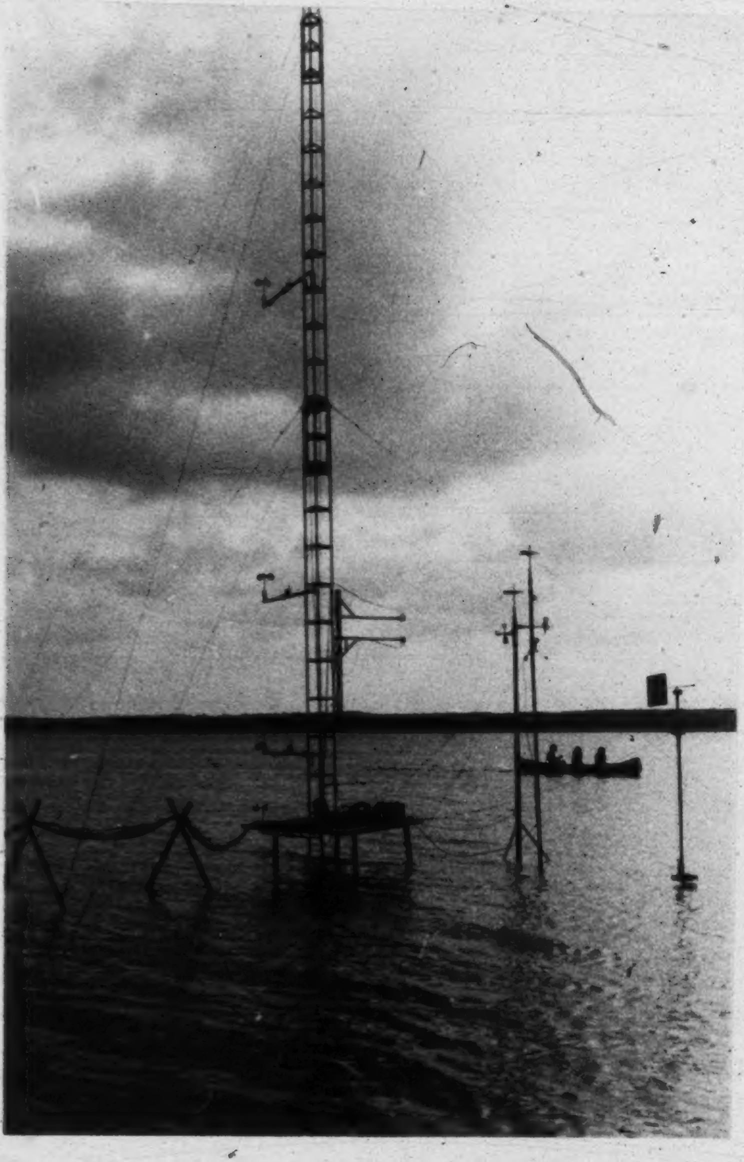

FIGURE 3. Point Alison instrumentation site, Lake Wabamun, 1972.

across the lake. The profile instruments were located near the ends of 1 m booms oriented southeastward toward the hot water plume. Thus the booms were aligned approximately into the wind during data collection and blockage effects were minimized. The sonic anemometer-thermometer and the Lyman-alpha humidiometer were attached to a boom extending southwestward from the tower 3 m above the lake surface. The shear-stress meter, resistance thermometer, net radiometer, and wind direction indicator were movable and were arrayed across wind from the tower before each day's runs. All masts and instruments were aligned with the vertical by using transit readings at three points along the shore.

2.3 Calibrations

Considerable effort was expended calibrating the instruments. The anemometers (cup and propeller) were calibrated against a hot-wire anemometer and a pitot tube in the University of Alberta Civil Engineering Department's wind tunnel, and against a secondary standard anemometer in a wind tunnel of the Defence Research Establishment at Suffield, Alberta. Further calibrations of the cup anemometers in both the laboratory and the field were necessary for low wind speeds (2 m/sec or less) because of different responses among the anemometers in this range.

The thermistor elements were calibrated using a temperature-controlled air flow in the laboratory spanning the entire range of temperatures encountered in the field experiments. Temperature dependent noise in the signal, discovered during these calibrations and affecting the integrating motors, eventually necessitated the discarding of the temperature profile data from the two August data collection days. The dew-point hygrometer was calibrated in both field and laboratory environments. As well the Assman psychrometer was used as a check on air temperature and moisture content during the actual data collection.

The fine-wire resistance thermometer was calibrated simply by measuring its resistance at several temperatures and fitting a linear relation to the points. The humidiometer calibration was determined by taking the reading for dry air. Because of the exponential relation between absorption and the water vapour amount, one reading defined a unique curve and complete calibration.

The sonic anemometer-thermometer has a built-in, electronically simulated, 30° phase shift. This phase shift was recorded both manually and directly onto magnetic tape permitting calibration to be carried out in the field before or after data collection.

2.4 Water Temperature Surveys

Temperature measurements in the lake were carried out from a small boat using a calibrated thermistor read through a YSI Model 42SL telethermometer (See Table 2). Surface temperatures were recorded by holding the thermistor in the upper layer of water with about 2 inches submersion. Temperature profiles were obtained by anchoring the boat and then lowering the thermistor by 2 foot increments. Bottom temperatures were recorded by dropping the weighted thermistor head into the mud bottom and waiting until equilibrium was obtained.

In August the boat's position was found by means of two simultaneous theodolite bearings from instruments set up on shore about 1200 feet apart. The base line distance was measured to within 0.1 ft and the angles recorded to the nearest 5 seconds of arc. Citizen's band radios were used for communication between the boat and theodolites.

Dense steam fog from the lake made it impossible to use the same procedure to determine the boat's position in October. Because of the extremely low visibility, only one traverse of the plume directly upwind of the tower was possible. The procedure was simply to start at the tower on a heading directly into the wind, continuing into the lake on the same heading until homogeneous lake temperatures were obtained. The boat's speed was estimated by measuring the time for objects on the water to pass from bow to stern of the boat in a manner similar to the casting of the log on a sailing ship. Of necessity then, the distribution of upwind water temperatures was subject to considerable uncertainty. However, because the width of the plume matched the known width on days with similar winds, the data for October were accepted.

2.5 Local Weather Conditions

Both August 24 and 25, 1972 were warm (75° F, 24° C) summer days with only scattered cloud. On August 24 light (3-4 m/sec), steady southeast winds prevailed through the day and into the evening. As was discovered during previous water temperature surveys with similar winds, the hot water plume was carried westward around Point Alison and directly on shore at the tower site (see Figure 4). Surface water temperatures reached 30° C in the plume so that the air arriving at the tower had been receiving heat from the lake surface for some 600 m and hence was likely to be unstable. The plume remained along the Point Alison shore until after data collection had ended. Data were collected from 1330 to 2045 MDT (Mountain Daylight Time).

A weak trough passed through Alberta during the night of August 24 and winds were steady from the southwest at about 2 m/sec through much of August 25. These winds carried the very shallow layer of hot water east of Point Alison and air reaching the tower site had passed over the cooler (22°C), ambient lake surface (See Figure 5). This meant that neutral or slightly stable conditions in the surface boundary layer could be expected to prevail through much of the day's data collection period. In the evening, wind speeds dropped to near calm and wind direction became variable. These two days were ideal for comparison of fluxes over the plume with fluxes over the rest of the lake. Useful data collection occurred between 1200 and 1630 MDT on August 25.

On the morning of October 21, 1972, a low pressure area in the southern parts of British Columbia and Alberta produced overcast stratocumulus cloud conditions, some periods of snow, and east winds in the Lake Wabamun region. By mid-afternoon the winds had veered to eastsoutheast and this direction was maintained well into the night. Once again these winds brought the heated water in along the shore of Point Alison in a situation similar to that shown for August 24 in Figure 4. Thus air with a temperature near 0° C had a trajectory of at least 300 m over water whose surface temperature approached 17° C (See Figure 6). This temperature gradient produced unstable conditions in the atmospheric surface boundary layer. A steam fog formed over the entire lake and was particularly dense over the warm waters of the plume. Data collection was carried out between 1830 and 2130 MDT.

CHAPTER III

THEORETICAL ANALYSIS

3.1 Introduction

In the past twenty-five years investigators of the surface boundary layer have used three main approaches to study and describe the motions of the air near the ground. The earliest method examined the average profiles of wind and temperature and through existing theory tried to infer turbulent structures and flux magnitudes. For the sake of simplicity the bulk of this theory was developed for an infinite, homogeneous, level surface. A large lake approximates these conditions very well and the profile approach was chosen as an appropriate one to apply to the Lake Wabamun data. The most serious departure from the profile-theory assumption at Lake Wabamun was the change in surface temperature because of the heated water but it was believed that the profiles would have adjusted sufficiently at the levels of interest for this not to be a serious problem.

Another approach uses accurate, fast-response instruments to examine the structure of the turbulence and the fluxes etc. directly. This method was also employed at Lake Wabamun. The third approach in common use involves numerical modelling of the surface boundary layer. The computer has proved particularly useful in extending theory to cover more complicated flows such as occur over changes in surface roughness and temperature, problems that have received increasing attention over the past fifteen years. The results of one such model will be discussed very briefly in chapter four. The theory of the other two approaches will be developed in this chapter.

The intent of this chapter is to provide a logical development of the theoretical formulas used with the Lake Wabamun data. A more complete treatment of surface boundary-layer profiles and turbulence can be found in a number of texts (see e.g. Lumley and Panofsky, 1964) and their contents need not be duplicated here.

3.2 Profile Theories

3.2.1 Introduction

Most of the recent advances in understanding of the distribution of wind, temperature and moisture near the earth's surface have been brought about by the use of the Monin-Obukhov "similarity theory." Because of its importance, and because much of the present surface boundary-layer profile theory is based on it, similarity theory has been chosen as the starting point for this discussion.

The complexity of the problem makes it impractical to completely and theoretically describe the state of the surface boundary-layer for the perfectly general case of air moving over a varying surface. For this reason numerous assumptions were found to be necessary in order to simplify the theoretical description of the mean flow.

When applied to meteorology, the equation for the mean motion in vector notation can be written as (see e.g. Lumley and Panofsky, 1964):

$$\frac{d\vec{V}}{dt} = f\,\vec{V} \times \hat{k} - \frac{1}{\rho}\nabla p + \frac{1}{\rho}\frac{\partial\vec{\tau}}{\partial z}$$

Here $\vec{V}$ is the horizontal wind vector, f the Coriolis parameter, ρ the density, ∇p the pressure gradient, $\vec{\tau}$ the tangential stress vector acting on a horizontal surface, and $\hat{k}$ the vertical unit vector. For micrometeorological studies of the surface boundary layer the magnitudes of the Coriolis force and the pressure gradient force are small enough to be neglected leaving as the expression for the mean flow:

$$\frac{d\vec{V}}{dt} = \frac{1}{\rho}\frac{\partial\vec{\tau}}{\partial z}$$

Two standard surface boundary-layer assumptions are that there is no external pressure gradient and the earth's rotation need not be considered. Both assumptions limit the scales to which the results of theory are applicable. A condition necessary for the theoretical development is that the turbulence characteristics exhibit stationarity in a statistical sense which implies that the mean flow is in equilibrium. Thus stationarity becomes a third assumption. A further restriction which limits the applicability of the results, reduces the problem to a two dimensional one by assuming horizontal homogeneity and aligning the horizontal axis with the mean flow. Finally, molecular transport and radiative flux divergence are neglected although the latter assumption may not be realistic in stable conditions.

Under these restrictions the shear stress or momentum flux and the heat flux vary little with height near the ground. In fact the surface boundary layer is frequently called the "constant-flux" layer defined as the layer in which the shear stress varies by less than 20%. Stress divided by density has units of velocity squared so that the constant shear stress condition makes it possible to define a "friction velocity" u^*, constant with height, by:

$$u^* = \sqrt{\frac{\tau}{\rho}} \qquad (3-1)$$

where τ is the surface shearing stress and ρ is density.

For the turbulent flow problem simplified by the previously-mentioned assumptions, Monin and Obukhov (1954) argued that the terms governing the flow characteristics, andhence the important terms for dimensional analysis purposes were $g/\overline{T}$, $\overline{\rho}$, u^*, H and Z. Here g denotes the acceleration of gravity, $\bar{T}$ a mean air temperature, $\bar{\rho}$ a mean air density, H the heat flux, and z the height above ground. This set of five variables involves four dimensions, mass, length, time and temperature, which, by the Buckingham $-\pi$ theorem, means that all mean flow parameters are expressible as a function of one nondimensional quantity. This quantity was chosen to be z/L where

$$L = \frac{-u^{*3}}{k\,(g/\bar{\bar{T}})\,(H/c_p\bar{\rho})} = -\frac{u^{*3}\,c_p\,\bar{\rho}\,\bar{\bar{T}}}{k\,g\,H} \qquad (3\text{-}2)$$

The constant c_p is the specific heat of air at constant pressure. The von Karman constant k is included arbitrarily because it is dimensionless. This constant was used historically to describe the wind profile and has a numerical value of about 0.4. All mean turbulence characteristics, when placed in nondimensional form, should be functions of z/L.

A scaling length L and a scaling velocity u^* have been found for the flow and for completeness a scaling temperature T^* has been determined from the same dimensionally-important quantities (see e.g. Lumley and Panofsky, 1964):

$$T^* = -\frac{1}{k u^*}\,\frac{H}{c_p \bar{\rho}} \qquad (3\text{-}3)$$

The wind shear is related to the stress by

$$\frac{\vec{\tau}}{\rho} = K_M \frac{\partial \vec{V}}{\partial z} \qquad (3\text{-}4)$$

where K_M is the scalar eddy viscosity. Since K_M is a scalar, the stress and wind shear have the same direction everywhere in the surface boundary layer. But the stress is constant in this layer so that the wind shear is constant and the wind direction remains constant with height and equals the stress direction. Because only one direction is involved the vector notation can be dropped and the quantities considered as scalars.

The heat flux H is related to the potential-temperature gradient in a similar manner:

$$H = -c_p \bar{\rho} \; K_H \frac{\partial \bar{\theta}}{\partial z} \qquad (3\text{-}5)$$

where K_H is the eddy conductivity and $\bar{\theta}$ is the potential temperature.

3.2.2 Profiles in Neutral and Near-Neutral Conditions

It has long been known that the velocity profile in neutral air is logarithmic in height. A simple derivation notes that the ratio

$$\frac{u^*}{\left(\frac{\partial V}{\partial z}\right)} \qquad (3\text{-}6)$$

has dimensions of length. As well, in neutral air the lapse rate of potential temperature is zero and by (3-5) the heat flux H must be zero also. This means that L goes to infinity for neutral stability leaving the height z as the only remaining characteristic length. Traditionally the von Karman constant is included in the equation so that (3-6) is set equal to kz and the differential equation for the wind profile becomes

$$\frac{\partial V}{\partial z} = \frac{u^*}{kz} \qquad (3\text{-}7)$$

Its integrated form is

$$V = \frac{u^*}{k} \ln\left(\frac{z}{z_0}\right) \qquad (3\text{-}8)$$

The term z_0 is the "roughness length" and arises from the integration as the height at which the wind velocity becomes zero.

Perfectly neutral conditions in the atmosphere are rare of course so that it is desirable to extend the theory to cover non-neutral conditions by including the effect of the buoyant energy production term.

The term z/L is an indicator of stability based upon the heat flux H contained in the denominator of L. For neutral conditions H = 0 and (z/L) = 0 while for potential temperature decreasing with height (i.e. unstable conditions) the heat flux is upward or positive and z/L becomes negative. In stable conditions, the potential temperature increases with height, the heat flux is downward or negative and z/L increases in the positive sense with increasing stability. If z/L is small in magnitude and negative then the rate of production of convective energy ($gH/c_p \rho T$) is positive but small compared to the rate of production of mechanical energy ($u^{*2}\, \partial V/\partial z$). Under these conditions the boundary layer is said to be in a state called forced convection. According to Lumley and Panofsky (1964) this occurs when the magnitude of z/L is less than 0.03. Small deviations from neutral stability, namely forced convection and slightly stable stratification, will be considered next in this discussion.

Following the lead of Monin and Obukhov, a nondimensional wind shear S can now be introduced as

$$S = \frac{kz}{u^*} \frac{\partial V}{\partial z} \qquad (3\text{-}9)$$

Considering (3-7) it can be seen that this is unity in neutral air. A nondimensional temperature lapse rate R can be analogously defined by

$$R = \frac{z}{T^*} \frac{\partial \theta}{\partial z} \qquad (3\text{-}10)$$

But similarity theory predicts that all nondimensional mean turbulence characteristics should be functions of z/L so that (3-9) and (3-10) become

$$S = \phi_1(z/L) = \frac{kz}{u^*}\frac{\partial V}{\partial z} \qquad (3\text{-}11)$$

and

$$R = \phi_2(z/L) = \frac{z}{T^*}\frac{\partial \theta}{\partial z} \qquad (3\text{-}12)$$

Thus the understanding of the behavior of $\phi_1(z/L)$ and $\phi_2(z/L)$ become essential to the theoretical development of expressions for non-neutral profiles.

As was done by Monin and Obukhov, ϕ_1 can be expanded in a Taylor series. Since the nondimensional profile equals unity in neutral conditions, $\phi_1(0)$ equals one and for small z/L

$$\phi_1(z/L) = 1 + \frac{\beta z}{L} \qquad (3\text{-}13)$$

where β is a constant. Integration of (3-11) after substituting (3-13) yields the log + linear velocity profile

$$V = \frac{u^*}{k}\left[\ln\left(\frac{z}{z_0}\right) + \frac{\beta z}{L}\right] \qquad (3\text{-}14)$$

provided $z >> z_0$. The constant β must be determined from observations in near-neutral conditions.

The evaluation of the term z/L often poses a problem in the experimental situation because L depends upon the vertical heat flux. If only the profiles are available z/L cannot be determined. Panofsky (1963) defined a new scale length L' that depended only upon the gradients as

$$L' = \frac{u^* \ (\partial V/\partial z)\ T}{kg \ (\partial \theta/\partial z)} \qquad (3\text{-}15)$$

where L' and L are related by

$$L' = L \ K_H / K_M \qquad (3\text{-}16)$$

The L' expression is derived simply by substituting in (3-2) for u^{*2} and H from (3-4) and (3-5).

The relative size of K_H and K_M has long been a topic for debate but almost all agree that the ratio K_H/K_M is close to unity for neutral air, increases in unstable air and decreases in stable air. Again following Panofsky (1963) it can be postulated that K_H/K_M depends only on z/L implying that $S = \phi_3(Z/L')$. Then for small z/L'

$$V = \frac{u^*}{k}\left[\ln\left(\frac{z}{z_0}\right) + \frac{\beta' z}{L'}\right] \qquad (3\text{-}17)$$

where $\beta' = \beta\,(K_H/K_M)$. Estimates of the empirical constant β' in near-neutral conditions have varied from 0.6, by Monin and Obukhov in their original investigation, to 6, with most investigators proposing values between 4 and 6 for the range where the nonlinear terms of the Taylor expansion can be dropped.

Now from (3-4)

$$K_M = \frac{u^{*2}}{(\partial V/\partial z)} = \frac{k\ u^* z}{\phi_1\ (z/L)} \qquad (3\text{-}18)$$

and from (3-5)

$$K_H = \frac{-H}{c_p \rho (\partial \theta/\partial z)} = \frac{k u^* z}{\phi_2\ (z/L)} \qquad (3\text{-}19)$$

whence

$$\phi_2 (z/L) = \phi_1 (z/L)\ K_M / K_H \qquad (3\text{-}20)$$

If the ratio K_H/K_M is near unity in near-neutral air, then the temperature profile for forced convection and slightly stable conditions is given by

$$\theta - \theta_0 = T^* \left[\ln \frac{z}{z_0} + \frac{\beta' z}{L'} \right]$$

where θ_0 is the potential temperature at $z = z_0$.

The term z/L is not the only term used as a measure of stability in the surface boundary layer. A logical stability parameter is the ratio of the rates of buoyant energy production and mechanical energy production. This ratio is commonly called the flux Richardson number R_f and like z/L, is dependent upon the fluxes so that it is advantageous to evaluate it in terms of the gradients.

$$R_f = \frac{-gH / c_p \rho \theta}{u^{*2} (\partial V / \partial z)} \tag{3-22}$$

$$= \frac{g}{\theta} \frac{K_H \; (\partial \theta / \partial z)}{K_M \; (\partial V / \partial z)^2}$$

$$R_f = \frac{K_H}{K_M} \cdot Ri \tag{3-23}$$

The term Ri has been defined as the gradient Richardson number but because it is used so commonly it is usually referred to as simply the Richardson number. It is related to the other stability parameter z/L as well:

$$Ri = \frac{g \; (\partial \theta / \partial z)}{\theta \; (\partial V / \partial z)^2} \tag{3-24}$$

$$= \frac{g}{\theta} \; \frac{-H}{c_p \rho \; K_H} \bigg/ \frac{u^{*2}}{K_M} \left(\frac{\partial V}{\partial z} \right) \cdot \frac{z}{z}$$

$$= \frac{K_M}{K_H} \left(\frac{-z}{u^{*3} \; c_p \rho \theta / k g H} \right) \bigg/ \frac{kz}{u^*} \left(\frac{\partial V}{\partial z} \right)$$

$$Ri = \frac{K_M}{K_H} \cdot \frac{z/L}{\phi_1 (z/L)} \tag{3-25}$$

The Richardson number has the great advantage that it can be estimated from measurements of winds and temperature at two levels. Because of this ease of calculation, it has become the standard stability parameter.

3.2.3 Profiles in Free Convection

Next to be considered is the extremely unstable case, the limit of which is called free convection. According to Lumley and Panofsky (1964) "free convection is the state of the boundary layer in which the vertical transfer of heat and momentum by mechanical turbulence can be neglected compared to that by heat convection." As Lumley and Panofsky have pointed out, this does not mean that the quantity of mechanical energy produced is negligible compared to the quantity of convective energy. It has been determined empirically that free-convection conditions exist when the absolute value of the Richardson number is unity. According to (3-25) and (3-22), this means that mechanical energy production and heat energy production are of the same order of magnitude. In fact Pandolfo (1966) and Priestley before him have claimed that free convection exists for Ri= -0.03. Apparently then mechanical turbulence is a very inefficient transporting agent compared to heat convection. Following Lumley and Panofsky (1964) again, the explanation of this lies in the fact that mechanical eddies have small wavelength and are more nearly isotropic while convectional eddies are larger and less isotropic, providing a much larger correlation between horizontal and vertical wind. Thus the small, isotropic mechanical eddies transfer relatively little momentum and heat compared with the large convectional eddies which have a directional preference in the vertical.

The absolute value of all the stability parameters is directly dependent upon the height z so that in every unstable constant-flux layer there is a height great enough to permit free-convection conditions to exist, and a height small enough to allow forced convection assumptions to hold. The temperature gradient determines the absolute heights at which the two extremes of turbulent transport in the unstable surface boundary layer can be considered valid.

Because mechanical transport can be neglected in free convection, u* is no longer important in the theoretical development. The dimensionally-important quantities for free convection become z, ρ, H, and g/θ_0 with dimensions of length (L), mass (M), time (T), and temperature (θ). This means that, by the Buckingham -π theorem, nondimensional arrangements of the variables are equal except for a multiplicative constant. Thus the units of the relevant variables in the free-convection potential temperature profile ($\partial\theta/\partial z$) are

$$[z] = L$$
$$[\rho] = M L^{-3}$$
$$[g/\theta_0] = L T^{-2} \theta^{-1}$$
$$[H/c_p \rho] = L T^{-1} \theta$$

and the units of the potential temperature profile equation can be determined from

$$\frac{\partial \theta}{\partial z} = z^{\alpha} \rho^{\beta} \left(\frac{g}{\theta}\right)^{\gamma} \left(\frac{H}{c_p \rho}\right)^{\delta}$$

$$[\theta L^{-1}] = [L]^{\alpha} [M L^{-3}]^{\beta} [L T^{-2} \theta^{-1}]^{\gamma} [L T^{-1} \theta]^{\delta}$$

Solving for the powers to keep the equation dimensionally consistent yields $\alpha = -4/3$, $\beta = 0$, $\gamma = -1/3$, $\delta = 2/3$ and the temperature equation becomes

$$\frac{\partial \theta}{\partial z} = C \left(\frac{g}{\theta_0}\right)^{-\frac{1}{3}} \left(\frac{H}{c_p \rho}\right)^{\frac{2}{3}} z^{-\frac{4}{3}} \qquad (3\text{-}26)$$

where C is a constant. Integration yields

$$\theta = B + 3C \left(\frac{g}{\theta_0}\right)^{-\frac{1}{3}} \left(\frac{H}{c_p \rho}\right)^{\frac{2}{3}} z^{-\frac{1}{3}} \qquad (3\text{-}27)$$

Here B is an integration constant. The value of C can be found if heat-flux measurements are available. From measurements by Priestley (1959) its value is 1.07 while Dyer (1965) has determined a value of C = 0.83.

The eddy conductivity, defined by $-H/c_p \rho \, (\partial \theta / \partial z)$ can be expressed using (3-26) as

$$K_H = C^{-1} \left(\frac{g H}{c_p \rho \, \theta_0}\right)^{\frac{1}{3}} z^{\frac{4}{3}} \qquad (3\text{-}28)$$

Using (3-28) and the eddy viscosity defined as

$u^{*2} / (\partial V / \partial z)$ gives

$$\frac{\partial V}{\partial z} = \frac{K_H}{K_M} u^{*2} \left(\frac{g H}{c_p \rho \theta_0} \right)^{-\frac{1}{3}} z^{-\frac{4}{3}} \qquad (3\text{-}29)$$

There are two problems associated with this result. In the original development of free-convection relationships, u* was assumed to be unimportant in determining the profiles but it appears explicitly in this wind profile. This seriously reduces the credibility of (3-29). In addition the variation of the ratio K_H/K_M with height in free convection is unknown. If this ratio is independent of height then the wind profile follows a $z^{-\frac{1}{3}}$ power law and becomes after integrating (3-29)

$$V(z_2) - V(z_1) = \frac{K_H}{K_M} u^{*2} \left(\frac{g H}{c_p \rho \theta_0} \right)^{-\frac{1}{3}} \left[z_1^{-\frac{1}{3}} - z_2^{-\frac{1}{3}} \right] \qquad (3\text{-}30)$$

According to Panofsky, Blackadar and McVehil (1960) for example, this fits wind observations on convective days with moderate wind speeds quite well.

Pandolfo (1966) has derived an alternative expression for the free-convection wind profile which still depends on u* explicitly but no longer makes the dubious assumption of a constant K_H/K_M ratio. Pandolfo based his derivation on a rearranged form of the free-convection temperature-gradient equation (3-26):

$$\frac{\partial \theta}{\partial z} = -C\left(\frac{H}{c_p\rho}\right)^{\frac{2}{3}}\left(\frac{g}{\theta_0}\right)^{-\frac{1}{3}} z^{-\frac{4}{3}}$$

$$= \frac{-1}{u^*kz}\,\frac{H}{c_p\rho}\cdot k^{\frac{4}{3}}C\left|\frac{-u^{*3}}{k(g/\theta_0)(H/c_p\rho\theta)}\right| z^{-\frac{1}{3}}$$

$$= \frac{\theta^*}{kz}\,\frac{C_1}{3}\left|\frac{z}{L}\right|^{-\frac{1}{3}}$$

where $\theta^* = -H/(u^* c_p\rho)$ and $C_1 = 3k^{\frac{4}{3}} C$. Pandolfo then postulated that the free-convection wind profile took the similar form

$$\frac{\partial V}{\partial z} = \frac{u^*}{kz}\,\frac{C_1}{3}\left|\frac{z}{L}\right|^{-\frac{1}{3}}\frac{K_H}{K_M} \tag{3-31}$$

He then presented strong empirical evidence for $z/L = Ri$ which, using (3-25), leads to

$$\frac{K_H}{K_M} = \frac{1}{\phi_1(z/L)} \tag{3-32}$$

Substituting (3-32) and (3-11) into (3-31) yields

$$\frac{K_H}{K_M} = \left(\frac{3}{C_1}\right)^{\frac{1}{2}}\left|\frac{z}{L}\right|^{\frac{1}{6}} \tag{3-33}$$

Then integrating (3-31) after substituting (3-33) allowed

Pandolfo to express the free-convection wind profile as a $z^{-1/6}$ power law

$$V(z_2)-V(z_1) = \frac{u^*}{k}\, 6 \left(\frac{C_1}{3}\right)^{1/2} \left[\left|\frac{z_1}{L}\right|^{-1/6} - \left|\frac{z_2}{L}\right|^{-1/6} \right] \qquad (3\text{-}34)$$

Pandolfo (1966) then presented evidence that wind profiles in free-convection conditions fit (3-34) well. Later in this discussion (3-31) and (3-34) will be tested against free-convection wind profiles obtained at Lake Wabamun.

3.2.4 General Profiles in Unstable Air

Next to be considered are the profiles for unstable conditions in between the two extremes of free and forced convection. Priestley (1955) has suggested that the transition from forced to free convection is quite sharp taking place at a Richardson number of -0.03. Other measurements, including some by Priestley (1959), indicate a gradual transition. Apart from this debate, there is obviously some advantage in being able to describe the structure of wind and temperature through the entire unstable range by means of one relationship. Such an equation was first found by interpolation between free and forced convection by Ellison (1957). The same equation was independently obtained by Kazanski, Yamamoto, Panofsky and Sellers and the relationship has become known as the Keyps equation after the first letter of the names of the originators. This relation between the nondimensional wind shear S and z/L is

$$S^4 - \gamma (z/L) S^3 = 1 \qquad (3\text{-}35)$$

Lumley and Panofsky (1964) showed that the relation is quite good with the constant $\gamma = 14$.

An analogous equation using L' instead of L, and hence using temperature profiles instead of heat flux, is obtained by substituting (3-16) in (3-35).

$$S^4 - \gamma' (z/L') S^3 = 1 \qquad (3\text{-}36)$$

Here γ' is defined as $\gamma K_H/K_M$. Lumley and Panofsky (1964) claimed that γ' is also constant at about 18 which implies that K_H/K_M must also be constant at 1.3. This result is highly controversial and disagrees with the observation of Pandolfo (1966) that $K_H/K_M = 1/\phi_1(Z/L)$.

Following Panofsky (1963), the condition

$$S = \phi_3(z/L') = \frac{kz}{u^*}\left(\frac{\partial V}{\partial z}\right)$$

can be integrated to give

$$V = \frac{u^*}{k}\left[\ln\frac{z}{z_0} - \int_{-\frac{z_0}{L'}}^{-\frac{z}{L'}} \frac{1-\phi_3(\xi)}{\xi}\, d\xi\right] \qquad (3\text{-}37)$$

The roughness Z_o is always small compared with L' and because the integral is well behaved at the origin (3-37) can be written

$$V = \frac{u^*}{k}\left[\ln\frac{z}{z_o} - \psi_1(z/L')\right] \tag{3-38}$$

where ψ_1(z/L') is another universal function which is related to ϕ_3(z/L') by

$$\psi_1(z/L') = \int_0^{-z/L'} \frac{1-\phi_3(\xi)}{\xi}\,d\xi \tag{3-39}$$

In a similar fashion the temperature profile can be expressed as

$$\theta - \theta_o = T^*\left[\ln\frac{z}{z_o} - \psi_2(z/L')\right] \tag{3-40}$$

$$\psi_2(z/L') = \int_0^{-z/L'} \frac{1-\phi_4(\xi)}{\xi}\,d\xi$$

Paulson (1970) has integrated (3-39) to get

$$\begin{aligned}\psi_1(z/L') = 1 - \phi_3 - 3\ln\phi_3 + 2\ln[(1+\phi_3)/2] \\ + 2\tan^{-1}\phi_3 - \frac{\pi}{2} + \ln[(1+\phi_3^2)/2]\end{aligned} \tag{3-41}$$

Thus, having calculated (z/L') from profile measurements, ϕ_3(z/L') can be determined by numerically solving (3-36) and ψ_1(z/L') can be obtained from (3-41). The velocity profile (3-38) is then specified for unstable conditions. The temperature profile can be obtained from (3-40) using (3-20) and assuming that K_H/K_M is constant.

Another profile representation for unstable conditions was independently suggested by Businger (1966) and Dyer (unpublished). This scheme uses the interpolation formula (3-35) and the same hypothesis suggested by Pandolfo (1966) that $(Z/L) = Ri$. As was previously shown this leads to $K_H/K_M = 1/\phi_1(z/L)$.

Now by definition of the terms involved

$$z/L' = S\,Ri \qquad (3\text{-}42)$$

Substituting this into (3-36) yields

$$S^4 - \gamma'\,Ri\,S^4 = 1$$

$$S = (1 - \gamma'\,Ri)^{-1/4}$$

$$\phi_1 = [1 - \gamma'(z/L)]^{-1/4} \qquad (3\text{-}43)$$

From (3-20) and (3-32)

$$\phi_1 = (K_H/K_M)\,\phi_2 = \phi_2/\phi_1$$

$$\phi_2 = \phi_1^2 = [1 - \gamma'(z/L)]^{-1/2} \qquad (3\text{-}44)$$

Paulson (1970) integrated (3-40) to get ψ_1 and ψ_2 for the

Businger-Dyer model and obtained

$$\psi_1 = 2 \ln [(1+x)/2] + \ln[(1+x^2)/2] - 2 \tan^{-1} x + \pi/2 \qquad (3\text{-}45)$$

$$\psi_2 = 2 \ln [(1+x^2)/2]$$

where

$$x = [1 - \gamma'(z/L)]^{1/4}$$

In free convection, as -z/L becomes large, the Keyps representation predicts that both wind and temperature vary asymptotically as $z^{-1/3}$ while the Businger-Dyer representation implies $V \propto Z^{-1/4}$ and $\theta \propto z^{-1/2}$.

In the paper by Paulson (1970) it was found that the Businger-Dyer representation gave the best fit to temperature profiles at Kerang,Australia and described the wind profiles for the same place equally as well as the Keyps model. There are more profile representations suggested in the literature but the two discussed here have received the most widespread acceptance.

3.2.5 Actual Method of Profile Analysis

It was originally intended that this thesis would compare the Businger-Dyer and Keyps profiles but a lack of data eliminated this possibility. The temperature profiles for August were completely lost because of equipment malfunction. In October, the cold air over warm water created extremely unstable conditions, well into the free-convection regime. It was then possible to compare the observed profiles with the unstable limits of the two theoretical profiles but not with the interpolation models themselves. To this end a least squares fit was performed on temperature and wind versus the appropriate power of the height Z.

In addition, flux estimates from the October free-convection profiles were desired for comparison with the flux estimates from the fast-response measurements. The heat flux was obtained using Priestly's free-convection temperature profile (3-27). A least squares fit was applied to temperature against $z^{-1/3}$ which produced an equation of the form

$$\theta = B + D z^{-1/3} \tag{3-46}$$

where both B and D are known. But comparing with (3-27) it can be seen that

$$\begin{aligned} D &= 3C \left(\frac{H}{c_p \rho}\right)^{2/3} \left(\frac{g}{\theta_0}\right)^{-1/3} \\ H &= c_p \rho \left(\frac{D}{3C}\right)^{3/2} \left(\frac{g}{\theta_0}\right)^{1/2} \end{aligned} \tag{3-47}$$

Then if one of the values of C from the literature is chosen everything else in (3-47) is known and a profile estimate of the heat flux is available.

Knowing H permits K_H to be calculated using (3-28). Then, assuming that $K_H = K_W$, the eddy diffusivity coefficient for water vapour, the flux of water vapour and hence of latent heat can be calculated from

$$E = L K_W \frac{\partial e}{\partial z} \qquad (3\text{-}48)$$

where E is the evaporative heat flux, e the absolute humidity and L the specific latent heat of evaporation.

The shear stress τ or friction velocity u* can be determined using either of the free-convection wind profiles of Priestley (3-30) or of Pandolfo (3-34). Considering (3-30), a least-squares fit of V and $z^{-1/3}$ produces a constant F which must be defined by

$$F = \frac{K_H}{K_M} u^{*2} \left(\frac{gH}{c_p \rho \theta_0} \right)^{-1/3}$$

$$u^{*2} = F \frac{K_M}{K_H} \left(\frac{gH}{c_p \rho \theta_0} \right)^{1/3} \qquad (3\text{-}49)$$

The term $(gH/c_p \rho \theta_0)$ can be taken from the temperature-profile equation which leaves K_H/K_M as the only unknown. This ratio was already assumed constant in deriving (3-30). The value 1.3 from Lumley and Panofsky (1964) was chosen to complete the equation.

A similar procedure fitting V to $z^{-1/6}$ according to (3-34) yields another constant G such that

$$G = \frac{u^*}{k} \; 6 \left(\frac{C_1}{3}\right)^{1/2}$$

$$u^* = \frac{Gk}{6} \left(\frac{C_1}{3}\right)^{-1/2} \qquad (3\text{-}50)$$

where $C_1 = 3k^{1/4} C$ and C is the same constant as the C in (3-47) for which there are values already calculated. This method does not require the dubious assumption of a constant K_H/K_M.

All derivatives were approximated by

$$\left(\frac{\partial F}{\partial z}\right)_{(z_1 z_2)^{1/2}} \approx \frac{F_2 - F_1}{(z_1 z_2)^{1/2}} \; \ln\left(\frac{z_2}{z_1}\right)$$

following a suggestion by Panofsky (1965), where F is a profile variable. The approximation applies at the geometric mean height of the observation levels and is rigorous for logarithmic profiles (i.e. neutral conditions). For $F \propto z^{-1/3}$ the error was estimated by Paulson (1970) to be ~6% for observation heights of 0.5 and 16 m and should be less for the heights used in the present study.

3.3 Vertical Fluxes by Eddy Correlation

3.3.1 Introduction

It is a standard procedure when examining the characteristics of turbulence and turbulent transport to assume that all quantities subject to variation because of turbulence can be written as the sum of a time mean and a fluctuating part (see e.g. Lumley and Panofsky 1964), where the mean of the fluctuating part is zero. In the present study an overbar will indicate mean or average values and the prime will indicate the perturbation from the mean which has zero average. Thus the instantaneous value of some physical parameter X in a turbulent flow can be expressed as

$$X = \overline{X} + X' \tag{3-51}$$

3.3.2 Turbulent Fluxes

The equations governing flow in the surface boundary layer are given by (see e.g. Lumley and Panofsky 1964):

$$\left.\begin{aligned} \frac{\partial u_i}{\partial t} + U_j \frac{\partial U_i}{\partial x_j} &= -\frac{1}{\rho_0} \frac{\partial P}{\partial x_i} + \frac{g}{T_0} T \delta_{3i} + \nu \frac{\partial^2 U_i}{\partial x_k^2} \\ \frac{\partial U_i}{\partial x_i} &= 0 \\ \frac{\partial T}{\partial t} + U_i \frac{\partial T}{\partial x_i} &= \kappa \frac{\partial^2 T}{\partial x_i^2} \end{aligned}\right\} \tag{3-52}$$

These are the equations of motion for a viscous, Newtonian medium in a uniform gravitational field, neglecting rotation. Subscripts imply summation over the three coordinate directions and x_3 is the vertical axis. The fluid speed is denoted by U_i, g is the acceleration due to gravity, ν is the kinematic viscosity and κ is the thermal diffusivity. The temperature T is a deviation from the undisturbed adiabatic value denoted by T_0. In the same way P refers to a small deviation from the undisturbed atmospheric pressure P_0 and ρ refers to a deviation from the undisturbed atmospheric density ρ_0. The Kronecker delta, δ_{ij}, is unity if the indices are equal but otherwise is zero. Motions at very low Mach numbers in an atmosphere consisting of a perfect gas of constant composition have been assumed, and variations in the viscosity and thermal diffusivity were neglected.

Writing the velocity, temperature and pressure in the form of (3-51)

$$
\begin{aligned}
U_i &= \bar{U}_i + u_i' \\
T &= \bar{T} + T' \\
P &= \bar{P} + P'
\end{aligned}
\qquad (3\text{-}53)
$$

and substituting into (3-52) yields:

$$\frac{\partial \bar{U}_i}{\partial t} + \frac{\partial u_i'}{\partial t} + \bar{U}_j \frac{\partial \bar{U}_i}{\partial x_j} + u_j' \frac{\partial \bar{U}_i}{\partial x_j} + \bar{U}_j \frac{\partial u_i'}{\partial x_j} + u_j' \frac{\partial u_i'}{\partial x_j}$$

$$= -\frac{1}{\rho_0} \frac{\partial \bar{P}}{\partial x_i} - \frac{1}{\rho_0} \frac{\partial P'}{\partial x_i} + \nu \frac{\partial^2 \bar{U}_i}{\partial x_j^2} + \nu \frac{\partial^2 u_i'}{\partial x_j^2} + \frac{g}{T_0} \bar{T} \delta_{i3} + \frac{g}{T_0} T' \delta_{i3}$$

$$\frac{\partial \bar{U}_i}{\partial x_i} + \frac{\partial u_i'}{\partial x_i} = 0 \qquad (3\text{-}54)$$

$$\frac{\partial \bar{T}}{\partial t} + \frac{\partial T'}{\partial t} + \bar{U}_i \frac{\partial \bar{T}}{\partial x_i} + u_i' \frac{\partial \bar{T}}{\partial x_i} + \bar{U}_i \frac{\partial T'}{\partial x_i} + u_i' \frac{\partial T'}{\partial x_i} = \kappa \frac{\partial^2 \bar{T}}{\partial x_j^2} + \kappa \frac{\partial^2 T'}{\partial x_j^2}$$

Taking averages produces the equations for the mean motion of the turbulent fluid:

$$\frac{\partial \bar{U}_i}{\partial t} + \bar{U}_j \frac{\partial \bar{U}_i}{\partial x_j} + \overline{u_j' \frac{\partial u_i'}{\partial x_j}} = -\frac{1}{\rho_0} \frac{\partial \bar{P}_i}{\partial x_i} + \nu \frac{\partial^2 \bar{U}_i}{\partial x_j^2} + \frac{g}{T_0} \bar{\bar{T}} \delta_{i3}$$

$$\frac{\partial \bar{U}_i}{\partial x_i} = 0 \qquad (3\text{-}55)$$

$$\frac{\partial \bar{\bar{T}}}{\partial t} + \bar{U}_i \frac{\partial \bar{\bar{T}}}{\partial x_i} + \overline{u_i' \frac{\partial T'}{\partial x_i}} = \kappa \frac{\partial^2 \bar{\bar{T}}}{\partial x_j^2}$$

Subtracting the middle members of (3-54) and (3-55) gives $\partial u_i'/\partial x_i = 0$ and the term $\overline{u_j' \, \partial u_i' / \partial x_j}$ can be transformed to $\partial/\partial x_j \left(\overline{u_i' u_j'} \right)$. Multiplying this by the density ρ_0 produces the divergence of a momentum flux which represents a force due to the turbulent transport of momentum. This term is frequently written on the right-hand side of the first of (3-55) and added to the stress giving

$$\frac{\partial \bar{U}_i}{\partial t} + \bar{U}_j \frac{\partial U_i}{\partial x_j} = \frac{1}{\rho_0} \frac{\partial \tau_{ij}}{\partial x_i} + \frac{g}{T_0} \overline{T} \delta_{i3} \qquad (3\text{-}56)$$

where

$$\tau_{ij} = -\bar{P} \delta_{ij} + \rho_0 \nu \left[\frac{\partial \bar{U}_i}{\partial x_j} + \frac{\partial \bar{U}_j}{\partial x_i} \right] - \rho_0 \overline{u_i u_j} \qquad (3\text{-}57)$$

The analogous term in the temperature equation $\overline{u_i' \, \partial T' / \partial x_i}$ when multiplied by $c_p \rho_0$ can be transformed in the same way to give the divergence of a heat flux, representing the heat transferred by turbulent temperature fluctuations. Similarly this term can be taken to the right-hand side of the third member of (3-55) and a heat flux vector defined as

$$H_j = -\rho_0 c_p \mathcal{K} \frac{\partial \bar{T}}{\partial x_j} + c_p \rho_0 \overline{T u_j'} \qquad (3\text{-}58)$$

Neglecting molecular viscosity and diffusivity and assuming no external pressure gradient (3-57) and (3-58) become

$$\tau_{ij} = -\rho_0 \overline{u_i' u_j'}$$

$$H_j = c_p \rho_0 \overline{u_j' T'}$$

Finally the assumption of horizontal homogeneity reduces the expressions for the shear stress and heat flux to

$$\tau = -\rho_0 \overline{u'w'} \qquad (3\text{-}60)$$

$$H = \rho_0 c_p \overline{w'T'} \qquad (3\text{-}61)$$

Here u' is the perturbation of the horizontal wind and w' is the perturbation of the vertical velocity.

The vertical turbulent flux of a quantity then is determined by the covariance of the perturbations in the quantity and perturbations in the vertical wind. If, for example, upward fluctuations in the vertical wind correspond to an increase in X or a positive X' and downward fluctuations occur with a decrease in X then a net upward flux of X results. The easiest way to visualize the significance of the covariance is to consider that upward vertical motion is bringing air with a certain X value up from somewhere below and downward vertical motion brings air with another value of X down from above. If there is a gradient of X with height then higher values of X will be carried to levels having a lower value of X and a flux of X "down" the gradient of X results. Then, corresponding to (3-60) and (3-61), if the vertical wind is denoted by $w = \bar{w} + w'$, the turbulent flux of X is given by

$$F_x = w'X' \qquad (3\text{-}62)$$

The perturbations (e.g. w' and X') were not measured directly for the evaluation of equations of the form of (3-62). However, the covariance of the perturbations, and hence the flux, can be related to the quantities that were measured, namely the total quantity (w and X) and the mean quantity ($\bar{w}$ and $\bar{X}$). Using (3-51) the covariance of the perturbations can be related to the measured quantities by

$$\begin{aligned}\overline{w'X'} &= \overline{(w - \bar{w})(X - \bar{X})} \\ &= \overline{wX - \bar{w}X - w\bar{X} + \bar{w}\bar{X}} \\ &= \overline{wX} - \bar{w}\bar{X} - \bar{w}\bar{X} + \bar{w}\bar{X} \\ &= \overline{wX} - \bar{w}\bar{X} \qquad (3\text{-}63)\end{aligned}$$

In stationary, homogeneous flow $\bar{w} = 0$ and the second term on the right is zero. The turbulent fluxes of heat ($H = c_p \rho \overline{w'T'}$), water vapour ($E = \overline{w'e'}$), and momentum ($-u_*^2 = \overline{u'w'}$) can be calculated if values of vertical wind w, temperature T, water vapour content e, and horizontal wind velocity u are measured with sufficiently fast-response instrumentation to make the covariances with w accurate.

3.3.3 Fluxes Associated with a Mean Vertical Wind

If the mean vertical velocity is not zero then the conditions of stationarity and horizontal homogeneity no longer hold and the turbulent flux at a certain height cannot be considered representative of the flux from the surface. The fluxes due to the mean vertical wind can be estimated, however, and a better estimate of the surface flux can be obtained by adding the turbulent and mean wind fluxes.

The contribution to the vertical fluxes by the mean vertical wind arises from the second terms of the first and third equations of (3-55). The term $\bar{U}_j \, \partial \bar{U}_i / \partial x_j$ can be taken to the right hand side of (3-56) and incorporated into the shear stress τ using the equation of continuity in (3-55). Assuming horizontal homogeneity and neglecting molecular viscosity and horizontal pressure gradients, the expression for the shear stress, including the contribution from the mean vertical wind, becomes

$$\tau = -\rho_0 \overline{u'w'} - \rho_0 \bar{w} \bar{u} \tag{3-64}$$

Similarly, the expression for the heat flux, including the contribution of a mean vertical wind, is given by

$$H = c_p \rho_0 \overline{w'T'} + c_p \rho_0 \bar{w} \bar{T} \tag{3-65}$$

where again $\bar{T}$ is the deviation from adiabatic conditions caused by the heat added at the surface.

CHAPTER IV

RESULTS

4.1 Introduction

Before any measurements could be properly interpreted the reliability of each had to be estimated. This was done using available literature on the instruments and calibrations carried out at the University of Alberta. Tables 4 and 5 give the estimated errors of measurement of the slow-response and fast-response instruments, respectively. Errors caused by terrain slope do not apply here of course because the lake surface is always nearly horizontal but errors in aligning the fast-response instruments with the vertical must be considered to be of possible significance. Such errors were estimated to be less than 15 minutes of arc for the transit procedure used at Lake Wabamun.

If θ is the deviation from the vertical then the error in vertical velocity is approximately u sin θ or 1-2 cm/sec for the horizontal wind speeds of interest to this project. This does not appreciably affect the turbulent fluxes because the mean vertical wind is subtracted from the flux estimate. However, estimates of the mean vertical velocity and associated fluxes are definitely influenced.

TABLE 4

Slow-Response Instrument Error

Sensor	Element	Error
Cup Anemometer	Wind Speed	5%
Thermistors	Air Temperature	± 0.1 °C
Hygrometers	Dew-Point	± 0.2 °C
Thermistor	Water Temperature	± 0.2 °C

TABLE 5

Fast-Response Instrument Error

Sensor	Element	Error
Sonic Anemometer	Vertical Wind Speed	4%[1]
Propeller Anemometer	Vertical Wind Speed	5%[2]
Propeller Anemometer	Horizontal Wind Speed	10%
	V component	as much as 30%[2]
Sonic Thermometer	Air Temperature	5%[1]
Resistance Thermometer	Air Temperature	5%
Lyman - α Humidiometer	Vapour Pressure	5%
Sonic Anemometer Thermometer	Heat Flux	10%[1]
Fluxatron	Heat Flux	10 - 25%[3]
Sonic-Lyman - α	Vapour Flux	10%
Shear-Stress Meter	Momentum Flux	12%[2]

---

[1] Kaimal and Businger (1963).

[2] B. B. Hicks (1972): For wind speeds of interest here.

[3] McBean (1972): Largest error for near-neutral conditions.

The shear-stress meter consisting of three orthogonal propeller anemometers was built so that the axes of the mount were within a few minutes of arc of being mutually orthogonal. Any error from non-orthogonal measurements was considered insignificant compared with the error introduced by the poor response of the propellers at large angles of attack to the wind. This latter error was included in the values given in Table 5.

4.2 August Tests

4.2.1 Local Weather Conditions

As was previously noted the weather conditions for the two days of data collection in August, 1972 were quite similar except for wind direction. The Edmonton International Airport, forty miles east of the lake, recorded maximum temperatures of 80 F and 79 F on August 24 and 25, respectively. Wind speeds for the two days averaged 3 m/sec and 2 m/sec with the greater speed occuring on August 24, the day of southeast winds and measurement of fluxes over the heated-water plume (see Figures 4 and 5). Scattered cumulus clouds were observed on both days.

4.2.2 Stability

Meaningful Richardson numbers could not be calculated for the test days in August because of the unavailability of temperature profiles. However Z/L was calculated for

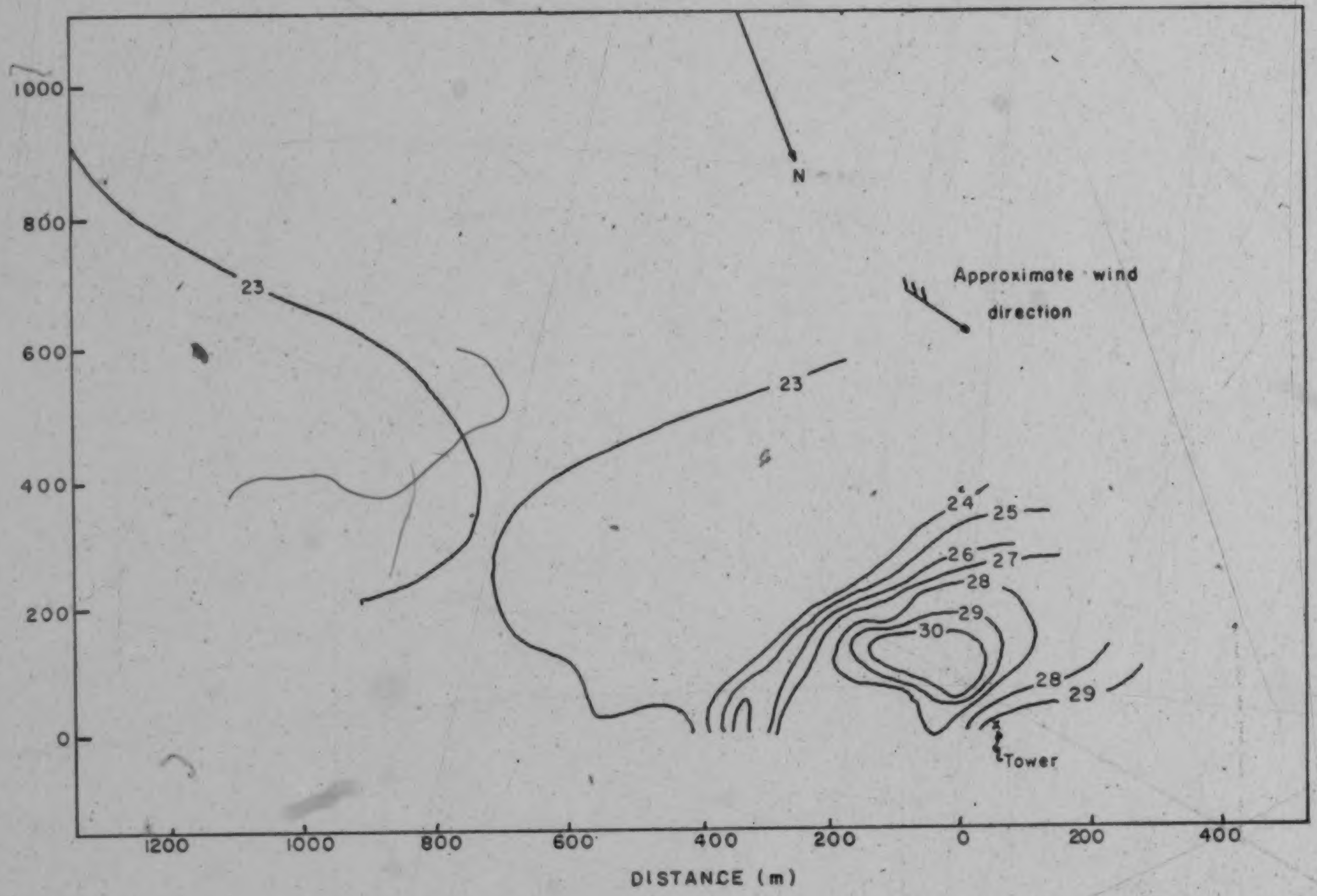
N
Approximate wind direction
23
23
24
25
26
27
28
29
30
28
29
Tower
1000
800
600
400
200
0
1200
1000
800
600
400
200
0
200
400
DISTANCE (m)

FIGURE 4. Lake Wabamun surface temperature, August 24. Isopleths are degrees Celsius.

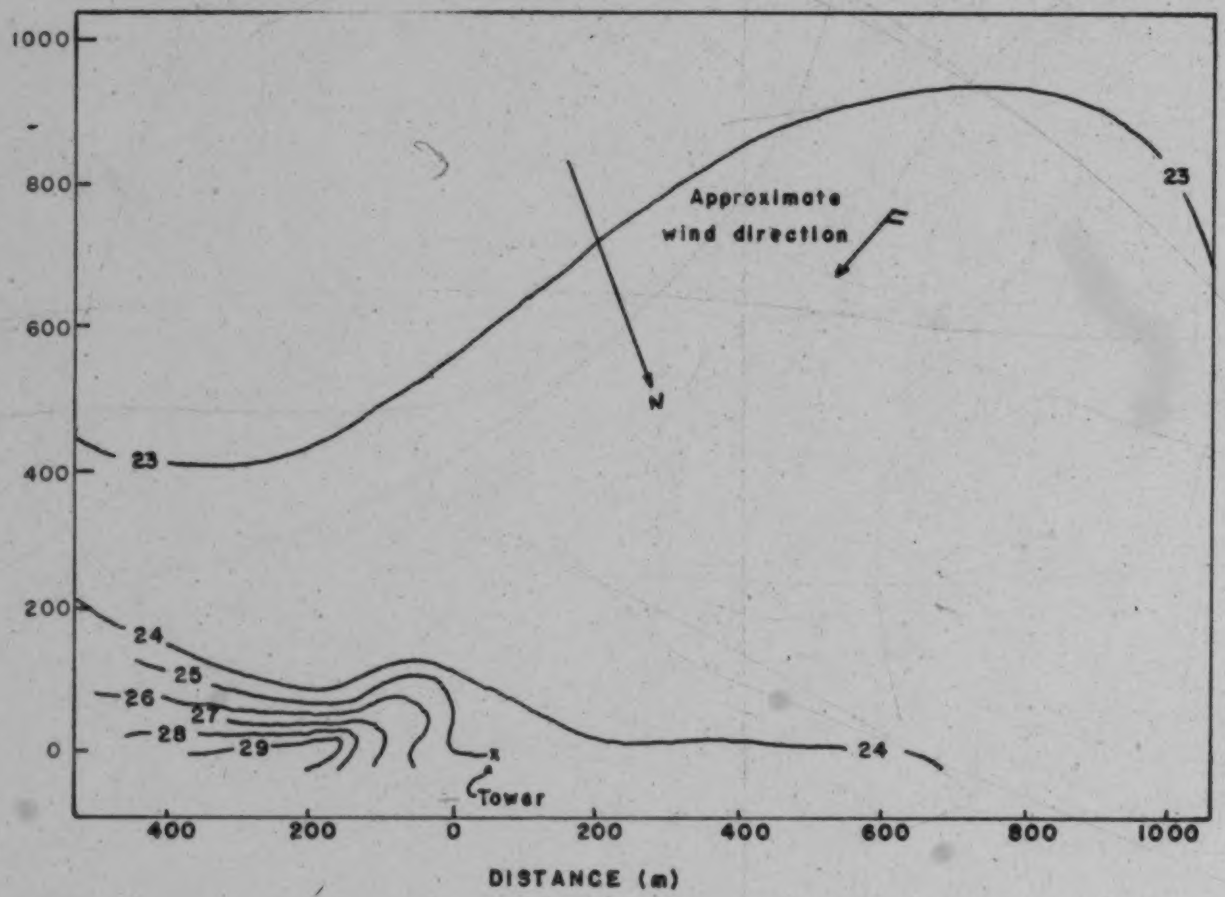

FIGURE 5. Lake Wabamun surface temperature, August 25. Isopleths are degrees Celsius.

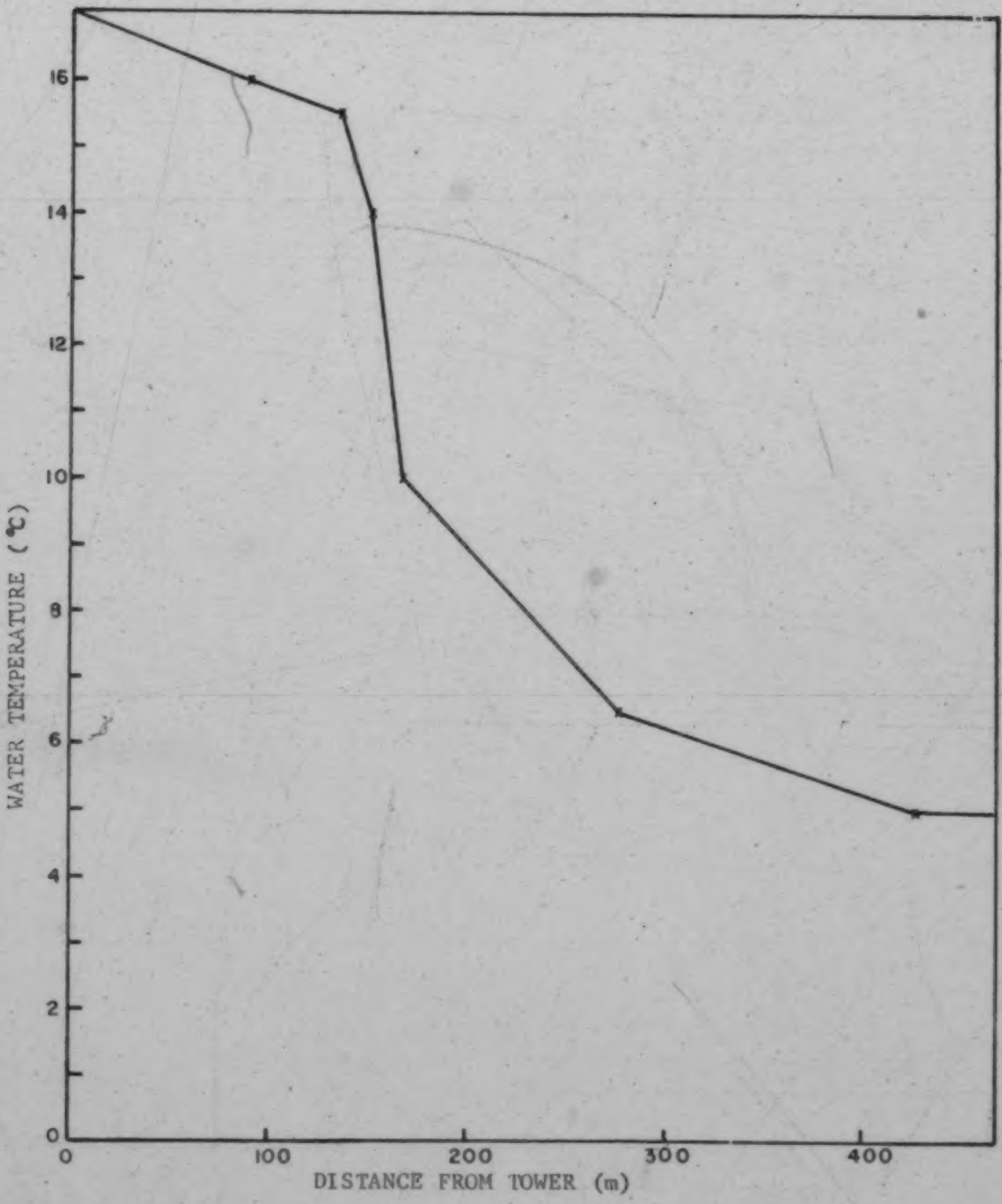

FIGURE 6. Surface temperature upwind from tower site; Lake Wabamun, October 21.

the two days using equation 3-2. These data, presented in Table 6, indicated near-neutral conditions in the flow across the unheated lake and instability on the day with flow across the heated plume. The Z/L values were based upon thirty-minute means of u* from the shear-stress meter and heat fluxes for the same intervals from the sonic anomometer-thermometer, hence the valid height is 3 m.

The values of u* are suspect for August 24 (see Table 7) because the vertical propeller of the shear-stress meter was not recording. The only record of vertical wind was from the sonic anemometer which was separated in space from the shear-stress meter and has a different response time. An average value of u* was used to calculate all of the L values in order to minimize the effect of these errors.

Typical wind profiles, averaged over 30 minutes, are presented in Figure 7.

4.2.3 Fluxes

The fluxes for the two test days in August, calculated from the fast-response instrument data, appear in Table 7. Over the plume (August 24), the heat fluxes were on the average considerably larger than those over the rest of the lake (August 25), while evaporation from the plume, as measured by the Lyman-alpha humidiometer and sonic anemometer, was 3 to 5 times greater. The inconsistent momentum flux on

TABLE 6

August Z/L Values

Date/Time	Wind Speed (cm/sec)	Sonic Z/L	Flux Z/L
24/1515	452	-0.0068	
1530	386	-0.0101	
1545	397	-0.0096	
1600	378	-0.0170	
1615	353	-0.0892	
1630	341	-0.120	
25/1330	193	-0.0020	-0.0011
1345	149	-0.0080	-0.0010
1400	136	-0.0072	-0.0013
1415	144	-0.0022	-0.0026
1430	160	-0.0013	-0.0015
1445	199	-0.0034	-0.0006

TABLE 7

August Fluxes

(30-Min Means)

Date/Time	Sonic Heat Flux (mW/cm^2)	Fluxatron Heat Flux (mW/cm^2)	Latent Heat Flux (mW/cm^2)	Momentum Flux (cm^2/sec^2)
Plume				
24/1515	1.43		4.13	8.5
1530	2.14		5.64	126.
1545	2.03		6.38	90.
1600	3.58		4.94	43.
1615	18.8		12.49	-
1630	25.2		17.6	325.
Average	8.86		8.53	119
Lake				
25/1330	2.11	1.21	1.85	194.
1345	5.75	0.70	1.76	149.
1400	3.24	0.58	1.41	109.
1415	0.46	0.55	1.50	67.
1430	0.54	0.62	1.63	105.
1445	3.28	0.56	1.73	182.
Average	2.56	0.70	1.65	151

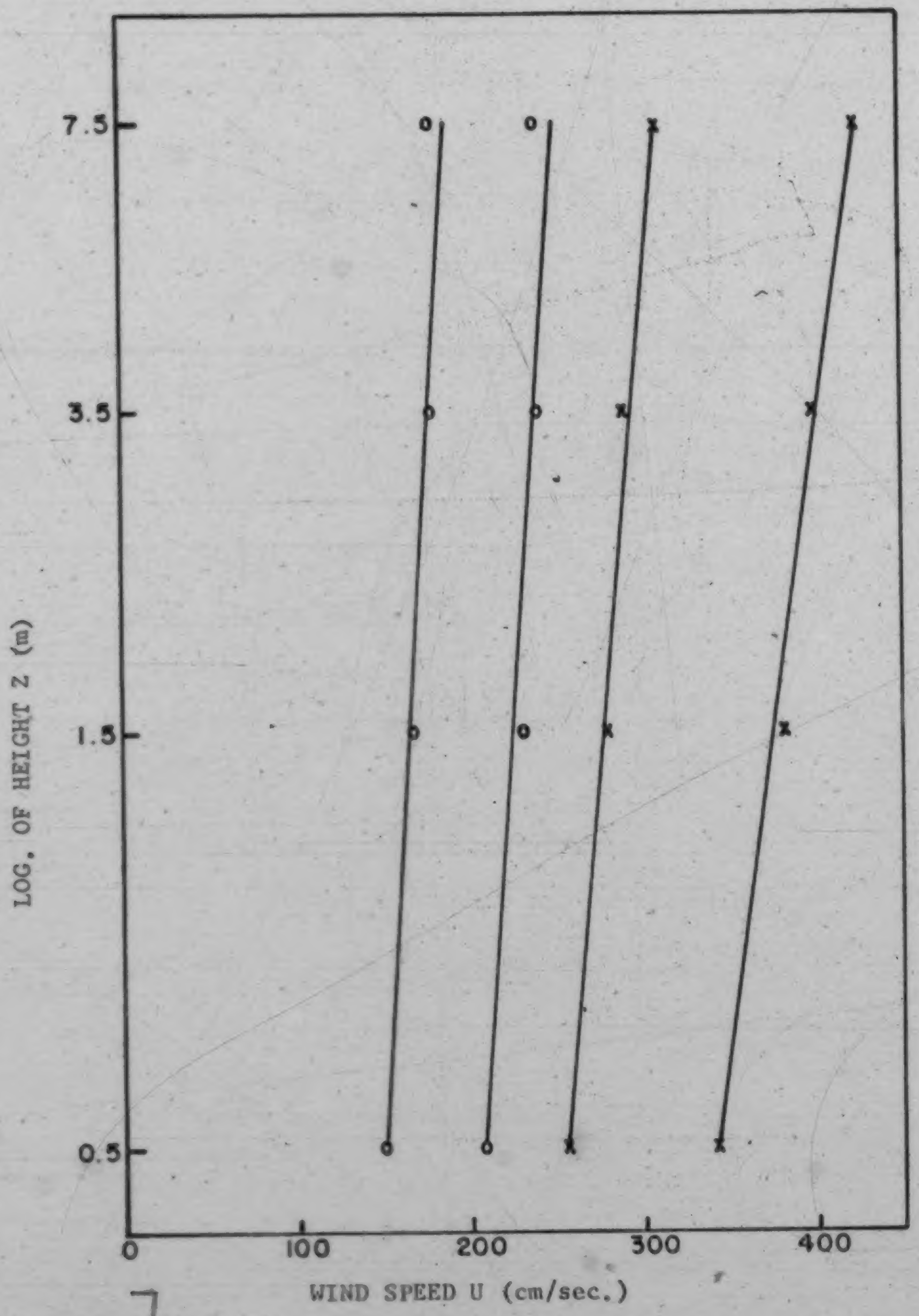

FIGURE 7. August wind profiles. August 24 observations indicated by x and August 25 observations by o.

August 24 was explained in 4.2.2.

The difference in fluxes on the two days is probably not entirely accounted for by the heated-water plume. Part of the decrease in magnitude of the fluxes on the second day can be explained by the lower wind speeds observed on that day. The lower wind speed would indicate less mechanical mixing and smaller fluxes. The difference in surface temperature was undoubtedly the dominant factor, however.

For August 25, with heat flux estimates from both the sonic equipment and the fluxatron available, a marked discrepancy between the two heat flux measurements existed as can be seen in Table 7. In almost every case the sonic estimates were higher than those of the fluxatron. One possible explanation is linked with the fact that the response time of the sonic anemometer is considerably less than that of the propeller of the fluxatron. This would result in an underestimate of the heat flux by the fluxatron. However, this should account for only 25-30% (See McBean, 1972) of the observed difference and a satisfactory explanation of the total discrepancy is unavailable.

4.3 October Tests

4.3.1 Stability

On October 21, 1972 there was a flow of cold air (+1°C) which crossed the heated plume before arriving at the instrumentation site. Unstable conditions were expected in such circumstances and the Richardson number and Z/L' as calculated from the profile measurements indicated extreme instability. Indeed, as Table 8 shows, |Ri| as calculated for 1.3 m was greater than 1.0 throughout the data collection period and the surface boundary layer was therefore well into the free-convection regime as defined in 3.2.3.

4.3.2 October Profiles

Because of the definite free-convection situation, an attempt was made to fit the theoretical free-convection profiles (see 3.2.3) of wind and temperature to the data. The fit was made for half-hourly mean values and the results are shown in Tables 9 and 10 and in Figures 8 and 9. Figure 8 shows observed temperature (crosses), the 1/3 power law (solid line), and the 1/2 power law (dashed line). The 1/3 law, of course, was predicted by the Priestley free-convection theory and is the value to which the Keyps formula is asymptotic. The Businger-Dyer theory is asymptotic to the 1/2 power curve. Both curves fit the data well but as is shown by the sums of squared differences in Table 9 the 1/3 power law was slightly better in every case.

The fit of the theoretical wind profiles to the measured was not as good because of a larger uncertainty

TABLE 8

October Ri and Z/L' (Valid at 1.3 m)

30 Min. Ending	Ri	Z/L'
2000	-4.39	-1.67
2015	-5.07	-1.85
2030	-2.68	-1.15
2045	-1.90	-0.88
2100	-2.08	-0.95
2115	-2.20	-0.99
2130	-2.20	-0.99

TABLE 9

Actual and Theoretical Temperature Profiles

October 21

30 Mins Ending	Ht. (m)	Actual T °K	$z^{-\frac{1}{3}}$ T °K	$z^{-\frac{1}{2}}$ T °K
2000	0.5	275.0	275.09	275.11
	1.5	274.3	274.26	274.21
	3.5	273.8	273.80	273.79
	7.5	273.4	273.49	273.54
	$\sum$(Difference)^2		.0086	.028
2030	0.5	275.2	275.25	275.27
	1.5	274.5	274.48	274.43
	3.5	274.0	274.05	274.03
	7.5	273.7	273.75	273.80
	$\sum$(Difference)^2		.0076	.0189

TABLE 9 (Continued)

30 Mins Ending	Ht. (m)	Actual T °K	$z^{-\frac{1}{3}}$ T °K	$z^{-\frac{1}{2}}$ T °K
2100	0.5	275.3	275.32	275.34
	1.5	274.8	274.66	274.62
	3.5	274.3	274.29	274.28
	7.5	274.0	274.04	274.08
$\sum$ (Difference)^2			.0174	.0345
2130	0.5	275.6	275.67	275.69
	1.5	275.1	274.96	274.91
	3.5	274.5	274.56	274.55
	7.5	274.2	274.28	274.33
$\sum$ (Difference)^2			.0313	.0562

TABLE 10

Actual and Theoretical Wind Profiles

October 21

30' Mins Ending	Ht. (m)	Actual u (cm/sec)	$z^{-\frac{1}{3}} u$ (cm/sec)	$z^{-\frac{1}{4}} u$ (cm/sec)	$z^{-\frac{1}{6}} u$ (cm/sec)
2000	0.5	187	185	185	185
	1.5	188	194	194	193
	3.5	203	199	199	199
	7.5	202	202	203	203
$\sum$ (Difference)^2			56.1	53.4	51.2
2030	0.5	229	228	228	228
	1.5	236	240	240	239
	3.5	249	247	247	247
	7.5	252	252	252	252
$\sum$ (Difference)^2			22.5	19.5	17.4

TABLE 10 (Continued)

30 Mins Ending	Ht. (m)	Actual u (cm/sec)	$z^{-\frac{1}{3}}$ u (cm/sec)	$z^{-\frac{1}{4}}$ u (cm/sec)	$z^{-\frac{1}{6}}$ u (cm/sec)
2100	0.5	229	228	229	229
	1.5	239	241	241	240
	3.5	250	248	248	248
	7.5	253	253	254	254
	$\sum$ (Difference)^2		8.0	7.1	6.9
2130	0.5	290	288	289	289
	1.5	299	303	302	302
	3.5	311	310	310	310
	7.5	317	316	316	317
	$\sum$ (Difference)^2		16.8	12.7	9.4

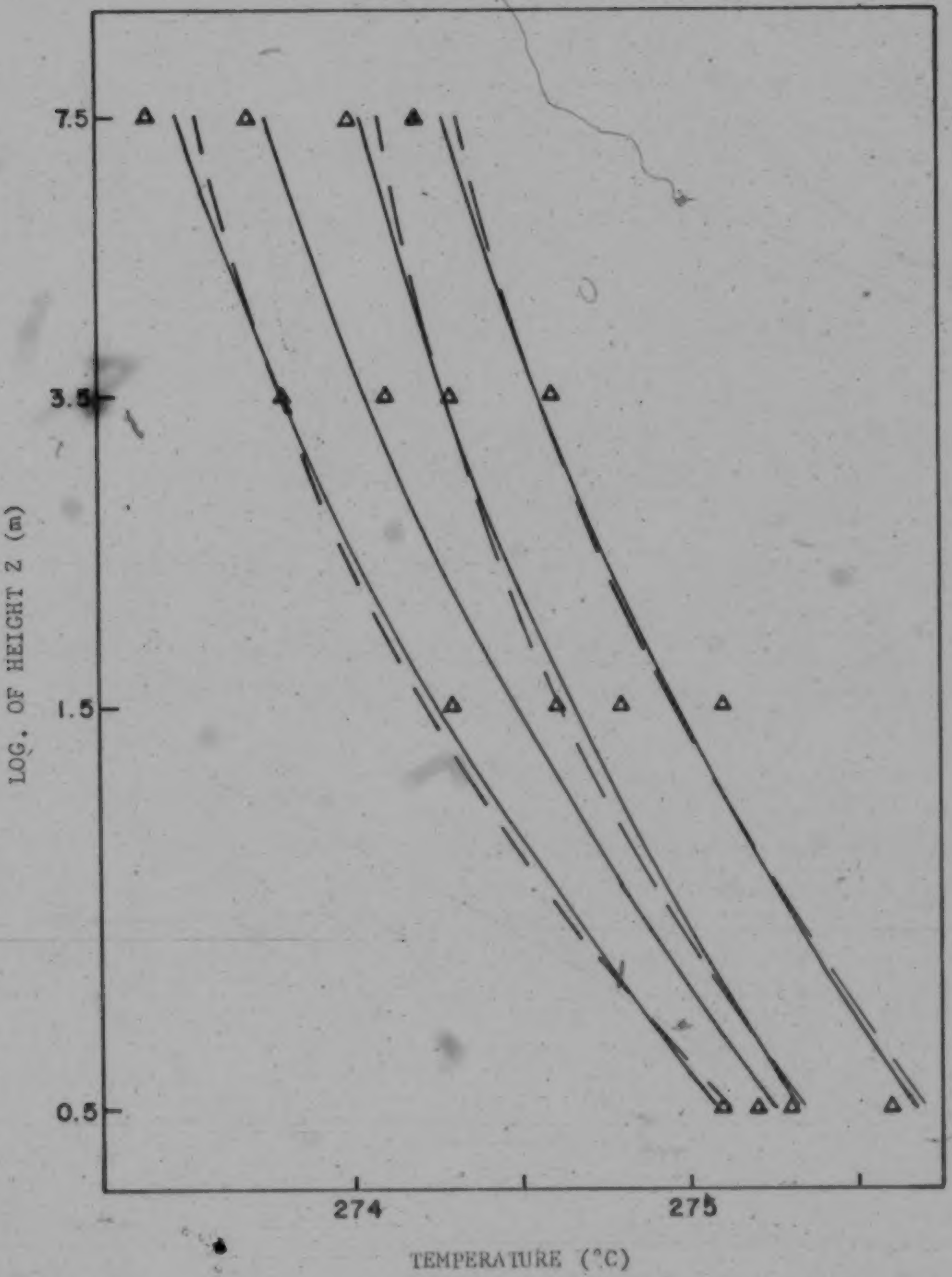

FIGURE 8. October temperature profiles. Observations are indicated by triangles. The solid curves represent the 1/3 power law and the dashed curves the 1/2 power law.

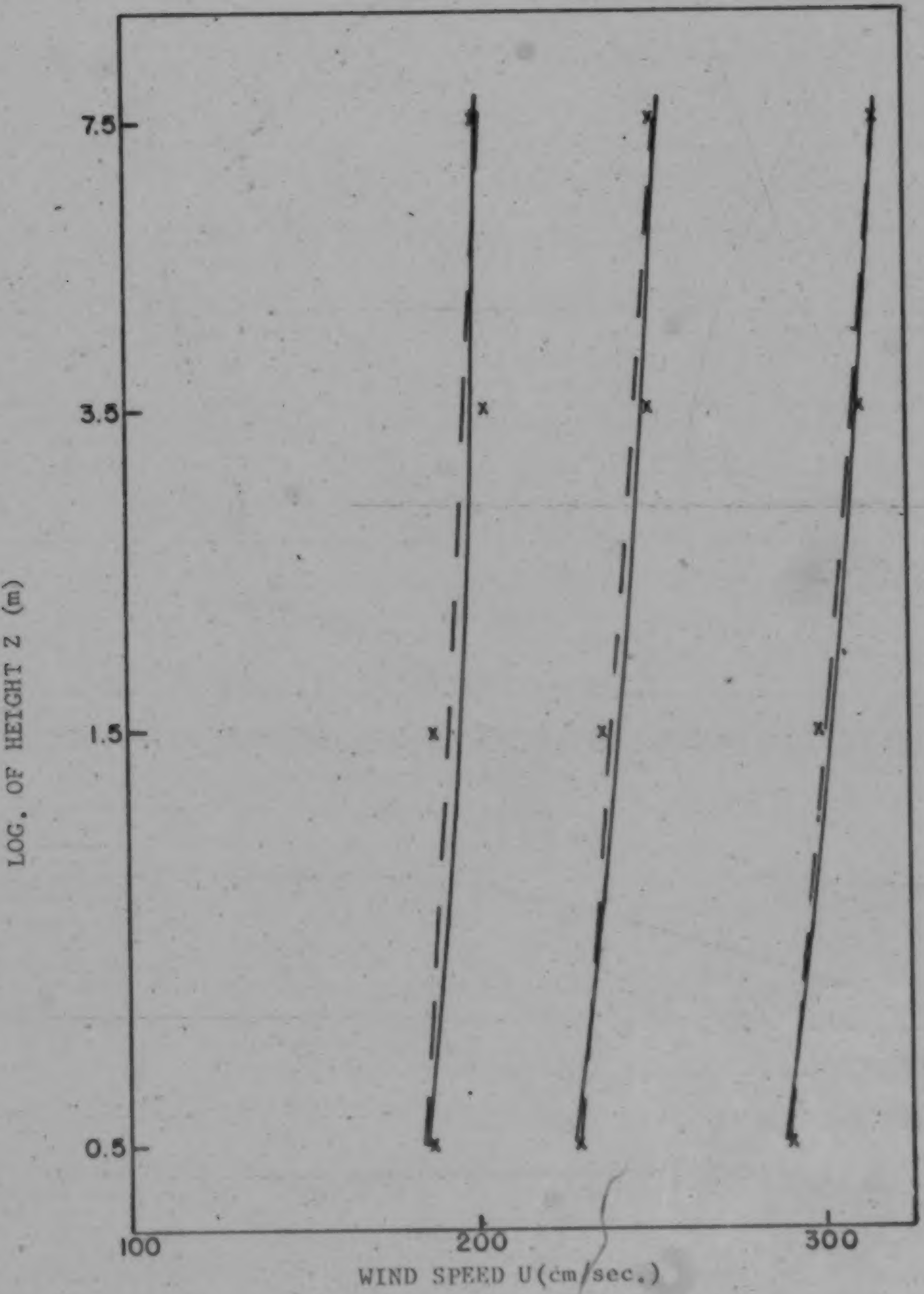

FIGURE 9. October wind profiles. Observations are indicated by x. Solid curves represent the 1/3 power law and dashed curves the 1/6 power law.

(see Table 4) in the wind measurements (see Figure 9). Once again, as is shown in Table 10, the departures of theoretical values from actual were all within the error of measurement although the Pandolfo 1/6 power law seemed to fit the observed values to a slightly better degree. The 1/3 power law corresponds to the Keyps free-convection prediction again while the Businger-Dyer formula is asymptotic to the 1/4 power law.

Taylor (1970) described a numerical model of a flow over a step change in surface temperature, a situation analogous to the actual conditions at Lake Wabamun on October 21. Comparison of the observed profiles with Taylor's results was difficult because Taylor presented all predictions in terms of deviations from an upstream neutral profile. At Lake Wabamun, no information on the profiles upstream of the heated water was collected. The numerical results indicated an acceleration of the flow in the lower levels to values above those at the same height upstream, with the fluid speed increase propagating upward with increasing distance downstream from the temperature change. The observed winds at 0.5 m. did indicate a trend in this direction as shown in Figure 9 but the deviations from the predicted profile were within the expected error of measurement of the anemometers. In addition, for the actual distance downstream of the increase in surface water temperature

(300 m), Taylor's model predicted profiles adjusted to the new surface to a height above the highest level on the tower. In short, the whole profile should have adjusted to the new surface conditions. It is possible that, if the low-level acceleration was real, it was the result of the air flow meeting higher temperatures as it approached the tower site. The warmest water was along the shore as shown in Figure 6. Further comparison with Taylor's numerical results would really only be speculation.

Calculations of the fluxes of momentum, heat and water vapour from the profiles were carried out as described in 3.2.5. The derived values of $u*$, and of sensible- and latent-heat fluxes appear in Table 11. The dew-point sensor results were unrealistic because of the dense fog conditions. The latent heat fluxes were obtained by assuming saturated air up to 7.5 m, equating air temperature to dew-point temperature and substituting into equation 3-48. This assumption seemed justified by the presence of fog extending above the highest level of measurement and by the observation of condensation on instruments and other equipment at all levels.

4.3.3 Directly-Measured Fluxes

The turbulent heat flux as measured by the sonic anemometer-thermometer and by the thermistor and propeller

TABLE 11

Profile Estimates of Turbulent Fluxes

October 21

30 Mins Ending	Sensible Heat Flux (mW/cm^2)	Latent Heat Flux (mW/cm^2)	Momentum Flux (mW/cm^2)
			Pandolfo Profile
2000	8.40	8.88	70.6
2015	8.32	8.64	84.6
2030	8.05	8.25	142.
2045	7.26	6.87	161.
2100	7.26	6.87	142.
2115	7.47	7.30	132.
2130	7.64	7.73	182.

anemometer were in good agreement with each other and with the profile estimates for the thirty-minute running means shown in Figure 10. There was a gap in the fast-response instrumentation data and the discrepancies in the last hour's results between fast-response and profile estimates were based on a rather large heat flux in the final fifteen minutes as calculated from the fast response data and not duplicated by the profile estimate. Generally the fast-response heat fluxes were within 10% of each other and within 15% of the profile estimates of heat fluxes except for the final 30-minute period.

As can be seen in Figure 11 the latent-heat fluxes as measured by the Lyman-alpha humidiometer and sonic anemometer were generally 30% lower than the values obtained from the profiles. There are at least two possible reasons for the difference. The humidity profile was based upon the temperature profile assuming saturation, but despite the fog this may have been an incorrect assumption. Also, the profile water-vapour flux was calculated assuming that the eddy coefficients for heat and water vapour transport were equivalent which may not have been the case. The vapour content as measured by the Lyman-alpha would produce a relative humidity of only 60% which is a serious but as yet unresolved inconsistency.

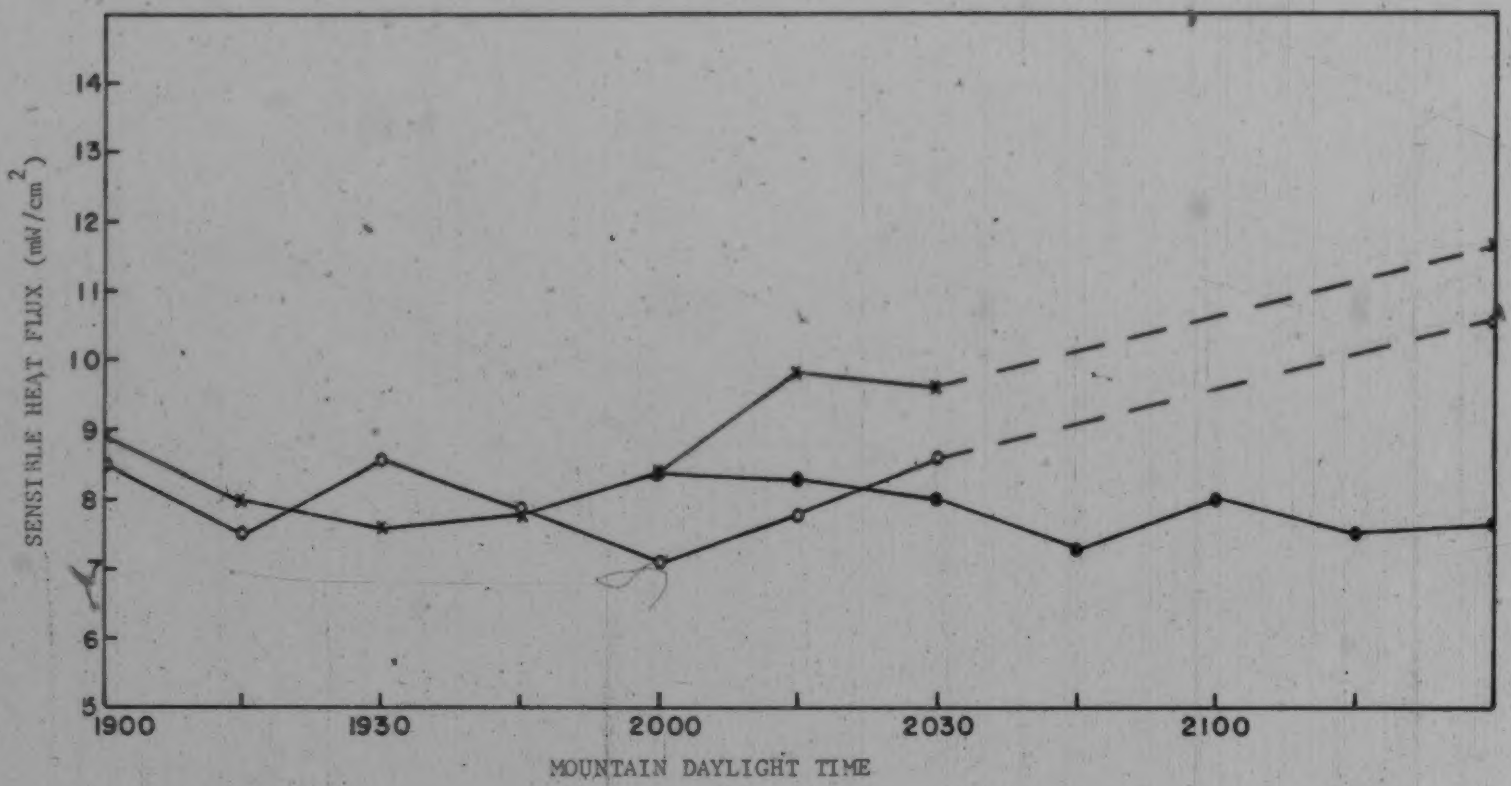

FIGURE 10. Heat flux comparisons, October. Fluxes calculated from profile data are indicated by ●, those from fluxatron data by x and those from sonic data by o. All plotted points are based on 30-minute means.

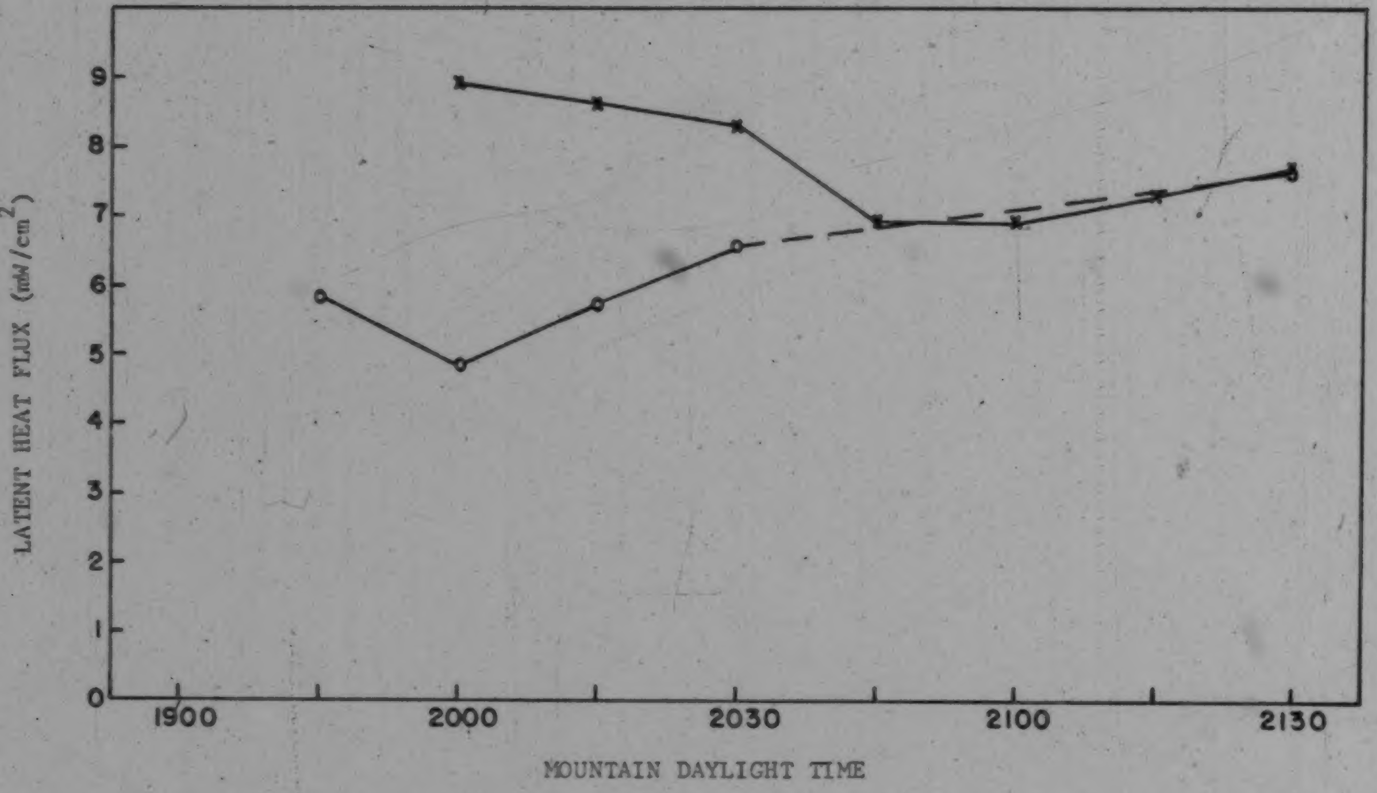

FIGURE 11. Latent heat flux comparisons, October. Fluxes calculated from profile data are indicated by x and those from fast-response instrument data by o. All plotted points are based on 30-minute means.

The momentum fluxes as calculated by the shear-stress meter were even more surprising. Not only did the shear stress u* differ markedly from the profile values of u* but, as can be seen in Figure 13 the momentum flux, or $-u*^2$, was frequently upward against the velocity gradient. In fact the average momentum flux over the entire data-collection period was upward.

4.3.4 The Anomalous Momentum Fluxes

Figure 13 shows five-minute averages of $-u*^2$ or of the momentum flux u'w' as measured by the three-component shear-stress meter. Momentum fluxes calculated from averages over periods as long as forty-five minutes did not show a difference in sign from that shown in Figure 13. The period from 115 to 150 minutes (2025-2100 MDT) was plotted as a horizontal line because no data were available for that period. In order to further investigate the cause of the upward momentum fluxes a few five-minute periods were chosen for a closer examination. The two largest upward spikes corresponding to 10-15 minutes (1840-1845 MDT) and 50-55 minutes (1920-1925 MDT) were considered to be the obvious intervals suitable for more intensive study, while the downward fluxes in the five-minute periods preceding each positive spike were used for comparison purposes. In addition several other intervals throughout the data collection period

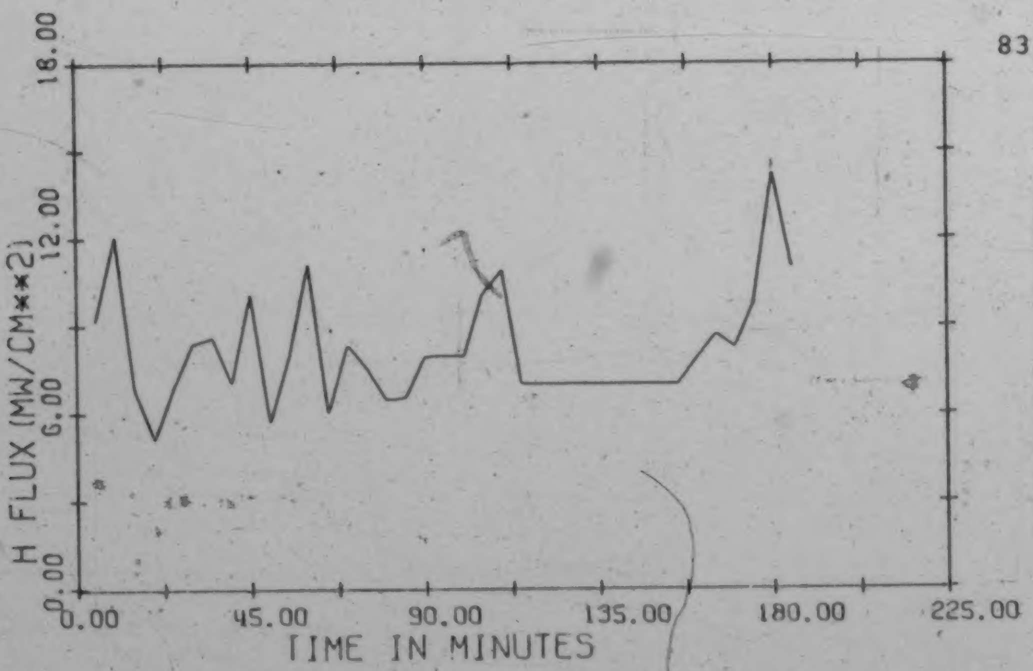

FIGURE 12. Five-minute heat fluxes (sonic); 1830-2130 MDT.

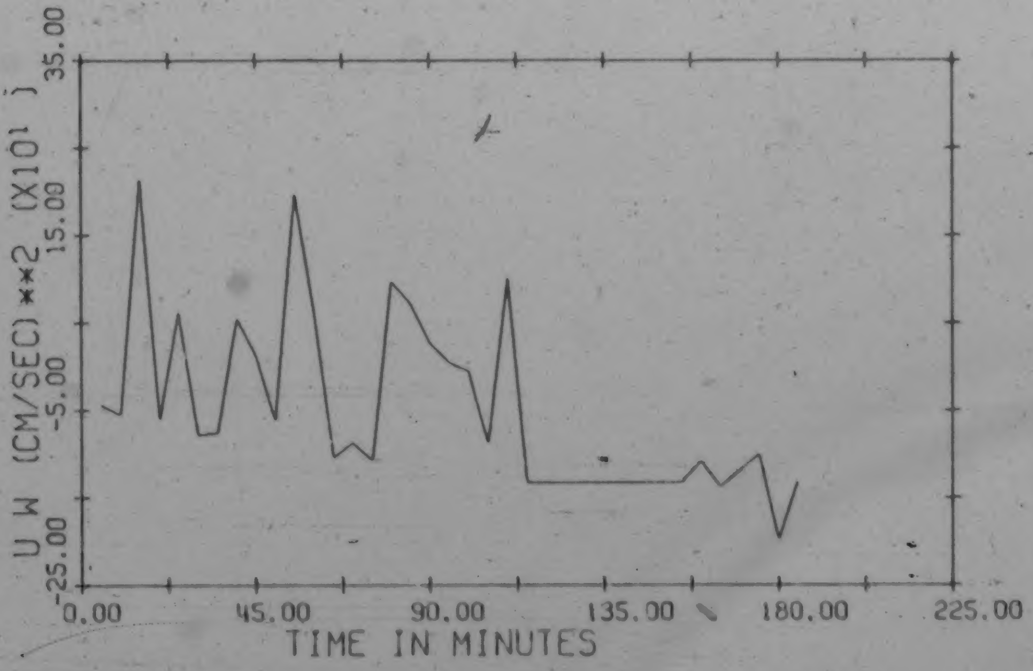

FIGURE 13. Five- minute momentum fluxes (shear-stress meter); 1830-2130 MDT.

were chosen randomly to be examined more closely.

In each chosen interval, means of total horizontal wind u and of vertical wind w from the shear-stress meter were examined as well as the fluxatron temperature T. The original intention was to find a time period over which to average, large enough to eliminate the fine-scale fluctuations but short enough to isolate the correlation of u and w necessary for the upward momentum flux. Normally of course, the horizontal wind increases with downward vertical velocity as faster moving air from above is brought down and vice versa for upward vertical velocity. For an upward momentum flux the opposite must occur at some scale and upward vertical velocity must correlate with an increase in horizontal wind. After some trial and error, thirty-second means were found to show best the anomalous correlation between vertical and horizontal velocities.

Figures 14 to 20 show the plotted values of the thirty-second means. In each case u is the top curve (stars), w is the bottom curve (squares) and temperature T (crosses) is plotted in the middle. The vertical scale represents cm/sec for u, (cm/sec)/10 for w and deviation of temperature in °K/100 for T. Every test interval showed both the normal situation with u increasing with downward w and the anomalous situation of u increasing with upward w. Some of the more accentuated examples of the latter are indicated

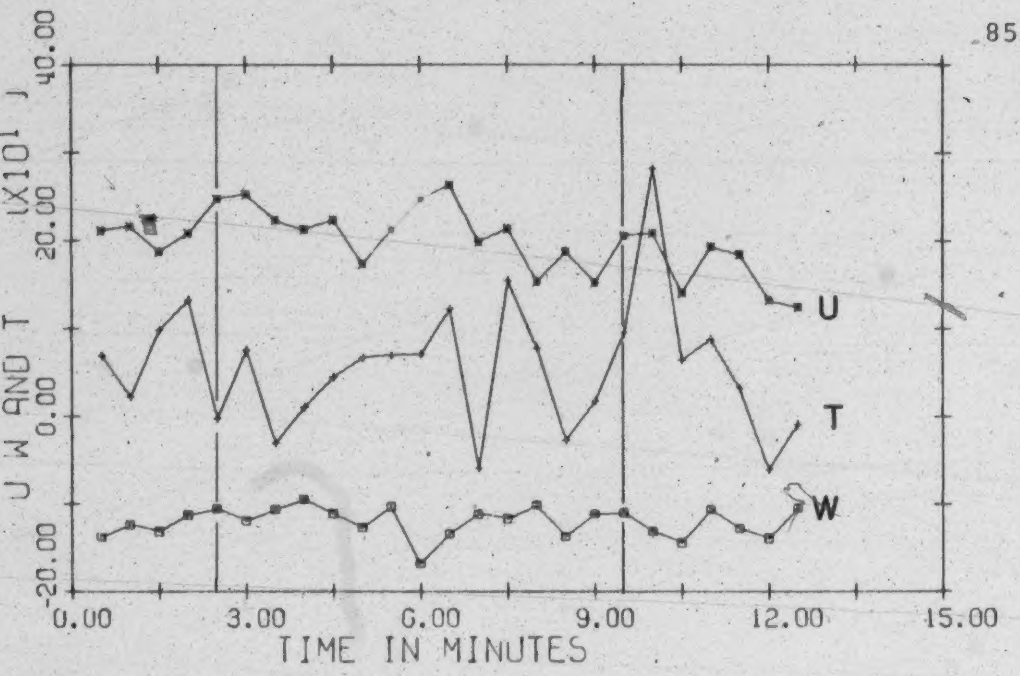

FIGURE 14. October 30-second means; 1833-1845 MDT.

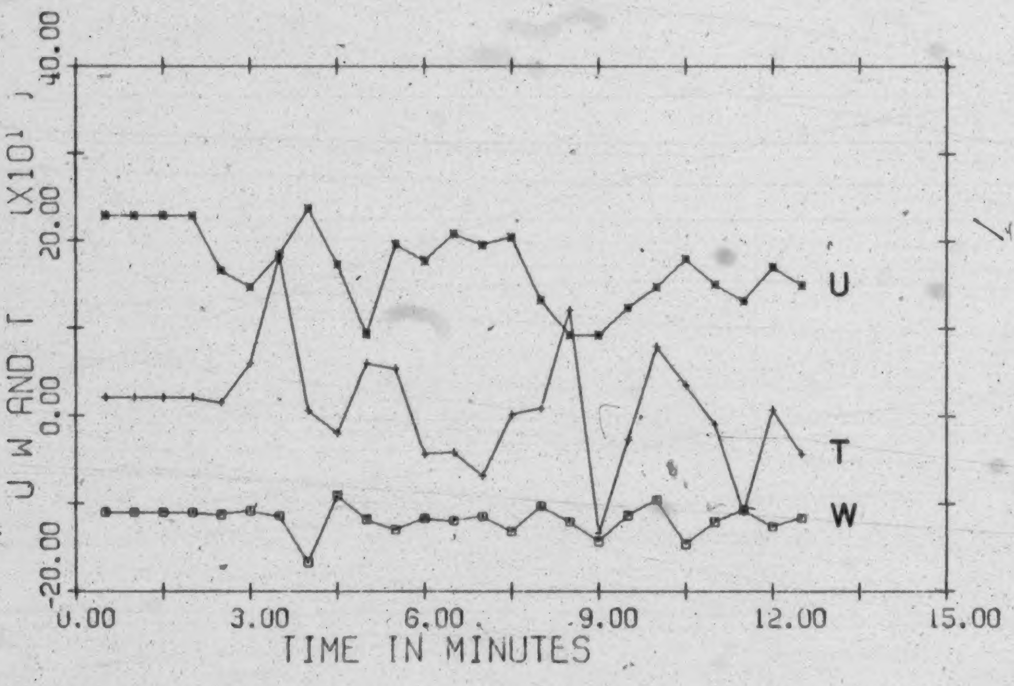

FIGURE 15. October 30-second means; 1900-1913 MDT.

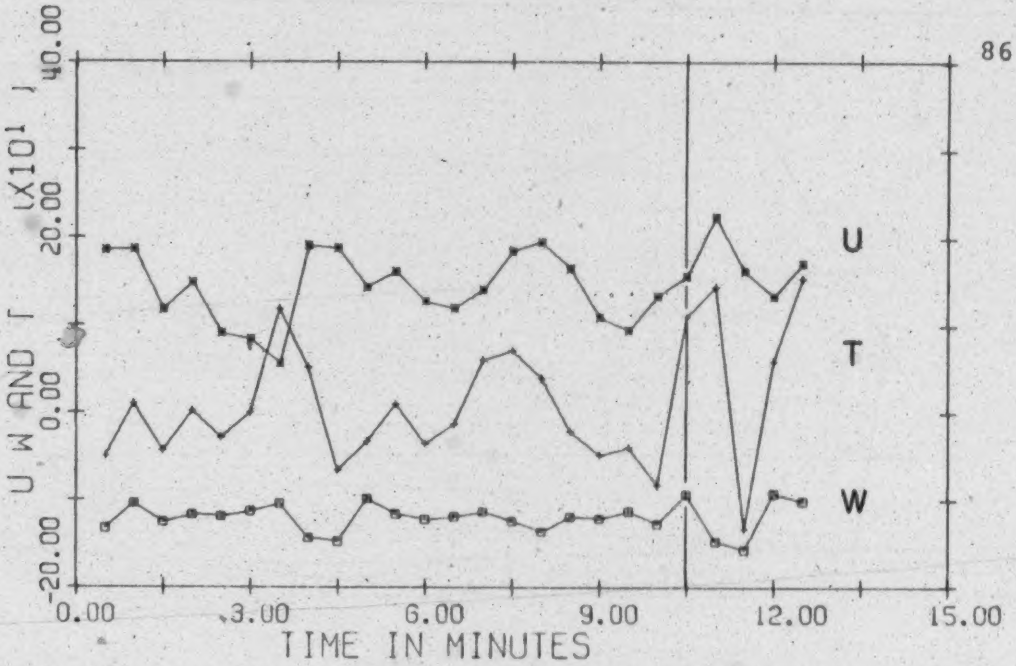

FIGURE 16. October 30-second means; 1916-1924 MDT.

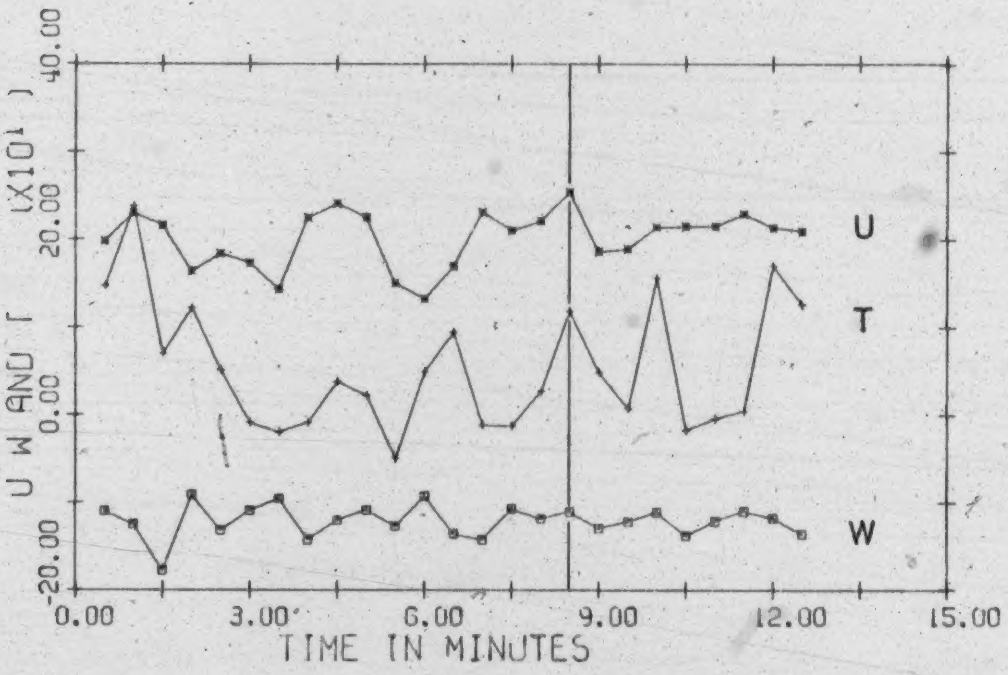

FIGURE 17. October 30-second means; 1925-1938 MDT.

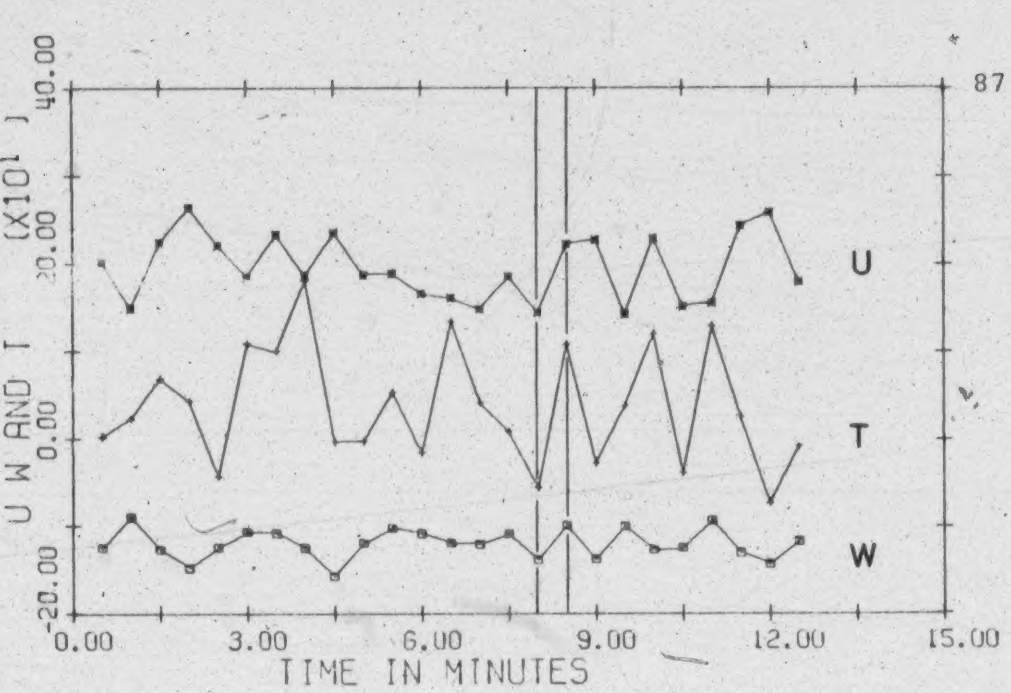

FIGURE 18. October 30-second means; 1938-1950 MDT.

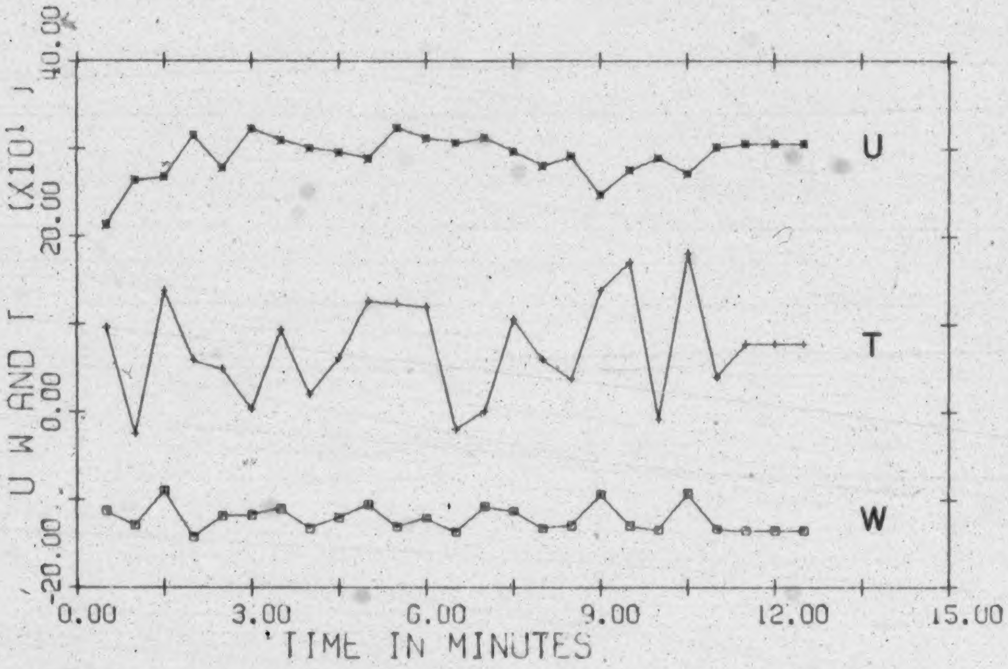

FIGURE 19. October 30-second means; 2105-2116 MDT.

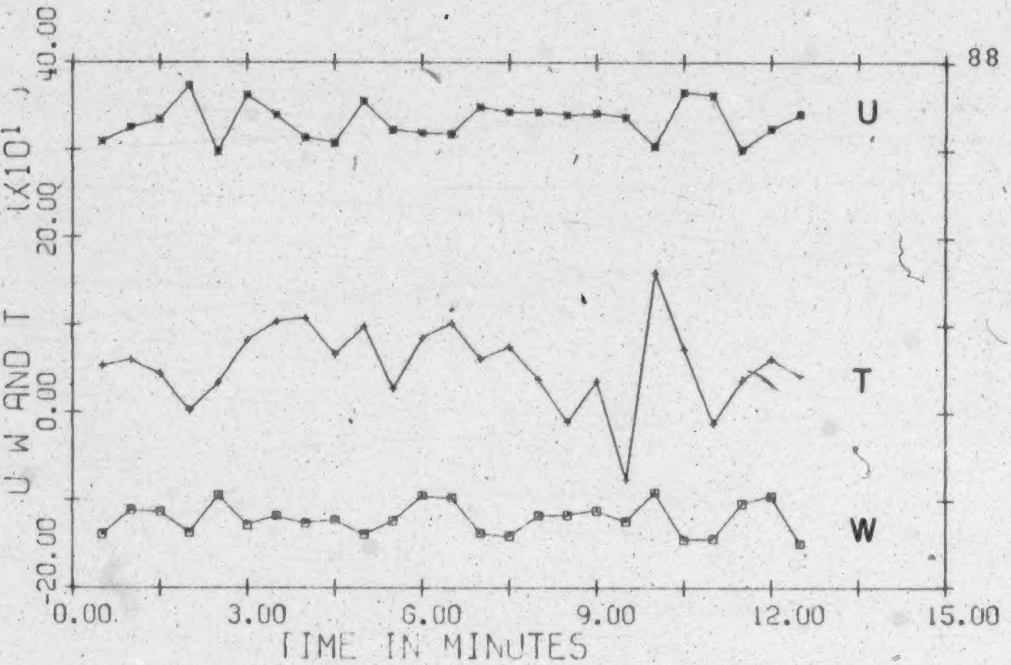

FIGURE 20. October 30-second means; 2118-2130 MDT.

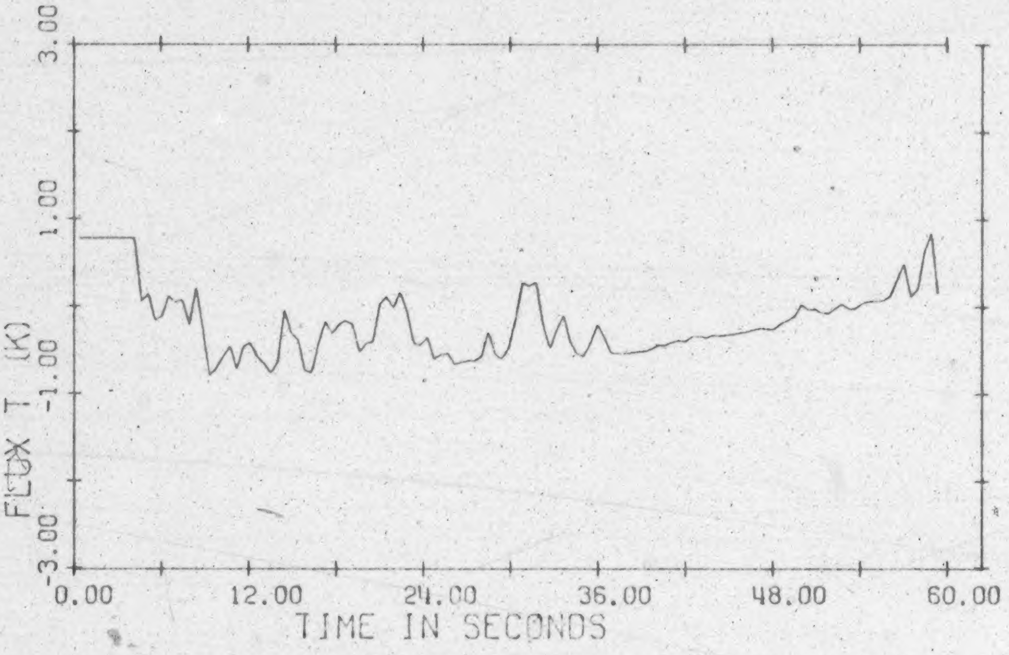

FIGURE 21. October half-second values; 1835-1836 MDT: fluxatron T.

by vertical lines on the figures. All intervals show the expected correlation between w and T. Using these thirty-second means, suitable one-minute intervals were selected for which the fine-scale fluctuations were examined.

The one-minute intervals thus chosen were parts of the five-minute periods preceding and making up the two largest upward momentum flux spikes in Figure 13. For each minute chosen, half-second means of all the instrument output were computed and these values are plotted in Figures 21 through 49. The total u is the total horizontal wind computed from the horizontal components of the shear-stress meter. This in turn was broken down into a one-minute mean direction component and a component perpendicular to the mean direction, the latter being denoted by V. It should be noted that temperature and sonic vertical velocity values are given relative to some arbitrary zero.

The two minutes 1835-1836 and 1919-1920 (Figures 21 to 25 and 38 to 42) are parts of five-minute periods which yielded the expected downward momentum flux. In both minutes there was a strong correlation between increasing upward velocity and decreasing horizontal wind. As well, both show a strong positive correlation between the sonic temperature and vertical velocity indicating a large positive heat flux.

The period 1842-1843 (Figures 26 to 31) falling within the first large upward momentum spike, was probably

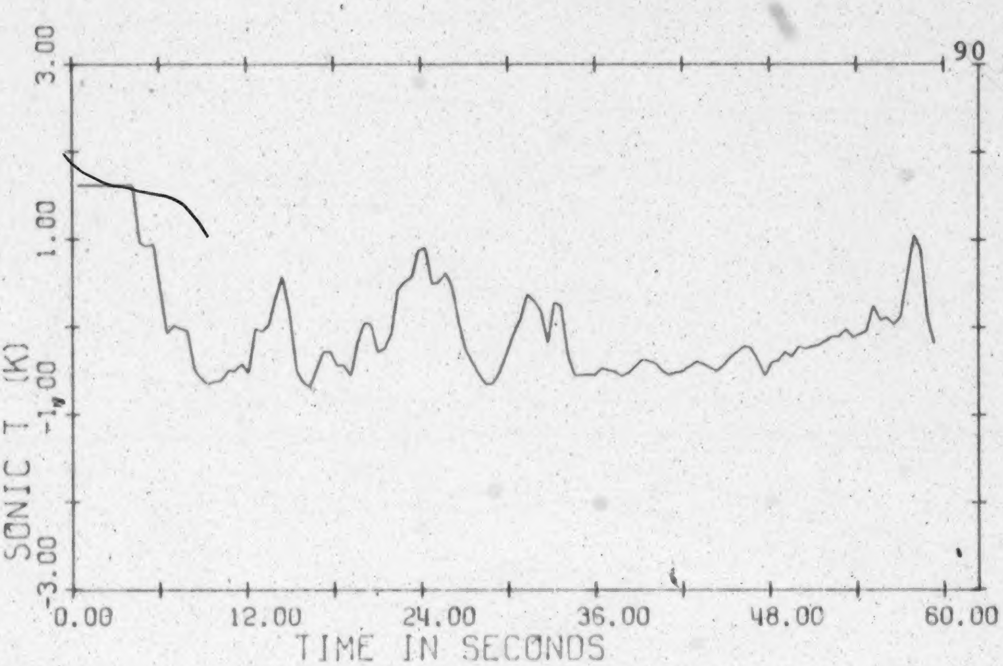

FIGURE 22. October half-second values; 1835-1836 MDT: sonic temperature.

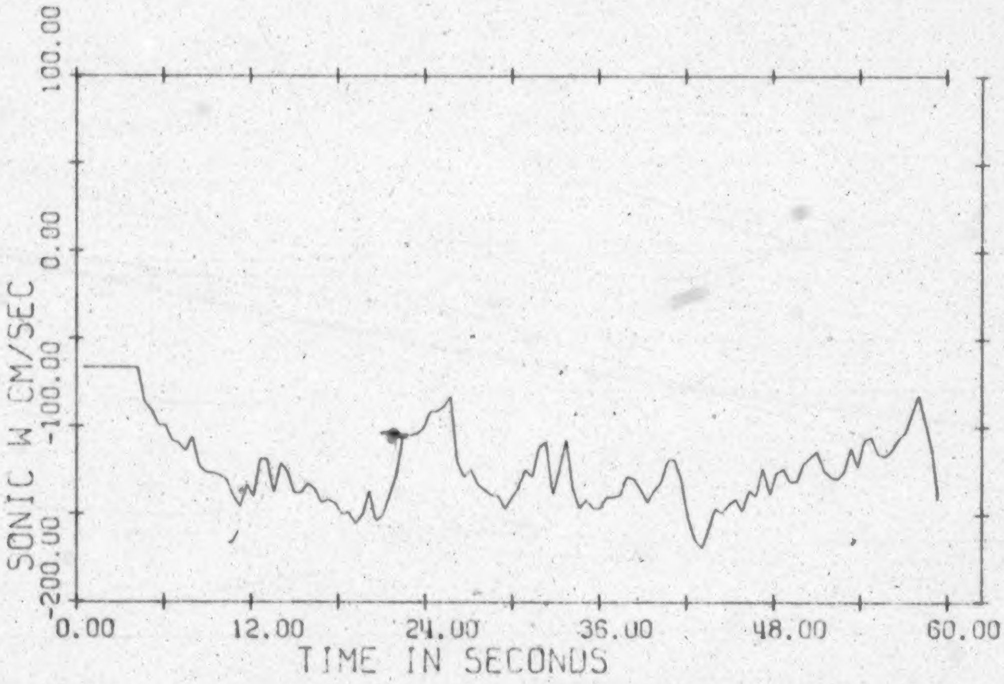

FIGURE 23. October half-second values; 1835-1836 MDT:sonic vertical wind.

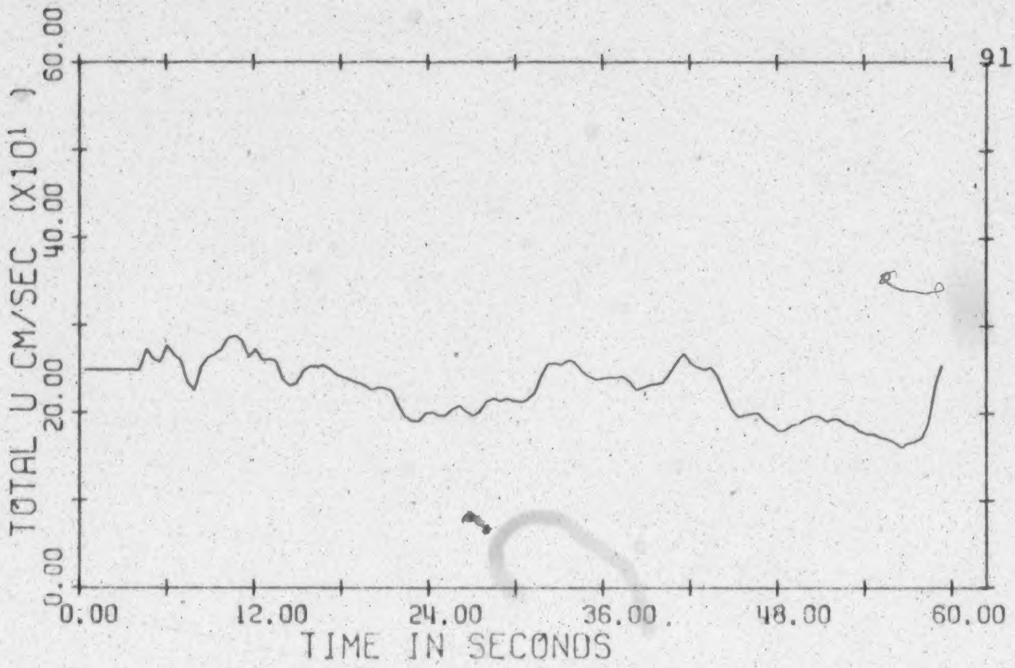

FIGURE 24. October half-second values; 1835-1836 MDT:total horizontal wind.

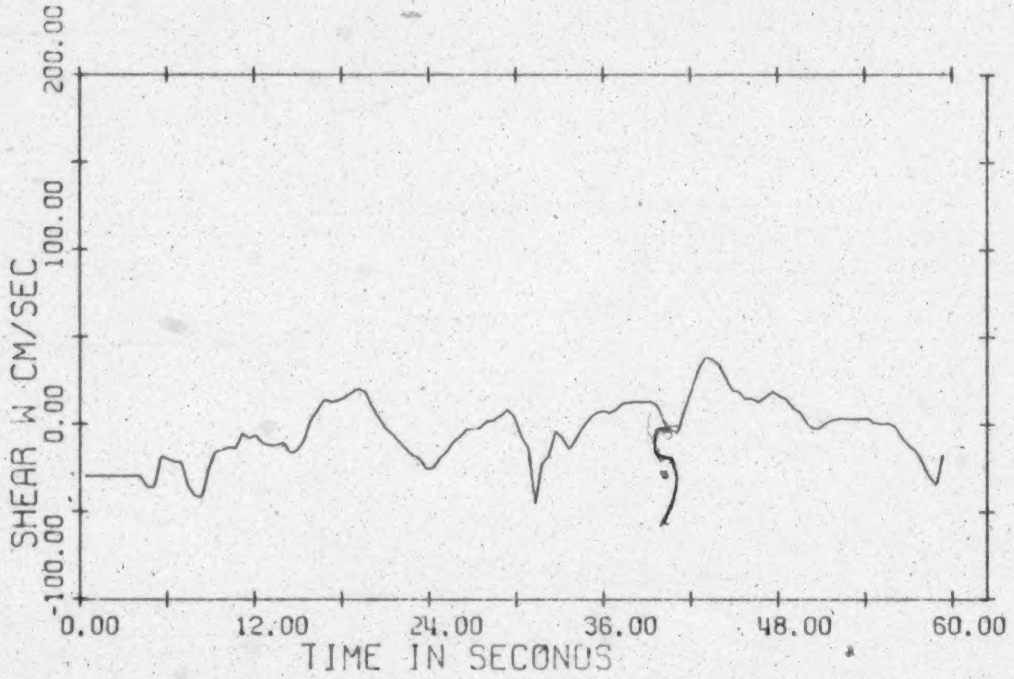

FIGURE 25. October half-second values; 1835-1836 MDT: shear-stress meter vertical wind.

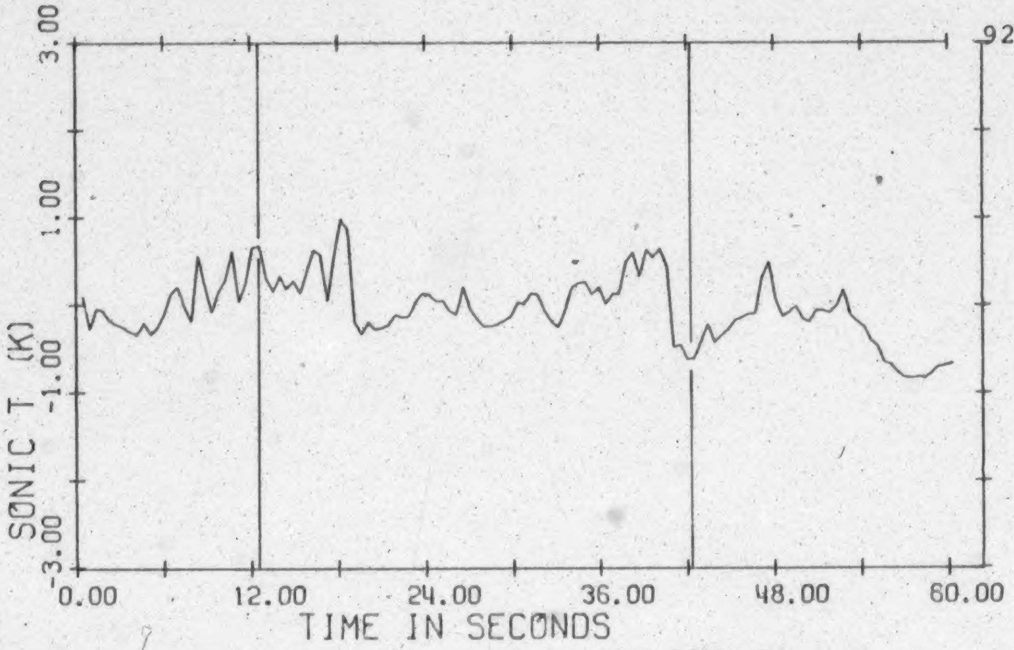

FIGURE 26. October half-second values; 1842-1843 MDT: sonic temperature.

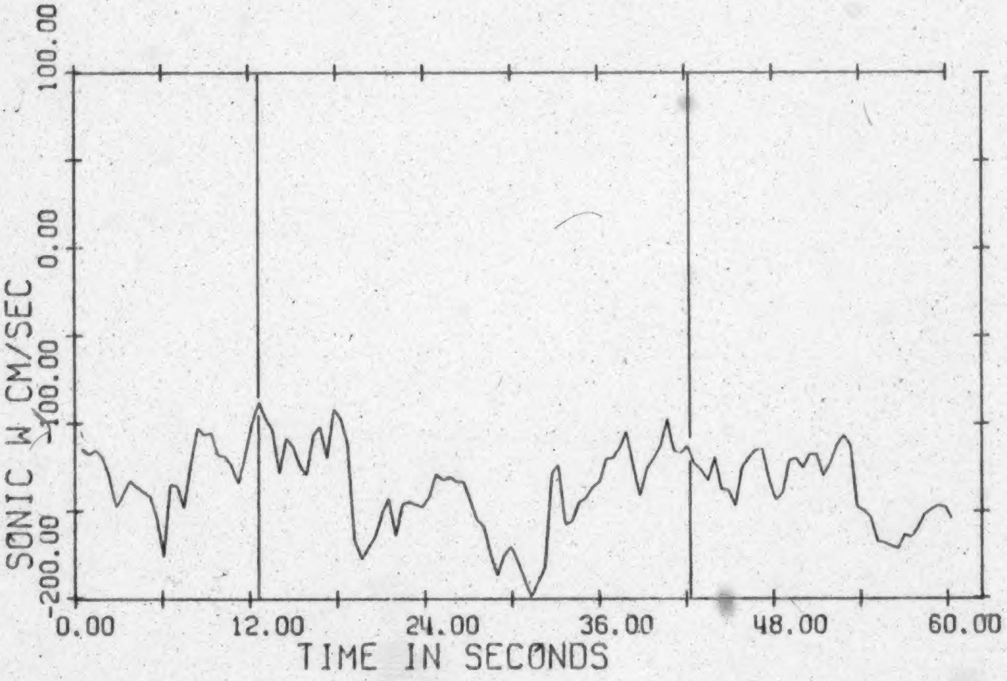

FIGURE 27. October half-second values; 1842-1843 MDT: sonic vertical wind.

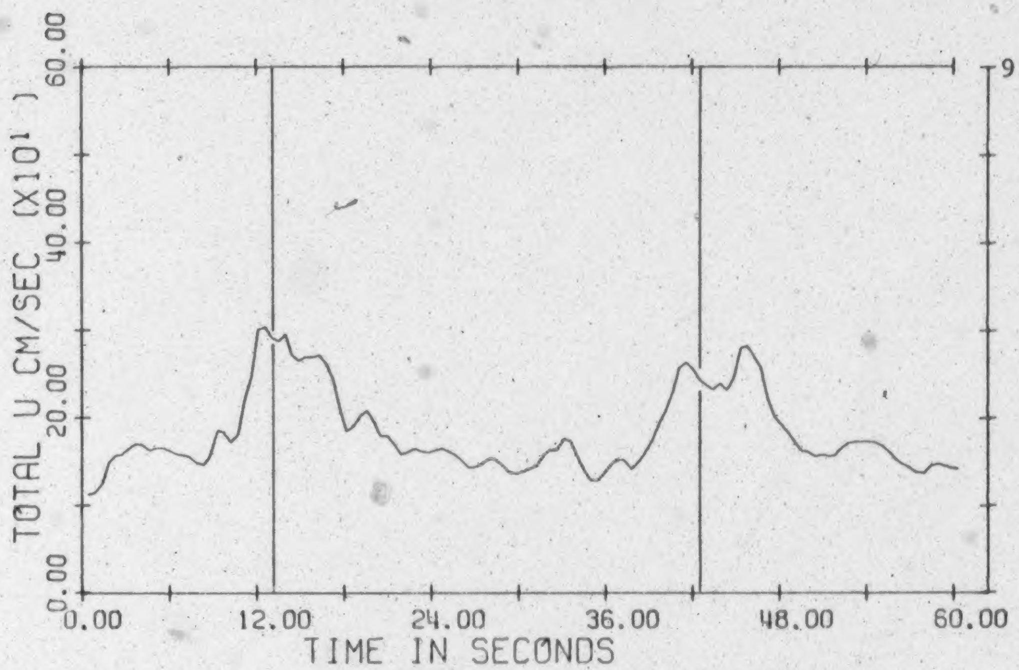

FIGURE 28. October half-second values; 1842-1843 MDT: total horizontal wind.

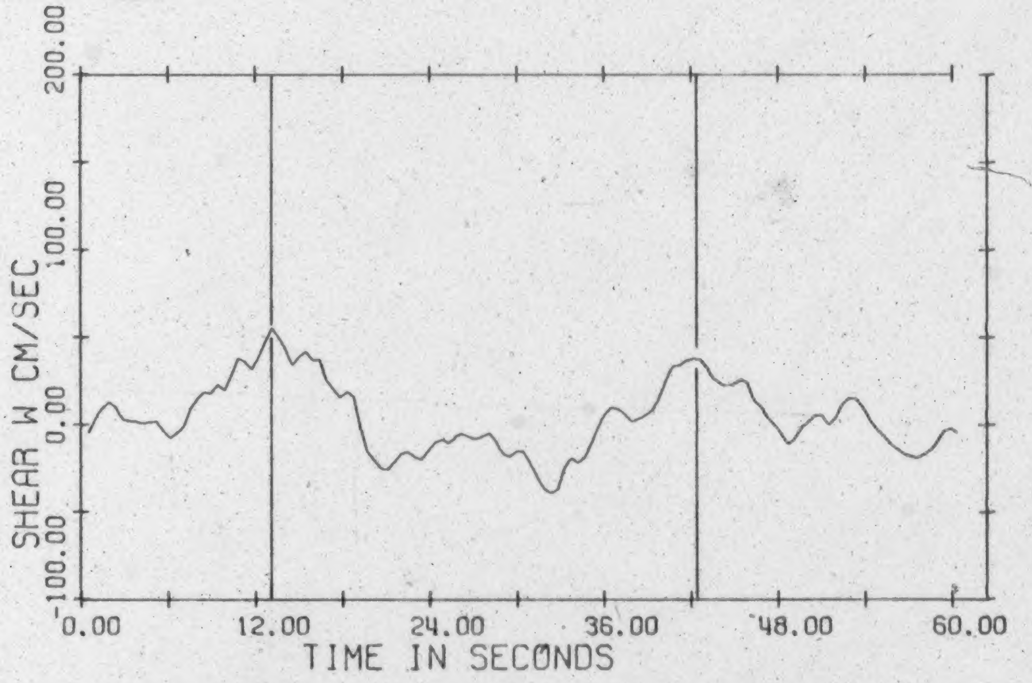

FIGURE 29. October half-second values; 1842-1843 MDT: shear-stress vertical wind.

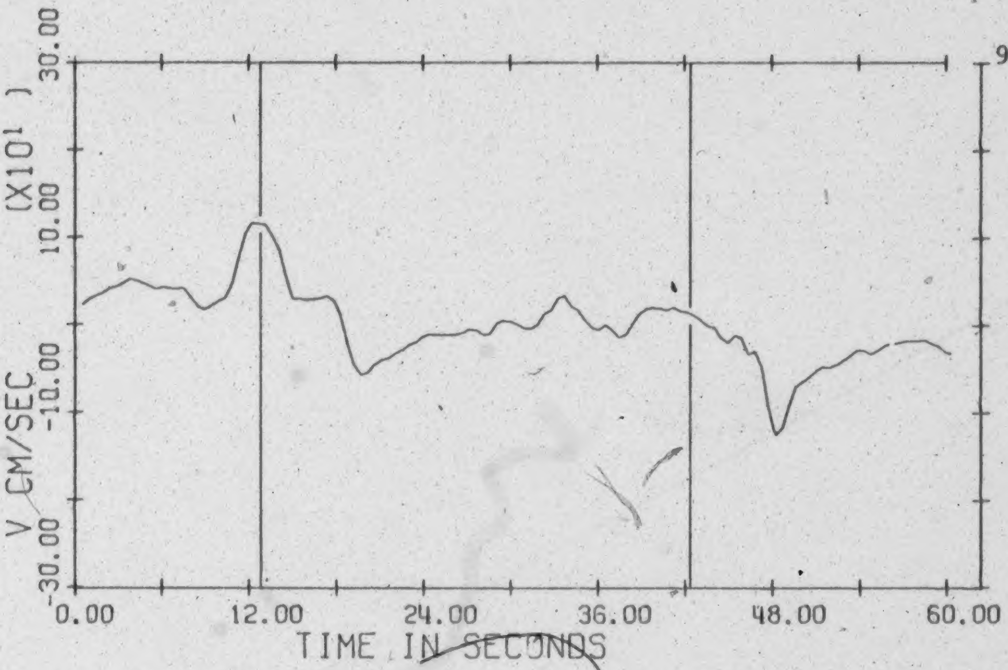

FIGURE 30. October half-second values; 1842-1843 MDT: horizontal wind, V component.

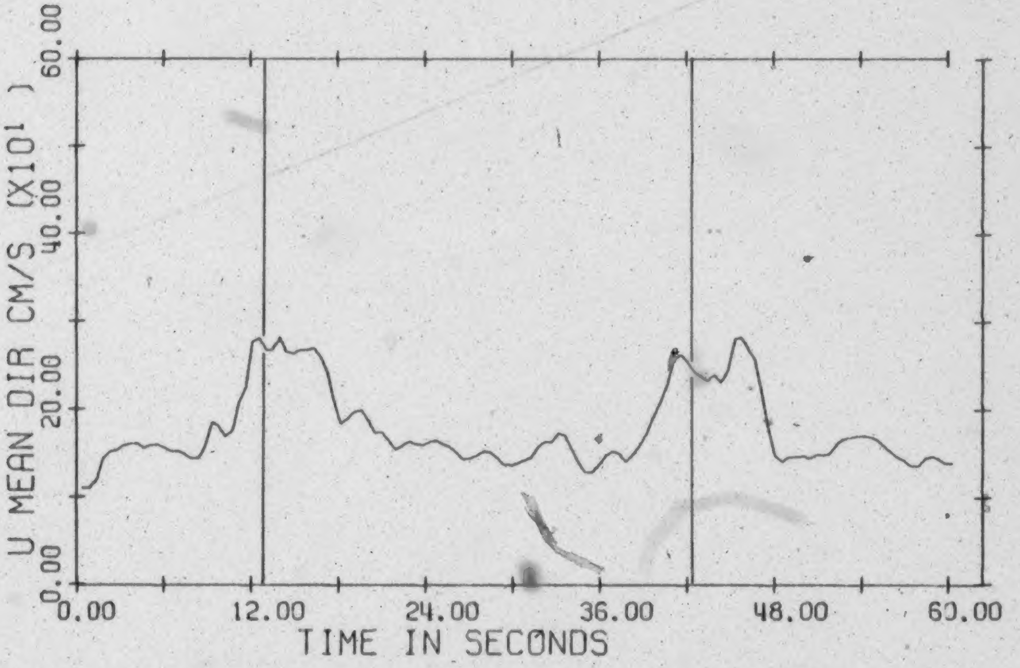

FIGURE 31. October half-second values; 1842-1843 MDT: horizontal wind, mean direction component.

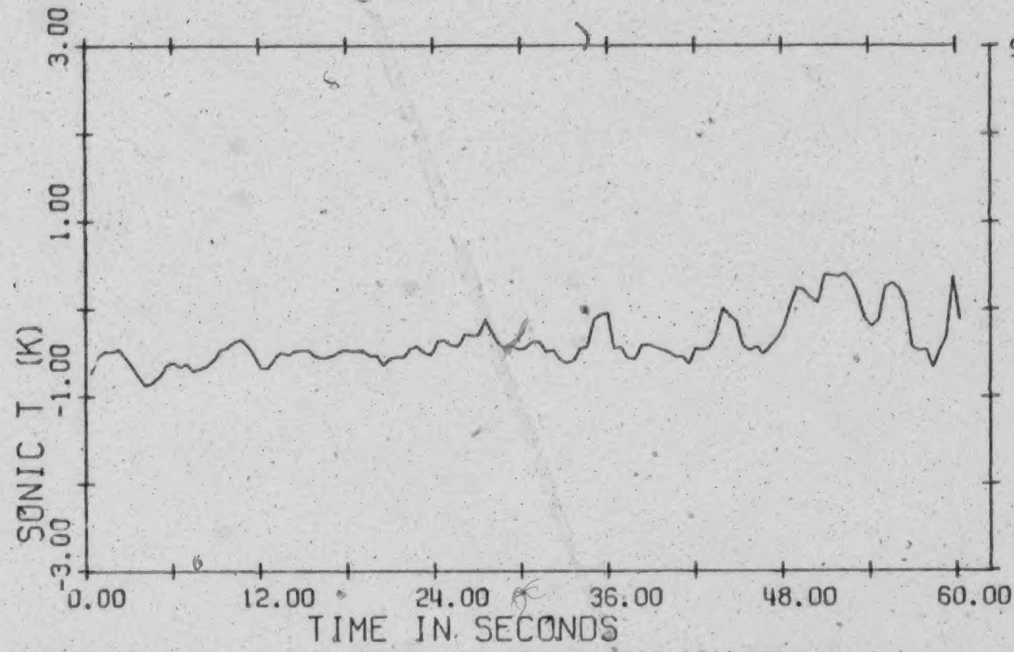

FIGURE 32. October half-second values; 1843-1844 MDT: sonic temperature.

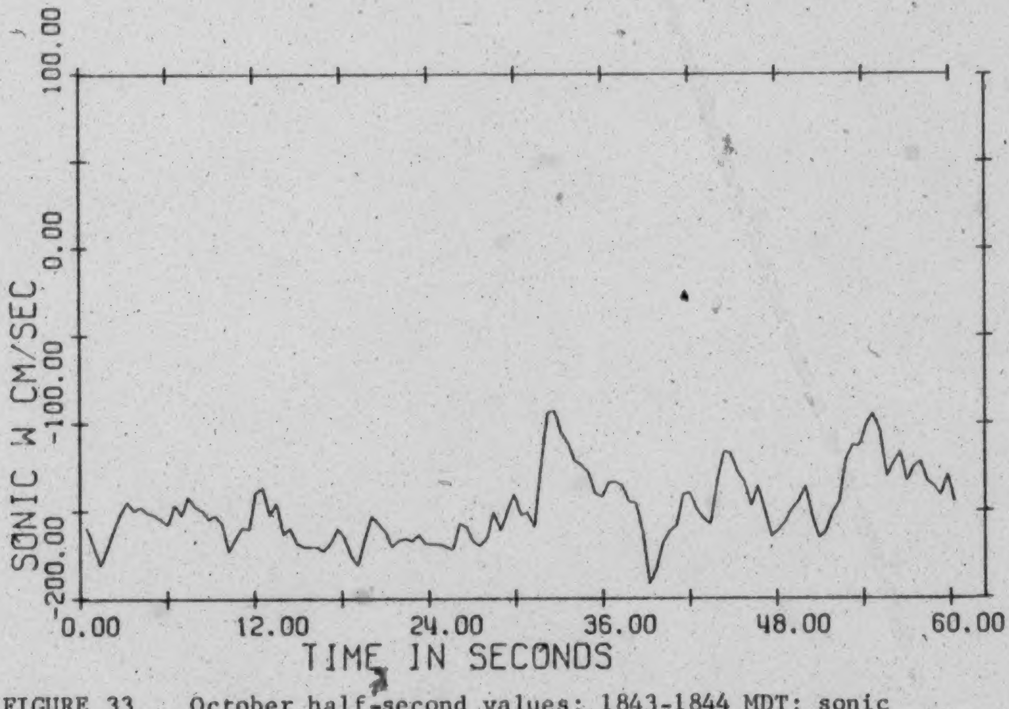

FIGURE 33. October half-second values; 1843-1844 MDT: sonic vertical wind.

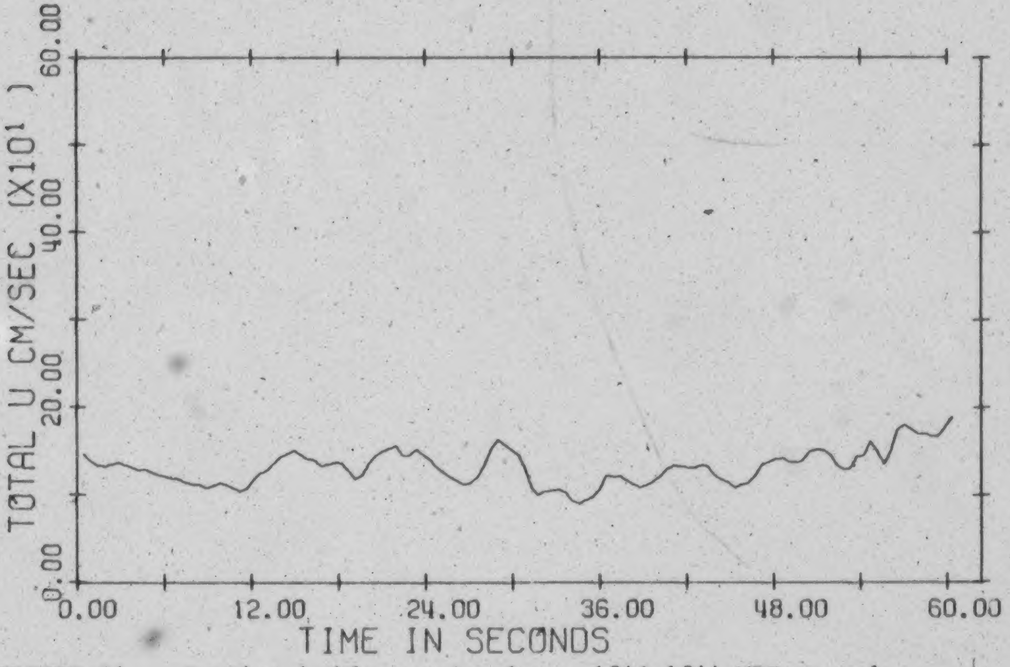

FIGURE 34. October half-second values; 1843-1844 MDT: total horizontal wind.

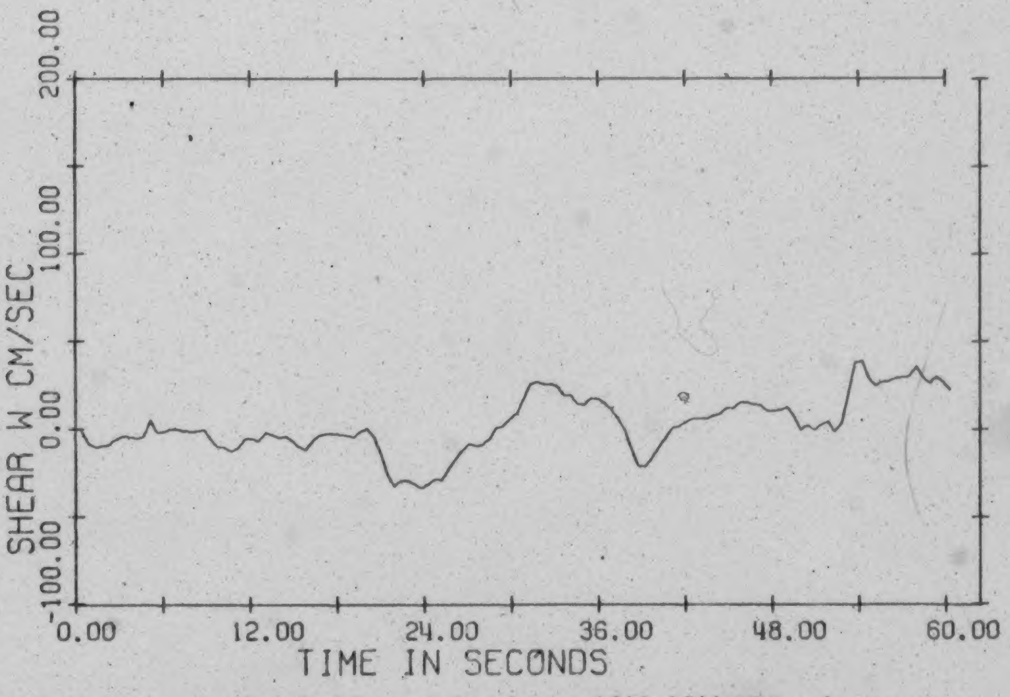

FIGURE 35. October half-second values; 1843-1844 MDT: shear-stress vertical wind.

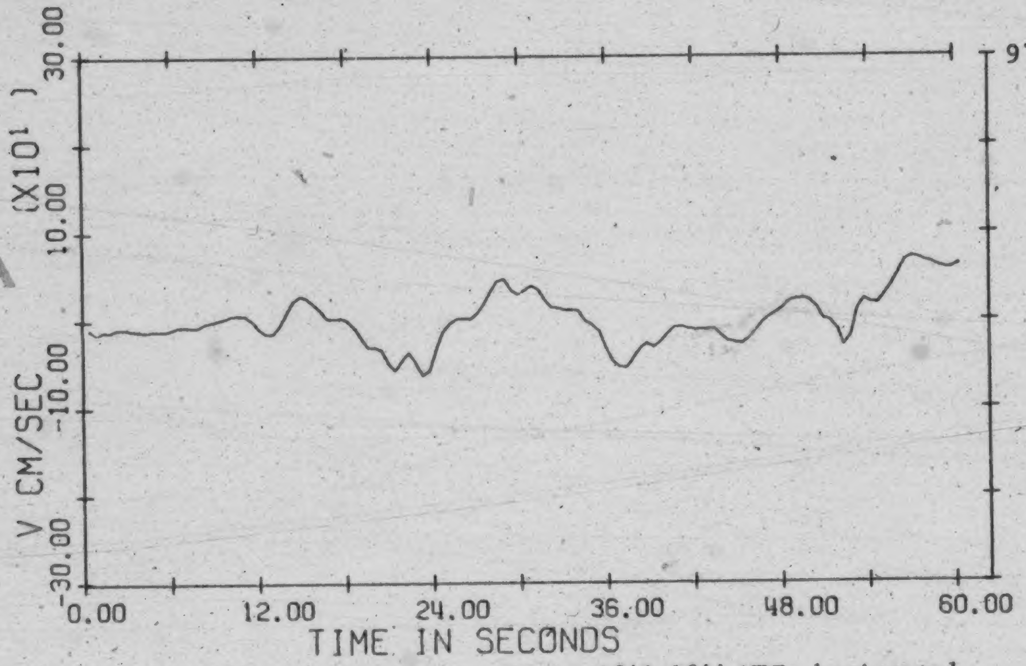

FIGURE 36. October half-second values; 1843-1844 MDT: horizontal wind, V component.

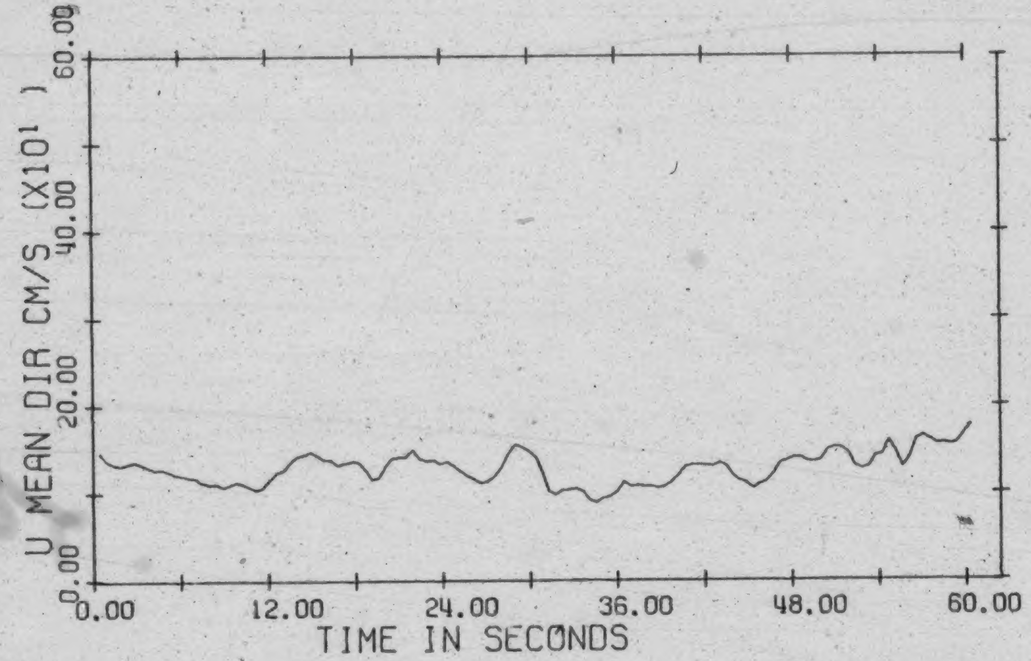

FIGURE 37. October half-second values; 1843-1844 MDT: horizontal wind, mean direction component.

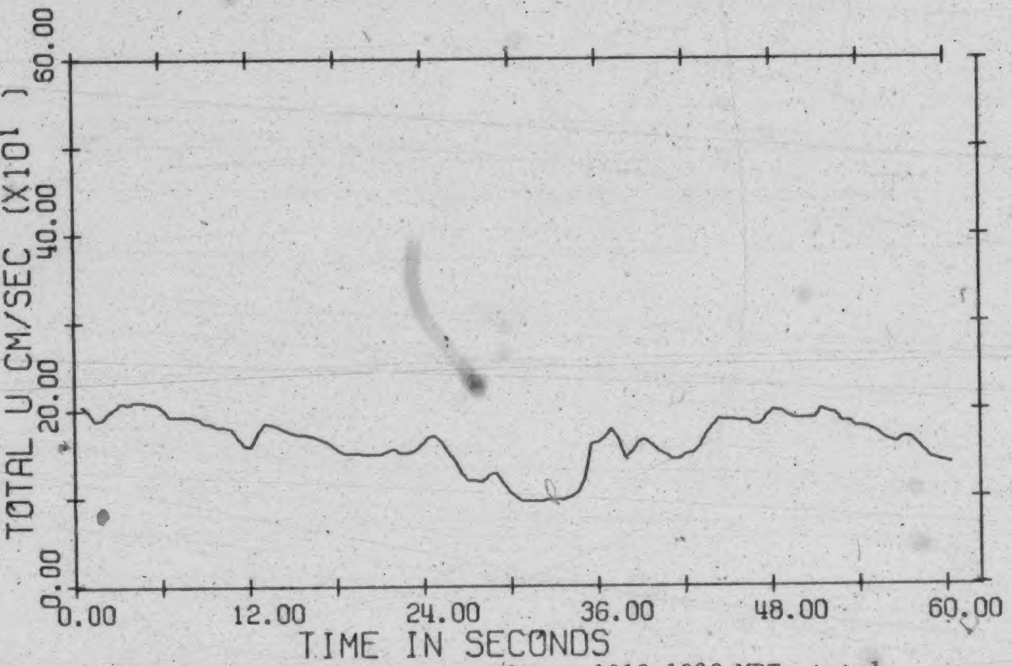

FIGURE 38. October half-second values; 1919-1920 MDT: total horizontal wind.

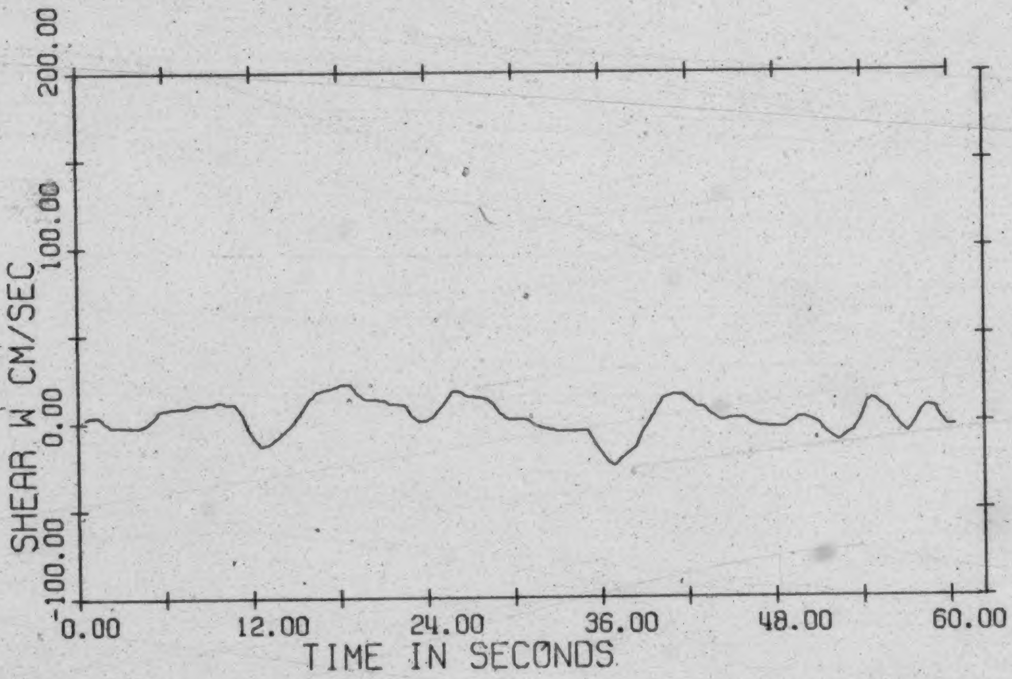

FIGURE 39. October half-second values; 1919-1920 MDT: shear-stress vertical wind.

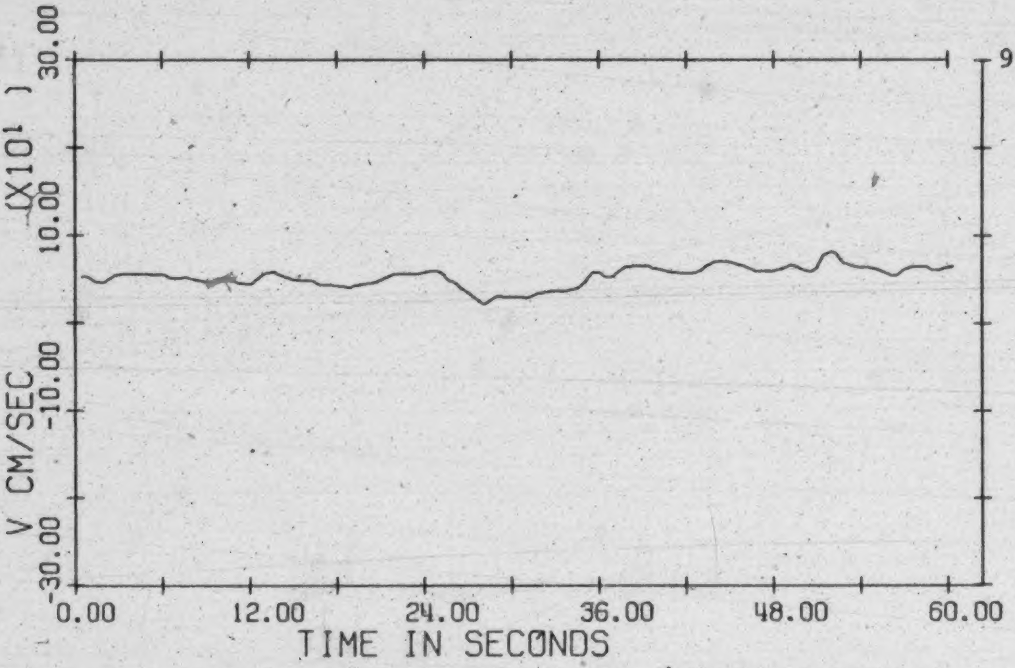

FIGURE 40. October half-second values; 1919-1920 MDT: horizontal wind, V component.

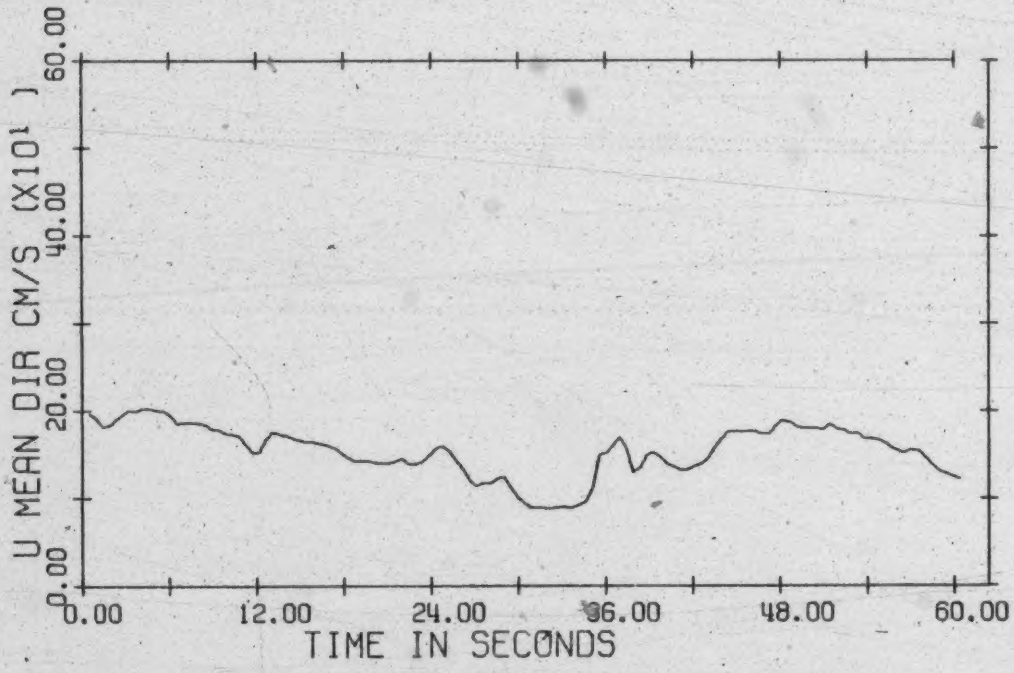

FIGURE 41. October half-second values; 1919-1920 MDT: horizontal wind, mean direction component.

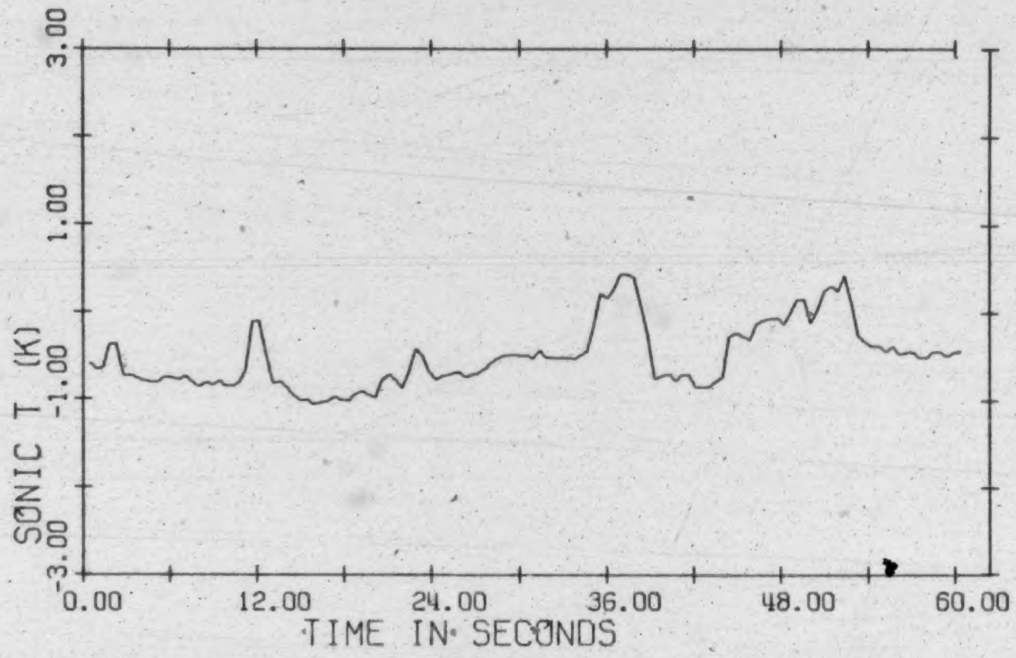

FIGURE 42. October half-second values; 1919-1920 MDT: sonic temperature.

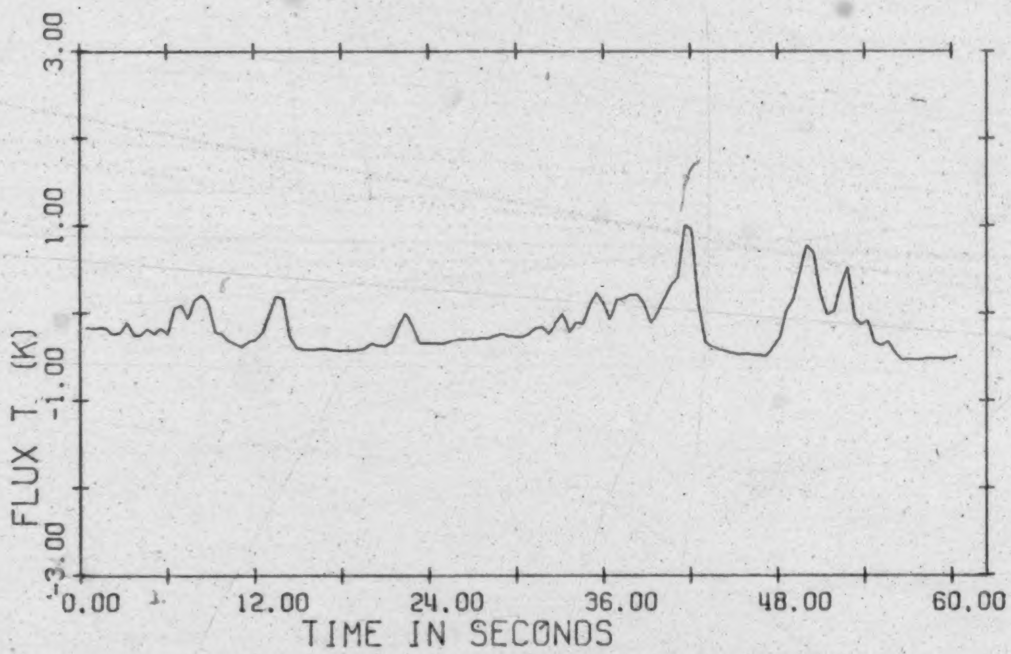

FIGURE 43. October half-second values; 1920-1921 MDT: fluxatron temperature.

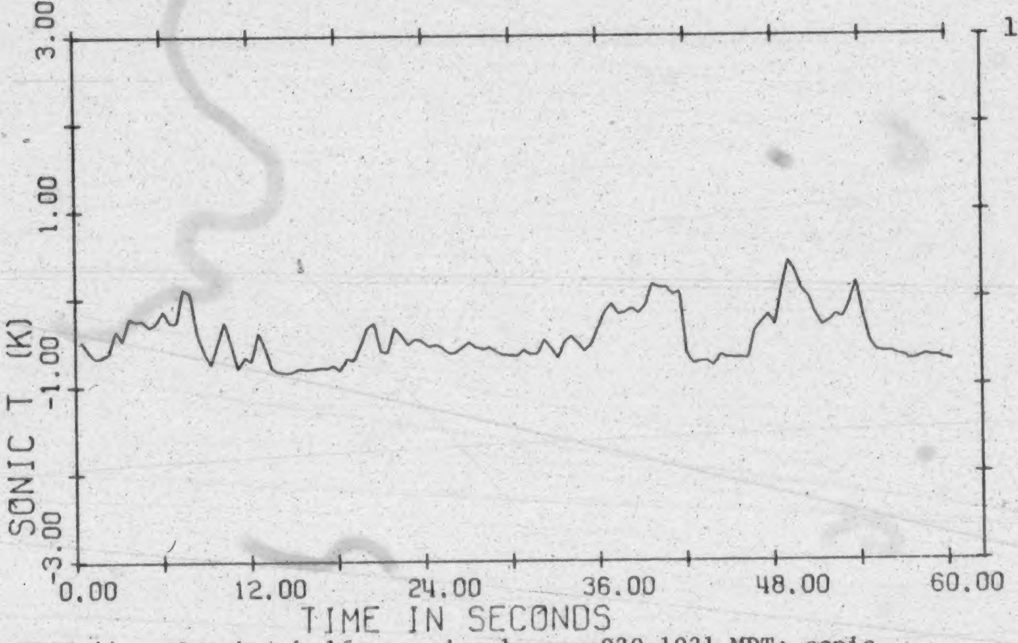

FIGURE 44. October half-second values; ;920-1921 MDT: sonic temperature.

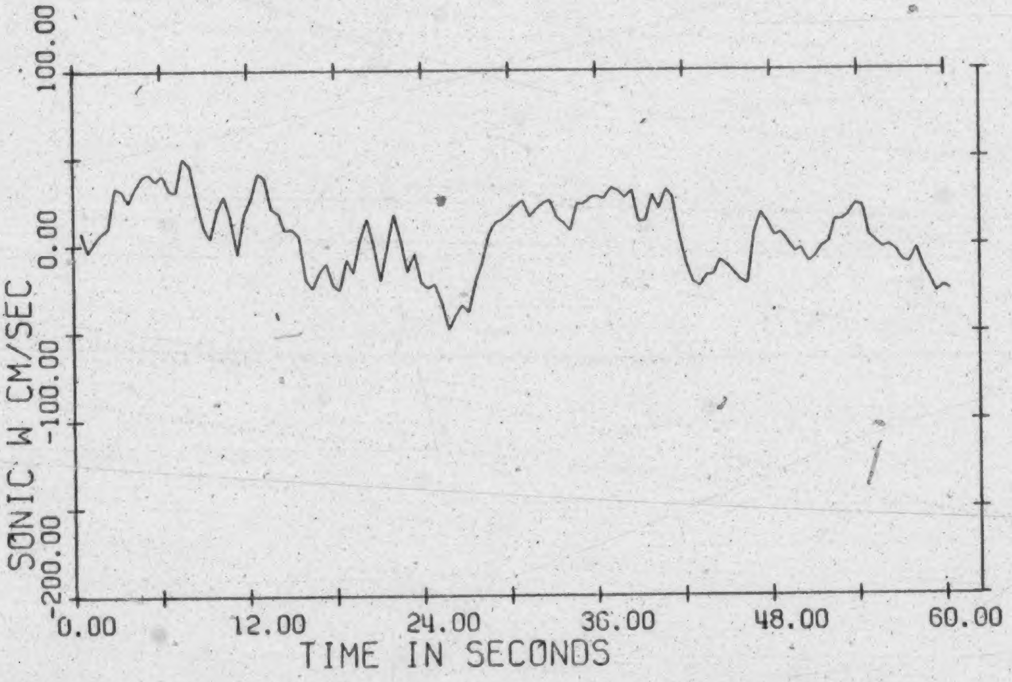

FIGURE 45. October half-second values; 1920-1921 MDT: sonic vertical wind.

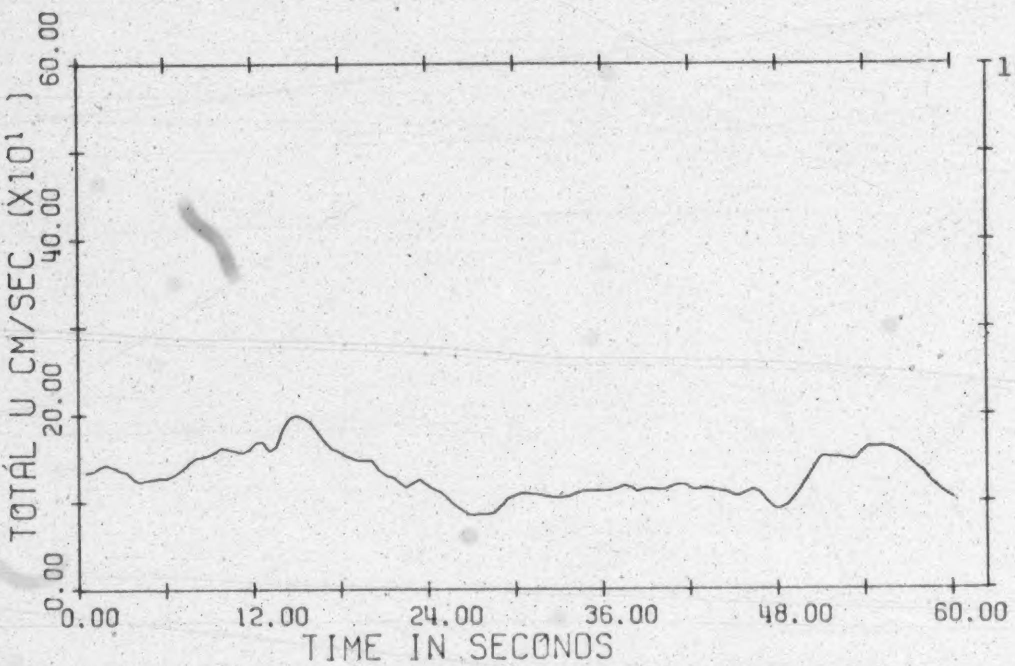

FIGURE 46. October half-second values; 1920-1921 MDT: total horizontal wind.

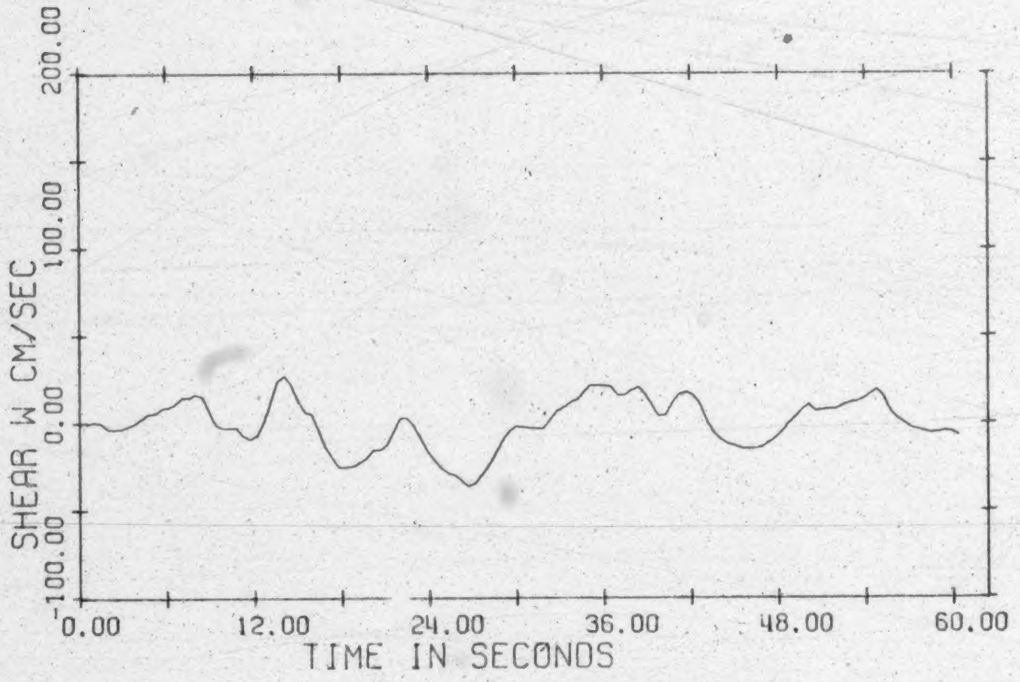

FIGURE 47. October half-second values; 1920-1921 MDT: shear-stress vertical wind.

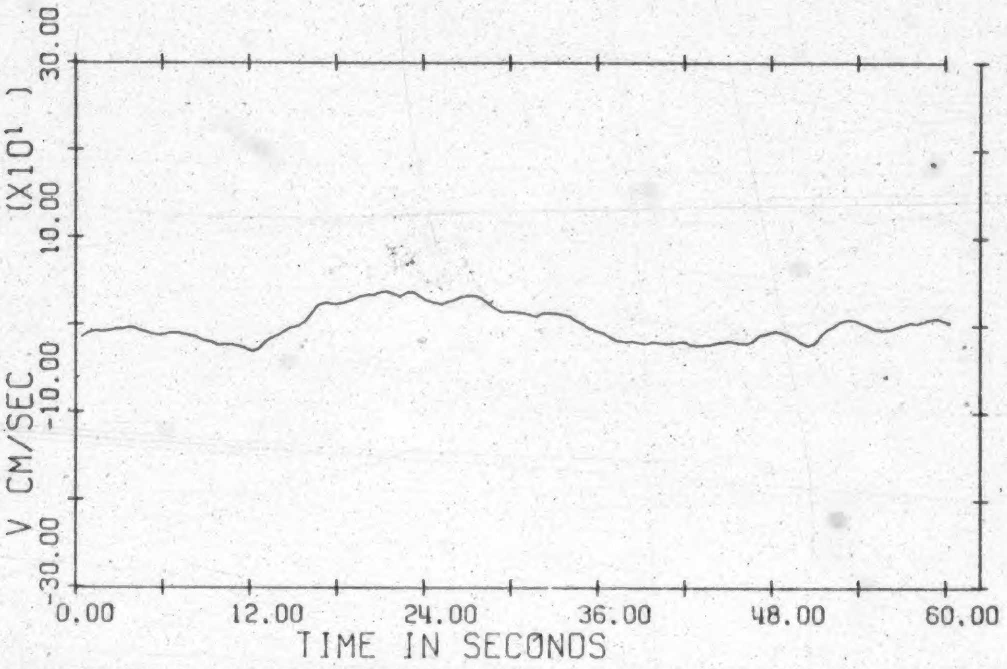

FIGURE 48. October half-second values; 1920-1921 MDT: horizontal wind, V component.

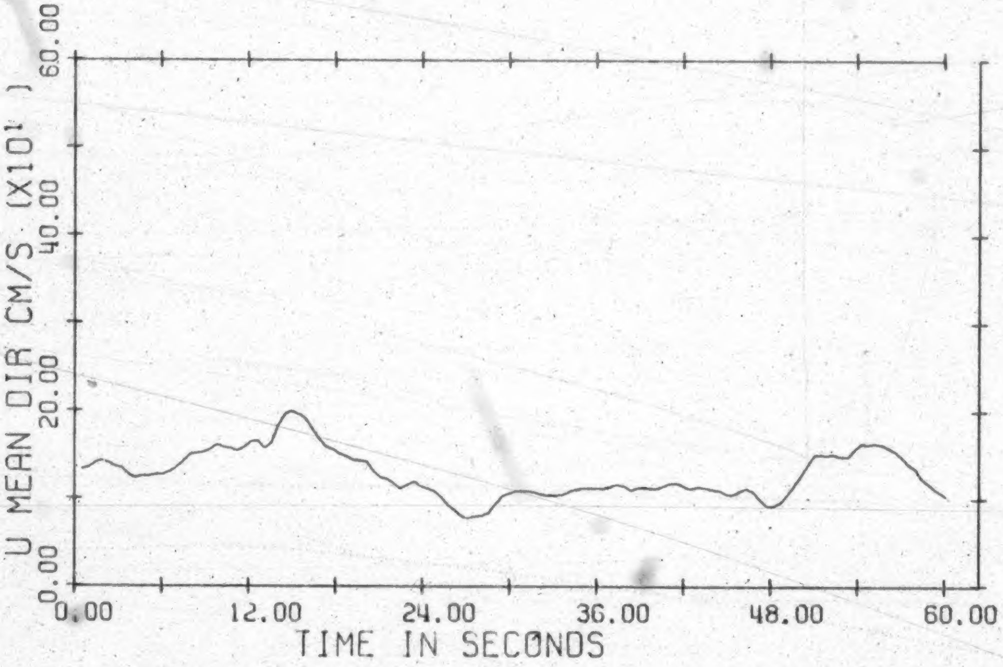

FIGURE 49. October half-second values; 1920-1921 MDT: horizontal wind, mean direction component.

the most interesting of all. The curves of shear stress w and horizontal wind u were strikingly similar and in phase, each having two fairly broad peaks within the 60- second interval (see Figures 28 and 29). Thus on this large scale the horizontal velocity increased as upward velocity increased. A close examination showed evidence of a finer scale fluctuation, superimposed upon the 30- second period oscillation described above, which had the expected increase of horizontal wind with increasing downward vertical velocity. Considering the larger scale again, the V component in Figure 30 showed a definite change in flow direction at the same time as maximum upward velocity was achieved. The sonic temperature and vertical wind were in phase for the first 30 seconds but were almost perfectly out of phase for much of the second 30 seconds.

The next minute, 1843-1844 (Figures 32 to 37), showed virtually none of the large-scale oscillation. Only the fine-scale fluctuations corresponding to the usual downward momentum flux were apparent. The sonic temperature and vertical wind traces showed no strong positive or negative correlation.

The final minute, 1920-1921 (Figures 43 to 49), was also taken from a period of large upward momentum fluxes and the corresponding data were similar in appearance to those for the interval 1842 to 1843, although the large-scale fluctuations were not as easily separated form the small scale. Reduced mean wind speed may have been an important factor in this regard. The V component indicated no truly significant direction change (Figure 48) and the sonic temperature and vertical wind were in phase (Figures 44 and 45).

In brief then there appeared to be a large-scale turbulence somewhat random in occurrence at the measuring site that accounted for a large upward transport of momentum. Superimposed on this was a small-scale turbulence continuously operating and transporting momentum in the conventional sense. When only the fine-scale turbulence occurred there was a small negative momentum flux but when the large-scale and small-scale turbulence occurred simultaneously there was a net upward transport of momentum. One can speculate that the large-scale phenomenon was some sort of organized convective eddy tilted in the flow direction to enable it to transport momentum against the mean velocity gradient whereas the fine-scale fluctuations represented mechanical turbulence. There was no evidence of a change in the temperature during the passage of the convective eddy and only a suggestion of some sort of turning of the horizontal wind, a rotation, during its occurrence.

It should be noted that Figure 12 shows strong downward momentum fluxes in the conventional sense for the period after 150 minutes (2100 MDT). Higher mean wind speeds in that period may have been responsible. It is conceivable that the stronger winds destroyed the organized convective cells, leaving a small-scale, more nearly isotropic turbulence accompanied by downward momentum transport.

Others have found similar counter-gradient momentum fluxes during highly unstable conditions. In particular Kaimal and Businger (1970) described in considerable detail such an occurrence in Kansas. They examined an irrotational convective plume and a rotational dust devil, both of which accounted for an upward momentum flux. The analogy between the Kansas and Wabamun data seems to end here, however, because the upward momentum flux in Kansas was accounted for by a burst of upward flux in the short-period or fine-scale turbulence. The Wabamun data on the other hand showed consistent downward fluxes by fine-scale turbulence. An upward flux was evident only when periods longer than 30 seconds were considered. Half-second and one-second average fluxes for the Kansas occurrences showed considerable upward momentum flux but one-second average fluxes for the Wabamun data in the time period 1842-1843 showed all downward fluxes.

The Kansas data were taken at higher levels (5.66 m and 22.6 m) but this should only have brought them into a region of Richardson numbers similar to those experienced at lower levels in the more unstable conditions existing at Lake Wabamun in October. The other difference of course was that the convective systems moved past the observing site in Kansas but at Lake Wabamun the site was fixed to the source of the convection, the hot water plume. An extensive observing set up enabled Kaimal and Businger to deduce a description of the Kansas convective systems but the limited data at Lake Wabamun prevented similar deductions about the structure of the Wabamun convection. The only possible conclusion is that the Kansas and Wabamun convective systems were dissimilar.

4.3.5 Turbulent Flux of Liquid Water

Because of the high concentration of liquid water (fog) in the air during the October experimentation an effort was made to estimate the vertical flux of this quantity. Because the liquid water had evaporated from the plume surface and then recondensed it represented a legitimate flux of latent heat from the surface.

No direct measurements of this quantity were made and several assumptions were necessary. The only indication of the quantity of liquid water present was based upon the visibility which was approximately 300 ft. Wiener et al. (1961) quoted a liquid water content for this visibility in ocean fog of 0.3 g/m^3 and this figure was accepted for the

Wabamun situation. This was an order of magnitude smaller than the water-vapour content measured at approximately 3 g/m^3 by the Lyman-alpha humidiometer. Then, assuming that the gradient of liquid water was the same as that for water vapour and the transporting mechanisms were similar, the flux of liquid water was also an order of magnitude less than that of water vapour. This would account for a 10% increase in the total flux of latent heat but because of the uncertainties involved in calculating the liquid water flux no further attempt was made to include it in the results.

4.3.6 Fluxes Associated With the Mean Vertical Wind

The mean vertical velocity at Lake Wabamun in October was not zero and in fact an upward velocity approximately six times larger than the possible instrument error was measured thoroughout the data collection period. As previously discussed, the existence of a mean vertical motion indicated that the turbulent fluxes no longer represent the total flux from the surface since the mean vertical wind carries a significant part of this total flux.

The vertical transport of quantities resulting from this mean upward motion were calculated as outlined in 3.3.3. The temperature of the undisturbed atmosphere was chosen as the temperature at 7.5 m for the purpose of calculating the temperature deviation from adiabatic because the temperature profiles seemed to be approaching the adiabatic lapse rate at this level. If this temperature deviation is denoted by T then the flux of sensible heat from the surface due to the mean W is given by (See 3.3.3)

$$H_w = c_p \rho \overline{T} \overline{w}$$

The vertical flux of water vapour associated with an average upward wind is the product of water vapour amount and vertical wind at that point. The situation is analogous to the heat case, however, and not all of this is a flux from the surface. Most of the moisture is brought into the area of upward velocity from elsewhere by convergent winds. The water vapour at a level above the heated water is therefore composed of what is advected in horizontally and what is added from below. The flux from the surface associated with the mean vertical motion is the product of the vapour added to the air by the surface and the mean w. The amount of vapour added by the surface was handled in a manner similar to the way the temperature deviation was calculated. As previously mentioned, the temperature of the undisturbed air away from the plume was assumed to be that of the 7.5 m level. For lack of information and to provide a minimum flux estimate, this air was assumed to be saturated. The estimated amount of water vapour in the undisturbed air was subtracted from the amount of water vapour in the air at the tower site to produce an estimate of the water vapour added by evaporation. The vapour flux from the surface associated with the mean vertical wind was then calculated by taking the product of this water vapour difference and the mean vertical wind as measured by the shear-stress meter.

The fluxes claculated in this way, along with the turbulent and total fluxes of sensible and latent heat are presented in Tables 12 and 13. In each period the sensible heat amounts transported by the two methods were of similar magnitude while the latent heat flux because of the mean vertical velocity was considerably less than its turbulent counterpart in every case. The rather large uncertainty in the vertical velocity (~2 cm/sec, see 4.1) produces a correspondingly large uncertainty in the flux estimates associated with the mean vertical velocity (~25%) but they still remain significant.

TABLE 12

Sensible Heat Flux Associated with Mean Vertical Wind

30-Min Means October 21

30 Mins Ending	$\bar{w}$ (cm/sec)	Heat Flux Due $\bar{w}$ (mW/cm^2)	Turbulent Heat Flux (mW/cm^2)	Total Heat Flux (mW/cm^2)
2000	5.8	4.8	7.1	11.9
2015	5.6	4.0	7.8	11.8
2030	6.8	4.9	8.6	13.5
2115	9.6	5.7	8.1	13.8
2130	8.8	6.3	13.0	19.3
Means	7.3	5.1	8.9	14.0

TABLE 13

Latent Heat Flux Associated With Mean Vertical Wind

30-Minute Means October 21

30 Mins Ending	$\bar{w}$ (cm/sec)	Latent Heat Flux Due $\bar{w}$ (mW/cm^2)	Turbulent Latent Heat Flux (mW/cm^2)	Total (mW/cm^2)
2000	5.8	1.8	4.8	6.6
2015	5.6	1.5	5.7	7.2
2030	6.8	1.8	6.6	8.4
2115	9.6	2.6	5.5	8.1
2130	8.8	2.4	7.6	10.0
Mean	7.1	2.0	6.0	8.0

CHAPTER V

CONCLUSIONS

The data collection program at Lake Wabamun in 1972 was in the nature of a preliminary investigation and interpretation of the results must take account of the severe limitations of the program in both space (one point) and time (parts of three days). Any attempt to extend the observed August ratio of fluxes over plume and lake to annual, seasonal or even monthly averages would be unjustified. Estimates of fluxes from the heated water plume have the additional complication of the changing size and shape of the plume itself and the changing volume of water discharged by the generating stations. Conclusions about the enhancement of evaporation and heat flux from the lake because of the hot water added to it must at present be almost totally qualitative.

In August, the time of the comparative observations of fluxes from the plume and the lake, the difference between plume and lake surface temperature should be approaching a minimum. Because the fluxes of heat and water vapour are directly dependent upon surface temperature, the difference in sensible and latent heat fluxes from the two surfaces should also be a minimum. Thus the value of approximately 5 (see Table 7) for the ratios of plume evaporation and heat flux to lake evaporation and heat flux should be a conservative one with the maximum value for this ratio occurring in the winter when all but the heated water is frozen.

If the plumes on the average cover 5% of the lake surface (see Nursall et al. 1972) and if the August data were representative then it could be concluded that the evaporation is enhanced 25% by the heated water. However, the question of representative data must remain unanswered until more data are available. In addition this estimate in no way takes account of the heat transferred by mixing and conduction into the rest of the lake possibly resulting in a net rise of temperature in the lake as a whole. The additional heat flux may not be significant when considered as part of the total energy budget of the lake but the increased evaporation may be a more serious problem (see Nursall et al. 1972).

Because profile measurements were available only for October 21, there were not enough data for a significant comparison of profile and fast-response estimates of the fluxes in general. However, a few comments about the comparison for free convection conditions should be valid keeping in mind the variation in surface temperature not allowed for in profile theory. The two estimates of heat flux were fairly well correlated being generally within 15% of one another for 30-minute means. The estimates of water vapour flux for the same intervals were not nearly as consistent with each other and in fact the profile estimates were greater by approximately 30%. This discrepancy may have been related to the near saturation conditions and to instrument error because of the presence of liquid water in the air but a full explanation is not available.

The profile estimates of momentum flux were in reasonable agreement with the momentum transported by the small scale eddies but of course, no allowance was made in the profile method for the momentum carried in the large-scale convective eddies. The profile procedure may provide good estimates of momentum flux in near-neutral stability or strong wind situations but in light wind and free convection conditions the picture from gradient information is over-simplified.

The dense fog at the lake in October was found to contribute to a 10% increase in the latent heat flux estimates but more accurate measurements of this quantity are necessary. With lower temperatures the liquid water flux should become more important in a fog situation and might have to be considered more rigorously.

The sensible and latent heat fluxes because of the non-zero vertical wind were found to contribute significantly to the total heat flux. This indicates that, in the winter months when mean upward vertical velocities over the heated water plumes are likely, the heat flux and evaporation are enhanced to a greater degree by the plumes than would be expected from the August comparison measurements.

Finally, the discovery of convective eddies above the plume transporting momentum upward against the horizontal velocity gradient during light winds was one of the most interesting products of the October field trip. These eddies were smaller than the heated water in extent but were of a larger scale than the ordinary boundary layer turbulence. Their occurrence at the tower site appeared to be random in nature with an observed duration of not less than 30 seconds. It was conjectured that these eddies were fairly extensive in the vertical with the vertical axis being tilted in the downwind direction in such a way that motion parallel to this axis would transport momentum upward. No information was available on the horizontal extent of the eddies and it is not known whether they are symmetrical in the cross-wind direction or extend the width of the plume. The latter might produce a structure similar to that of the large-scale convection forming cumulus in cloud streets higher in the troposphere as is frequently observed. With the source of these eddies fixed to the heated water plume it should be a relatively easy and rewarding task to gather more information on this convective turbulence at Lake Wabamun.

The problems encountered in this project emphasize the necessity of having profile observations outside the area of influence of the heated water, especially when large temperature differences between the air and water exist. As well, the largest part of the temperature gradient was found to be below the lowest level of profile measurement. More detailed profile observations in the low levels should therefore be worthwhile in any future data collection at Lake Wabamun.

BIBLIOGRAPHY

BIBLIOGRAPHY

Badgley, F. I., C. A. Paulson and M. Miyake, 1968: Profiles of Wind, Temperature and Humidity over the Arabian Sea. International Indian Ocean Expedition, Meteorol. Monographs No. 6, University Press of Hawaii, 60 pp.

Busch, N. E. and H. A. Panofsky, 1968: Recent spectra of Atmospheric Turbulence. Quart. J. Roy Meteor. Soc., 94, pp. 132-148.

Businger, J. A.,1966: Transfer of Momentum and Heat in the Planetary Boundary Layer. Proc. Symp. Arctic Heat Budget and Atmospheric Circulation,the RAND Corp., pp. 305-331.

Dyer, A. J., 1965: The flux-gradient Relation for Heat Transfer in the Lower Atmosphere. Quart. J. Roy. Meteor. Soc., 91, pp. 151-157.

________. 1967: The Turbulent Transfer of Heat and Water Vapour in an Unstable Atmosphere. Quart. J. Roy. Meteor. Soc., 93, pp. 501-508.

Ellison, T. H., 1957: Turbulent Transport of Heat and Momentum from an Infinite Rough Plane. J. Fluid Mech., Vol. 2, p. 456.

Estoque, M. A. and C. M. Bhumralkar, 1969: Flow Over a Localized Heat Source. Mon. Wea. Rev., 97, pp. 850-859.

Fleagle, R. G., F. I. Badgley, Y. Hsueh, 1967: Calculation of Turbulent Fluxes by Integral Methods. J. Atmos. Sci., 24, pp. 356-373.

________. and J. A. Businger, 1963: An Introduction to Atmospheric Physics. Chap. V: Transfer Processes and Applications, Pp. 180-196, Seattle Wash., University of Washington.

Hage, K. D., J. L. Honsaker and J. B. Nuttall, 1972: A Micrometeorological Study of Lake Wabamun. Paper presented at the Symposium on the Lakes of Western Canada, University of Alberta, Nov 16-17, 1972, 15 pp.

Haugen, D. A., J. C. Kaimal and E. F. Bradley, 1971: An Experimental Study of Reynolds Stress and Heat Flux in the Atmospheric Surface Layer. Quart. J. Roy. Meteor. Soc., 97, pp. 168-180.

Hicks, B. B., 1972: Propeller Anemometers as Sensors of Atmospheric Trubulence. Boundary-Layer Meteorology, 3, pp. 214-228.

Holland, J. Z., 1972: The Bomex Interaction Program: Background and Results to Date. NOAA Tech. Mem. ERL BAMAP -9, U.S. Dept. of Commerce NOAA Environmental Res. Labs. pp. 34.

Honsaker, J. L., F. McDougall and D. Oracheski, 1972: Data Acquisition System for Eddy Flux Measurements. Paper presented at the 6th annual congress of The Canadian Meteorological Society, Edmonton, May 31- June 2, 14 pp.

Kaimal, J. C. and J. A. Businger, 1963: A Continuous Wave Sonic Anemometer-thermometer. J. Appl. Meteor. 2, pp. 156-164.

________. and J. A. Businger, 1970: Case Studies of a Convective Plume and a Dust Devil. J. Appl. Meteor., 9, pp. 612-620.

________. J. C. Wyngaard, Y. Izumi, O. R. Cote, 1972: Spectral Characteristics of Surface-Layer Turbulence. Quart. J. Roy. Meteor. Soc., 99, pp. 563-589.

Lumley, J. L. and H. A. Panofsky, 1964: The Structure of Atmospheric Turbulence. New York, Interscience Publishers, 239 pp.

McBean, G. A., 1972: Instrument Requirements for Eddy Correlation Measurements. J. Appl. Meteor., 11, pp. 1078-1084.

Miyake, M., M. Donelan, G. McBean, C. Paulson, F. Badgley and E. Leavitt, 1970: Comparison of Turbulent Fluxes over Water Determined by Profile and Eddy Correlation Techniques. Quart. J. Roy. Meteor. Soc., 96, pp 132-137.

Monin, A. S. and A. M. Obunkhov, 1954: Basic Regularity in Turbulent Mixing in the Surface Layer of the Atmosphere. Trudy Geophys. Inst. ANSSSR, No. 24, p. 163.

Munn, R. E., 1966: Descriptive Micrometeorology. New York Academic Press Inc., 245 pp.

Nursall, J. R. and D. N. Gallup, 1971: The Responses of the Biota of Lake Wabamun, Alberta, to Thermal Effluent. Proc. Internat. Symp. on Ident. and Measurement of Environmental Pollutants, Ottawa, June 1971, pp. 295-304.

________. J. B. Nuttall and P. Fritz, 1972: The Effect of Thermal Effluent in Lake Wabamun, Alberta. Verh. Internat. Verein. Limmol., 18, pp. 269-277.

Pandolfo, J. P., 1966: Wind and Temperature Profiles for Constant-Flux Boundary Layers in Lapse Conditions with a Variable Eddy Conductivity to Eddy Viscosity Ratio. J. Atmos. Sci., 23, pp.495-502.

Panofsky, H. A., 1961: An Alternative Derivation of the Diabatic Wind Profile.Quart. J. Roy. Meteor. Soc., 87, p. 109.

________, 1963: Determination of Stress from Wind and Temperature Measurements. Quart. J. Roy. Meteor. Soc., 89, pp. 85-93.

________, 1965: Re-Analysis of Swinbank's Kerang Observations: Flux of Heat and Momentum in the Planetary Boundary Layer. Rept., Dept. of Meteorology, Pennsylvania State Univ., pp. 66-76.

________, 1969: Spectra of Atmospheric Variables in the Boundary Layer. Radio Science, 4(12), pp. 1101-1109.

________, A. K. Blackadar and G. E. McVehil, 1960: The Diabatic Wind Profile. Quart. J. Roy. Meteor. Soc., 86, p. 390.

Pasquill, F., 1972: Some Aspects of Boundary Layer Description. Quart. J. Roy. Meteor. Soc., 98, pp. 469-494.

Paulson, C. A., 1970: The Mathematical Representation of Wind Speed and Temperature Profiles in the Unstable Atmospheric Surface Layer. J. Appl. Meteor., 9, pp. 857-861.

Phelps, G. T. and S. Pond, 1971: Spectra of the Temperature and Humidity Fluctuations and the Fluxes of Moisture and Sensible Heat in the Marine Boundary Layer. J. Atmos. Sci., 28, pp. 918-928.

Plate, E. J., 1971: Aerodynamic Characteristics of Atmospheric Boundary Layers. AEC Critical Review Series, TlD - 25465, USAEC Tech. Info. Center, Oak Ridge, Tenn., 190 pp.

Pond, S., G. T. Phelps, J. E. Paquin, G. McBean and R. W. Stewart, 1971: Measurement of the Turbulent Fluxes of Momentum, Moisture and Sensible Heat Over the Ocean. J. Atmos. Sci., 28, pp. 901-917.

Priestley, C. H. B., 1955: Free and Forced Convection in the Atmosphere Near the Ground. Quart. J. Roy. Meteor. Soc., 81, p. 139.

________., 1959: Turbulent Transfer in the Lower Atmosphere, Chicago, University of Chicago Press, 130 pp.

Robinson, G. D., 1966: Another Look at Some Problems of the Air-Sea Interface. Quart. J. Roy. Meteor. Soc., 92, pp. 451-465.

Sellers, W. D., 1965: Physical Climatology. Chicago and London, The University of Chicago Press, 242 pp.

Sheppard, P. A., D. T. Tribble, J. R. Garratt, 1972: Studies of Turbulence in the Surface Layer Over Water (Lough Neagh): Part I: Instrumentation, Programme, Profiles. Quart. J. Roy. Meteor. Soc., 98, pp. 627-641.

Taylor, P. A., 1969: On Wind and Shear Stress Profiles Above a Change in Surface Roughness. Quart. J. Roy. Meteor. Soc., 95, pp. 77-91.

________., 1970: A Model of Airflow Above Changes in Surface Heat Flux, Temperature and Roughness for Neutral and Unstable Conditions. Boundary Layer Meteorology, 1(1), pp. 18-39.

U.S. Dept. of the Interior, 1954: Water Loss Investigations: Lake Hefner Studies. Technical Report, U.S.G.S. Professional Paper 269.

Webb, E. K., 1970: Profile Relationships: The Log Linear Range, and Extension to Strong Stability. Quart. J. Roy. Meteor. Soc., 96, pp. 67-90.

Wiener, F. M., J. H. Ball and C. M. Gogos, 1961: Some Micrometeorological Measurements in Ocean Fog. J. Geophys. Res., 66, pp. 3974-3978,